



**NTNU – Trondheim**  
Norwegian University of  
Science and Technology

# Multiphase performance validation

**Halfdan Rognes Knudsen**

Master of Energy and Environmental Engineering

Submission date: June 2013

Supervisor: Lars Erik Bakken, EPT

Norwegian University of Science and Technology  
Department of Energy and Process Engineering



EPT-M-2013-69

**MASTEROPPGAVE**

for

Stud.techn. Halvdan Knudsen

Våren 2013

**Validering av flerfase ytelse***Multiphase performance validation***Bakgrunn**

Flerfase trykkøkning er ny teknologi som prosessindustrien ønsker å utvikle for å redusere utbyggingskostnader og øke produksjonen fra eksisterende felt. Både operatører og leverandører av slikt utstyr satser tungt på utvikling av pålitelige konsepter som også kan brukes på havbunnen. Teknologien vil gi vesentlige energi og miljømessige besparelser ved at prosesseringsgraden og effektforbruket reduseres vesentlig i distribuerte anlegg. Med basis i eksperimentell forsøksdata undersøkes ytelsene til eksisterende konsepter. Av spesiell interesse er validering av instrumentering for nøyaktig bestemmelse av ytelse både ved ren væske og flerfase fluid.

**Mål**

Basert på litteratur og tilgjengelig eksperimentelt arbeid er det et mål å etablere pålitelige rutiner for validering av flerfase ytelse (gass volumfraksjon opp mot 0,90). Forholdet inkluderer både måletekniske og beregningstekniske aspekter.

**Oppgaven bearbeides ut fra følgende punkter:**

1. Prosjekttere laboratorierigg for å validere temperatursensorers evne til å gi pålitelige målinger av flerfase strømningsregime. Av spesiell interesse er driftsforhold hvor temperaturendringen er liten, samt forhold hvor termisk likevekt i fluidet (gass og væske) ikke er oppfylt.
2. Validere funksjonaliteten til «direkte integrasjon» i Hysys ved ulike driftsforhold fra ren væske og opp mot gass volumfraksjon 0,90.
3. Ved basis i «direkte integrasjon» i Hysys validere og dokumentere innvirkningen av tunge fluidkomponenter har på kompresjonsbanen og ytelser.

” - ”

Senest 14 dager etter utlevering av oppgaven skal kandidaten levere/sende instituttet en detaljert fremdrift- og eventuelt forsøksplan for oppgaven til evaluering og eventuelt diskusjon med faglig ansvarlig/veiledere. Detaljer ved eventuell utførelse av dataprogrammer skal avtales nærmere i samråd med faglig ansvarlig.

Besvarelsen redigeres mest mulig som en forskningsrapport med et sammendrag både på norsk og engelsk, konklusjon, litteraturliste, innholdsfortegnelse etc. Ved utarbeidelsen av teksten skal kandidaten legge vekt på å gjøre teksten oversiktlig og velkrevet. Med henblikk på lesning av besvarelsen er det viktig at de nødvendige henvisninger for korresponderende steder i tekst, tabeller og figurer anføres på begge steder. Ved bedømmelsen legges det stor vekt på at resultatene er grundig bearbeidet, at de oppstilles tabellarisk og/eller grafisk på en oversiktlig måte, og at de er diskutert utførlig.

Alle benyttede kilder, også muntlige opplysninger, skal oppgis på fullstendig måte. For tidsskrifter og bøker oppgis forfatter, tittel, årgang, sidetall og eventuelt figurnummer.

Det forutsettes at kandidaten tar initiativ til og holder nødvendig kontakt med faglærer og veileder(e). Kandidaten skal rette seg etter de reglementer og retningslinjer som gjelder ved alle (andre) fagmiljøer som kandidaten har kontakt med gjennom sin utførelse av oppgaven, samt etter eventuelle pålegg fra Institutt for energi- og prosesssteknikk.

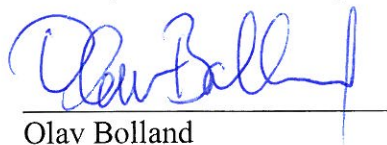
Risikovurdering av kandidatens arbeid skal gjennomføres i henhold til instituttets prosedyrer. Risikovurderingen skal dokumenteres og inngå som del av besvarelsen. Hendelser relatert til kandidatens arbeid med uheldig innvirkning på helse, miljø eller sikkerhet, skal dokumenteres og inngå som en del av besvarelsen. Hvis dokumentasjonen på risikovurderingen utgjør veldig mange sider, leveres den fulle versjonen elektronisk til veileder og et utdrag inkluderes i besvarelsen.

I henhold til "Utfyllende regler til studieforskriften for teknologistudiet/sivilingeniørstudiet" ved NTNU § 20, forbeholder instituttet seg retten til å benytte alle resultater og data til undervisnings- og forskningsformål, samt til fremtidige publikasjoner.

Besvarelsen leveres digitalt i DAIM. Et faglig sammendrag med oppgavens tittel, kandidatens navn, veileders navn, årstall, instituttnavn, og NTNUs logo og navn, leveres til instituttet som en separat pdf-fil. Etter avtale leveres besvarelse og evt. annet materiale til veileder i digitalt format.

- Arbeid i laboratorium (vannkraftlaboratoriet, strømningsteknisk, varmeteknisk)  
 Feltarbeid

NTNU, Institutt for energi- og prosesssteknikk, 14. januar 2013



Olav Bolland  
Instituttleder

  
Lars E Bakken  
Faglig ansvarlig/veileder

Medveileder;  
- Øyvind Hundseid, NTNU





## Abstract

The oil and gas industry wishes to further develop multi-phase technology in order to reduce construction costs and increase production from existing fields. Both suppliers and operators are investing in development of subsea equipment. The goal is to reduce environmental impact and energy costs.

Suppliers are extending their product portfolio with wet gas compressors or high GVF multi-phase pumps. Accurate predictions of performance are important to the customer, as the customer needs the predictions in order to estimate return of investments, and for designing the overall production plant.

Well-established models for predicting performance of single-phase and liquid dominated two-phase flow exists. But companies aim to extend these models, in order to also predict performance of gas dominated flow.

Based on literature study and available test data, the goal is to establish reliable routines on two-phase performance calculations. This includes solving challenges related to both calculations and measurements.

A laboratory rig have been planned in order to validate different temperature sensors ability to measure in two phase flow. Main focus has been on generating conditions where thermal equilibrium is absent. Different solutions on how to generate non thermal equilibrium two-phase mixtures have been presented. Relevant temperature sensors have been chosen and a sensitivity analysis has been performed to make sure they are accurate enough for the assignment. Solutions to challenges like gas phase humidity and local gas phase temperature measurements are presented. In the end a complete procedure on how to perform the tests is suggested.

This thesis aimed to validate the functionality of a Direct Integration method implemented in the process simulation tool HYSYS. Trough different examples it has been compared to Shultz and a Matlab implementation of the Direct Integration model presented in this thesis. The HYSYS implementation was found to differ from the original Direct Integration method presented by Huntington. For polytropic efficiency calculations it does not seem to be implemented at all. If the Direct Integration method is to be used in performance calculations, better results will be achieved by applying the Matlab implementation presented in this thesis.

Industry actors sometimes reduce analysis costs by neglecting heavier parts of the composition. The importance of knowing the exact fluid composition is discussed in this thesis. Results from simulations where heavier components are neglected are presented. It has been found that the accuracy of the performance calculations is highly dependent on the accuracy of the composition. The calculations of polytropic efficiency are especially sensitive when operating far into the two-phase area.





## Sammendrag

Olje og gass industrien ønsker å videreutvikle flerfase trykkøknings teknologi, for å redusere byggekostnader og for å øke produksjonen fra eksisterende felt. Både leverandører og operatører investerer i utviklingen av Subsea-utstyr og konsekvensene er redusert miljøpåvirkning og energiforbruk.

Flere leverandører utvider sin produktportefølje med våtgass kompressorer eller flerfasepumper. Nøyaktige beregninger av ytelse er viktig for kundene, ettersom kundene trenger beregningene for å estimere lønnsomheten av sine investeringer, og for å dimensjonere et omliggende produksjonsanlegg.

Veletablerte og aksepterte modeller for prediksjon av ren væske ytelse og væskedominert tofase ytelse eksisterer. Men selskapene ønsker å utvide disse modellene, slik at de også kan bli brukt til å prediktere ytelse ved gass dominert strømning.

Basert på litteraturstudier og tilgjengelige testdata, er målet å etablere pålitelige rutiner for tofase prediksjon. utfordringer knyttet til både beregninger og målinger er behandlet i denne oppgaven.

En laboratorierigg har blitt planlagt. Hensikten er å validere forskjellige temperatur sensorers evne til å gjøre pålitelige målinger i to fase strømnings regime. Hovedfokus har vært på å generere forhold der termisklikevekt er fraværende. Ulike løsninger på hvordan gas og væske kan mikses for å generere en temperaturforskjell mellom fasene, er presentert i oppgaven. Relevante temperatursensorer er valgt ut, og en sensitivetsanalyse er utført for å sørge for at sensorene er nøyaktige nok. utfordringer som gassfuktighet og lokale gass temperaturmålinger blir grundig gjennomgått. Til slutt blir det foreslått en fullstendig test prosedyre.

Denne oppgaven har forsøkt å validere funksjonaliteten til Direkte Integrasjon i prosess simuleringsverktøyet HYSYS. Gjennom forskjellige eksempler har Direkte Integrasjon i HYSYS blitt sammenlignet med Shultz og en implementering av Direkte Integrasjon i Matlab. Matlab implementeringen er presentert i denne oppgaven. Det har vist seg at Directe Integrasjon i HYSYS avviker fra den opprinnelige Direkte Integrasjons metoden presentert av Huntington. For beregning av polytropisk virkningsgrad ser det ut til at Direkte Integrasjon ikke er implementert i det hele tatt. Hvis det er ønskelig å benytte Direkte Integrasjon i fremtidige ytelses beregninger, vil man oppnå bedre resultat om man benytter Matlab modellen som blir presentert i denne oppgaven.

Aktører i Industrien forsøker noen ganger å redusere kostnader ved å neglisjere de tyngste fluid komponentene. Viktigheten av å kjenne til den nøyaktige fluid komposisjonen diskuteres i denne oppgave. Resultater fra simuleringer der tyngre komponenter er neglisjert viser at nøyaktigheten av ytelses beregninger er svært avhengig av nøyaktigheten av sammensetningen. Det ble også funnet at beregningene av polytropisk virkningsgrad er spesielt sensitive når det opereres i tofase området.



## **Acknowledgements**

This Master Thesis is performed at the Department of Energy and Process Engineering at the Norwegian University of Science and Technology, during spring 2013.

I would like to thank my supervisor Professor Lars Erik Bakken and my fellow students at the study hall, for their important inputs.

Trondheim 19. December 2012

---

Halfdan Rognes Knudsen



# Table of Contents

<b>FIGURES</b> .....	<b>2</b>
<b>TABLES</b> .....	<b>4</b>
<b>ROMAN SYMBOLS</b> .....	<b>6</b>
<b>GREEK SYMBOLS</b> .....	<b>7</b>
<b>SUBSCRIPTS</b> .....	<b>7</b>
<b>ABBREVIATIONS</b> .....	<b>8</b>
<b>1 INTRODUCTION</b> .....	<b>10</b>
1.1 Background .....	10
1.2 Objective .....	10
1.3 Approach .....	12
<b>2 MULTI-PHASE FLOW THEORY</b> .....	<b>14</b>
2.1 Simple definitions .....	14
2.2 Flow regimes .....	15
2.3 Mixed flow model .....	15
2.4 Two-fluid model .....	16
<b>3 SINGLE-PHASE PUMP THEORY</b> .....	<b>18</b>
3.1 Affinity laws .....	20
3.2 Viscosity .....	21
<b>4 MULTI-PHASE PUMP THEORY</b> .....	<b>24</b>
4.1 Affinity and Similarity laws .....	24
4.2 Two-phase multipliers .....	25
4.2.1 Analytical approach .....	26
4.2.2 MIT-model .....	26

4.3	Gas compression .....	27
4.3.1	Isothermal compression .....	27
4.3.2	Polytrophic compression .....	28
4.4	Viscosity.....	30
4.5	Phase transition .....	31
<b>5</b>	<b>TEMPERATURE MEASUREMENTS .....</b>	<b>34</b>
5.1	Accuracy .....	34
5.2	Sensor technologies.....	36
5.2.1	Thermocouples .....	36
5.2.2	Resistance temperature detectors (RTD).....	37
5.2.3	Thermistors .....	37
5.2.4	Pyrometers .....	38
5.3	Two-phase temperature measurements .....	38
<b>6</b>	<b>LABORATORY RIG .....</b>	<b>42</b>
6.1	Conditions and setup.....	43
6.2	Engineering .....	44
6.2.1	Temperature measurements .....	45
6.2.2	Test section .....	46
6.2.3	Gas phase humidity .....	50
6.2.4	Gas volume fraction.....	52
6.2.5	Generating liquid dominated flow .....	52
6.2.6	Generating gas dominated flow .....	54
6.3	Test procedure.....	56
6.4	Sources of Error .....	58
<b>7</b>	<b>VALIDATION OF DIRECT INTEGRATION IN HYSYS.....</b>	<b>60</b>
7.1	Direct Integration .....	60
7.2	Implementation of direct integration in HYSYS .....	61
7.3	Implementation of direct integration in Matlab .....	63
7.3.1	DirectIntegrationT().....	63

7.3.2	DirectIntegrationEtha().....	64
7.4	Validation.....	65
<b>8</b>	<b>INFLUENCE OF HEAVY COMPONENTS ON THE PERFORMANCE</b>	
	<b>CALCULATIONS.....</b>	<b>68</b>
8.1	Compositions .....	68
8.2	Compression path and performance parameters .....	70
<b>9</b>	<b>CONCLUSIONS AND SUGGESTIONS TO FURTHER WORK .....</b>	<b>74</b>
	<b>REFERENCES .....</b>	<b>76</b>
	<b>APPENDIX .....</b>	<b>80</b>
	<b>A - OFFER ON THERMO-NEEDLE-PROBE SYSTEM.....</b>	<b>82</b>
	<b>B - DATA SHEETS.....</b>	<b>84</b>
	<b>C - LIQUID DOMINATED MIXER CALCULATIONS.....</b>	<b>92</b>
	<b>D - SIMULATION ENVIRONMENT TEST RIG.....</b>	<b>94</b>
	<b>E - MATLAB IMPLEMENTATION OF DIRECT INTEGRATION .....</b>	<b>96</b>
	<b>F - COMPLETE DIRECT INTEGRATION RESULTS.....</b>	<b>102</b>





## Figures

Figure 1 Boosted production compared to natural production.....	10
Figure 2 Gas-liquid flow regime in horizontal pipes [ 3 ].....	15
Figure 3 Velocity diagrams of a centrifugal impeller. ....	18
Figure 4 Velocity diagram at impeller inlet. ....	18
Figure 5 Velocity diagram at impeller outlet. ....	19
Figure 6 Pump characteristics with specified losses. ....	19
Figure 7: Correction of head and efficiency [ 2 ]. ....	21
Figure 8 Phase envelope of a typical hydrocarbon.....	32
Figure 9 Temperature sensitivity analysis, with an inaccuracy of 0.2 K. ....	35
Figure 10 Temperature sensitivity analysis, with an inaccuracy of 0.002 K. ....	36
Figure 11 Comparison of RTDs, NTC thermistors and Thermo couples. ....	38
Figure 12 Temperature and conductivity measurement of a passing bobble [ 27 ]. ....	39
Figure 13 Simple drawing of the test rig.....	42
Figure 14 Heater and saturator simulations.....	44
Figure 15 Concept number one - CTC probe setup. ....	47
Figure 16 Concept number two - PT100 RTD shield setup.....	48
Figure 17 Concept number three - PT100 Gas suction setup.....	49
Figure 18 Saturation example .....	51
Figure 19 Perforated tube in mixer.....	53
Figure 20 Nozzle mounting.....	55
Figure 21 HYSYS test procedure simulations .....	57
Figure 22 HYSYS compressor calculation options.....	60
Figure 23 DirectIntegrationT() first step iteration.....	63
Figure 24 DirectIntegrationT() after last step iteration .....	64
Figure 25 DirectIntegrationEtha().....	65
Figure 26 Direct integration, Composition A VS B, Number of steps = 10, GVF 90%.....	71
Figure 27 Direct integration, Composition A VS B, Number of steps = 10, GVF 60%.....	72
Figure 28 Direct integration, Composition A VS B, Number of steps = 10, GVF 30%.....	72
Figure 29 Direct integration, Composition A VS B, Number of steps = 10, GVF 0%.....	73
Figure 30 Direct integration, Composition A VS B, Number of steps = 10, GVF 0% .....	103

Figure 31 Direct integration, Composition A VS B, Number of steps = 10, GVF 10% ..... 103  
Figure 32 Direct integration, Composition A VS B, Number of steps = 10, GVF 20% ..... 104  
Figure 33 Direct integration, Composition A VS B, Number of steps = 10, GVF 30% ..... 104  
Figure 34 Direct integration, Composition A VS B, Number of steps = 10, GVF 40% ..... 104  
Figure 35 Direct integration, Composition A VS B, Number of steps = 10, GVF 50% ..... 105  
Figure 36 Direct integration, Composition A VS B, Number of steps = 10, GVF 60% ..... 105  
Figure 37 Direct integration, Composition A VS B, Number of steps = 10, GVF 70% ..... 105  
Figure 38 Direct integration, Composition A VS B, Number of steps = 10, GVF 80% ..... 106  
Figure 39 Direct integration, Composition A VS B, Number of steps = 10, GVF 90% ..... 106

## Tables

Table 1 Temperature measurement sensitivity analysis.....	34
Table 2 Fluid conditions 2.....	43
Table 3 Temperature sensor data .....	46
Table 4 Sensitivity of liquid temperature measurements on gas temperature calculations.....	46
Table 5 Fluid conditions.....	47
Table 6 Effect of condensation on GVF.....	52
Table 7 Perforated tube Flow rate/Pressure calculations .....	53
Table 8 Nozzle GVF calculations option 1 .....	54
Table 9 Nozzle GVF calculations option 2 .....	55
Table 10 Conditions .....	62
Table 11 Outlet temperature calculations.....	62
Table 12 Conditions .....	62
Table 13 Polytropic efficiency calculations .....	62
Table 14 Conditions .....	66
Table 15 Outlet temperature calculations of a hydrocarbon mixture at 60% GVF.....	66
Table 16 Outlet temperature calculations of water .....	67
Table 17 Hydrocarbon composition Actual mixtures VS Low cost analyzes.....	69
Table 18 Imagined test results.....	70
Table 19 Performance Calculations .....	70
Table 20 Direct Integration results 90%-60% GVF.....	102
Table 21 Direct Integration results 50%-20% GVF.....	102
Table 22 Direct Integration results 10%-0% GVF.....	103



## Roman symbols

<i>A</i>	Area	$m^2$
<i>B</i>	Impeller discharge width	$m$
<i>B</i>	Pump performance Reynolds number	-
<i>c</i>	Absolute velocity	$m/s$
$C_p$	Heat capacity	$kJ/kg\ K$
<i>d</i>	Diameter	$m$
<i>F</i>	Friction effect on pressure loss	$Pa/m$
<i>f</i>	Correction factor	-
<i>G</i>	Gravitation effect on pressure loss	$Pa/m$
<i>g</i>	Acceleration due to gravity	$m/s^2$
<i>H</i>	Euler Head	$kJ/kg$
<i>h</i>	Enthalpy	$kJ/kg$
$\dot{m}$	Mass flow rate	$kg/s$
<i>n</i>	Rotational speed	$rad/s$
<i>n</i>	Polytrophic exponent	-
$n_q$	Specific speed	$rad/s$
<i>P</i>	Power	$W$
<i>p</i>	Pressure	$Pa$
<i>Q</i>	Volumetric flow rate	$m^3/s$
$q^*$	Flow rate on flow rate at best efficiency	-
<i>R</i>	Gas constant	$kJ/kg\ K$
<i>S</i>	Slip ratio	-
<i>T</i>	Temperature	$^{\circ}C$

$u$	Circumferential velocity	$m/s$
$v$	Specific volume	$m^3/kg$
$v$	Relative velocity	$m/s$
$X$	Compressibility function	-
$x$	Axial distance	$m$
$Y$	Compressibility function	-
$Z$	Compressibility factor	-
$z_{st}$	Number of stages	-

### Greek symbols

$\alpha$	Gas volume fraction(GVF)	-
$\beta$	Gas mass fraction(GMF)	-
$\beta$	Impeller outlet angle	$rad$
$\eta$	Efficiency	$\%$
$\theta$	Pipe elevation	$rad$
$\kappa$	Isentropic exponent	-
$\lambda$	Friction coefficient	-
$\nu$	Kinematic viscosity	$m^2/s$
$\rho$	Density	$kg/m^3$
$\phi$	Flow coefficient	-
$\psi$	Head coefficient	-

### Subscripts

$1$	Stage/Impeller inlet
$2$	Stage/Impeller outlet

<i>a</i>	Application
<i>d</i>	Drag
<i>ref</i>	Reference
<i>g</i>	Gas
<i>ISO</i>	Isothermal
<i>l</i>	Liquid
<i>M</i>	Model
<i>m</i>	Two-phase mix
<i>m2</i>	Radial component
<i>m1</i>	Axial component
<i>p</i>	Polytrophic
<i>SPL</i>	Single-phase liquid
<i>TP</i>	Two-phase
<i>th</i>	Theoretical
<i>tot</i>	Total
<i>u</i>	Circumferential component
<i>v</i>	Viscous
<i>v</i>	Volume corrected
<i>w</i>	Water

## **Abbreviations**

<i>BEP</i>	Best efficiency point
<i>DR</i>	Density ratio
<i>GLR</i>	Gas liquid ratio

<i>GMF</i>	Gas mass fraction
<i>GVF</i>	Gas volume fraction
LH	Liquid holdup
<i>VF</i>	Void fraction



# 1 Introduction

## 1.1 Background

Pumps are deployed onshore, offshore and subsea in order to increase oil recovery from fields where the natural reservoir pressure is insufficient. By reducing the back pressure of the well, pumps increase the flow rate. The purpose can either be to increase the daily production, or to extend the lifetime of an aging field. In both cases the total production increases.

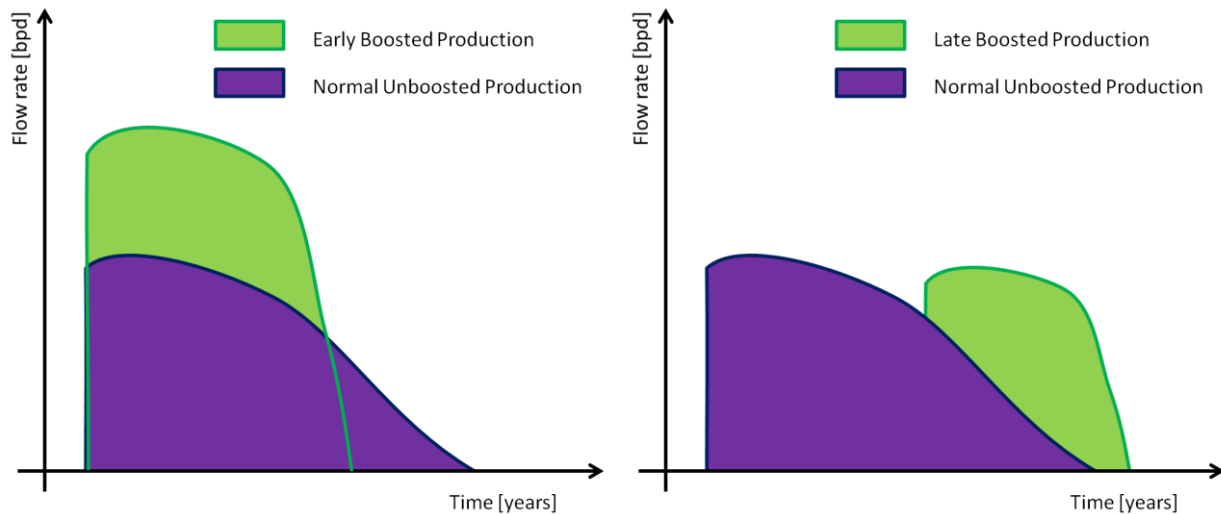


**Figure 1 Boosted production compared to natural production.**

A hydrocarbon well stream may contain oil, gas, water and sand. Separation at the seabed is an option, but a complete separation is associated with extensive maintenance work. Any operation at the seabed is complicated, and systems should be as robust as possible. As a result, subsea boosting will typically be exposed to multi-phase flow, either directly from a well, or from a sub-sea separator. Industry is therefore looking to multi-phase pumps and wet gas compressors to handle the subsea boosting.

## 1.2 Objective

Several Oil service companies are extending their product portfolio with wet gas compressors or high GVF multi-phase pumps. Accurate prediction of performance is important to the customer. The customer needs the predictions in order to estimate the return of investments, and for designing the overall production plant.

Based on literature study and available test data, the goal is to establish reliable routines on two-phase pump performance calculations. Well-established models for predicting performance of

single-phase pumps and liquid dominated two-phase pumps (0 – 60 % GVF) exists. But companies aim to extend these models, in order to also predict performance of gas dominated pumps (60 % - 90 % GVF). The models applied by the industry today are limited by the fact that they assume isothermal compression of the gas. The isothermal compression model neglects the heat generated from the compression of the gas and therefore causes a under estimation of the generated head. A under estimation of the generated head will in turn cause a under estimation of the efficiency.

Efficiency, head and power consumption data generated from tests are used as inputs in performance prediction of operating pumps. If the pump is operating close to the test conditions, outlet conditions can be predicted with good accuracy using the isothermal compression model. But when the pump is operating far from the tested conditions the simplified compression model becomes less accurate.

To improve predictions the isothermal compression model can be replaced by a polytropic compression model. It is more thermo dynamically correct, and does not neglect the heat generated from the gas compression. The challenge of applying a polytropic compression model is that it requires a polytropic efficiency. The polytropic efficiency can only be established from temperature measurements. The temperature measurements need to be highly accurate as the temperature increase across a stage is typically in the range of just 0.5 °C to 9 °C, depending on the GVF and the differential pressure.

Performances of multi-phase pumps are calculated stage by stage, as important performance parameters constantly changes trough out the compression. Uncertainties related to whether or not the gas and liquid phase is in thermal equilibrium exist. Stage to stage temperature measurements must therefore be able to measure temperature locally in both phases. A laboratory rig will be planned in order to validate different temperature sensors ability to do measurements in two-phase flow. Main focus will be on generating conditions where thermal equilibrium is absent.

This thesis will also aim to validate the functionality of the polytropic compression model Direct Integration, implemented in the process simulation tool HYSYS. Trough different examples it will be validated against other polytropic methods.

At least but not last the importance of accurate composition data will be assessed. Industry actors sometimes reduce analysis costs by neglecting heavier parts of the composition. The importance of knowing the exact fluid composition will be simulated and discussed.

### 1.3 Approach

Chapter 2 contains general theory on multi-phase flow in one-dimensional pipes. Performance parameters, flow-regimes and fluid models relevant for multi-phase pumps are discussed.

Chapter 3 describes general theory on single-phase pumps. It also discusses single-phase performance predictions.

Chapter 4 discusses different aspects of multi-phase performance predictions. Different calculation models are suggested and the challenges involved when applying them are discussed.

Chapter 5 contains general theory about temperature measurements. Different technologies, their advantages and disadvantages are discussed.

Chapter 6 describes a laboratory rig planned in order to enable validation of different temperature sensors. Main focus will be on generating conditions where thermal equilibrium is absent.

Chapter 7 is an attempt on validating and documenting the functionality of the Direct Integration method implemented in HYSYS. HYSYS is a process simulation tool delivered by AspenTec.

Chapter 8 discusses the importance of knowing the exact composition of test fluid. Results from simulations where the heavier components are neglected are presented.



## 2 Multi-phase flow Theory

A phase is simply one of the states of a matter and can either be a gas, a liquid, or a solid. Multi-phase flow is the simultaneous flow of several phases. Two-phase flow is the simplest case of multi-phase flow [ 1 ]. Fluids which flow from a reservoir can contain a mixture of oil, gas, water and sand. In this thesis only two-phase mixtures will be considered, either as air/water test fluids, or as hydrocarbon mixtures.

### 2.1 Simple definitions

Alpha is the gas volume fraction (GVF), while beta represents the gas mass fraction (GMF).

$$\alpha = \frac{Q_g}{Q_{tot}} = \frac{Q_g}{Q_g + Q_l} \quad \text{Eq. 2.1}$$

$$\beta = \frac{\dot{m}_g}{\dot{m}_{tot}} = \frac{\dot{m}_g}{\dot{m}_g + \dot{m}_l} \quad \text{Eq. 2.2}$$

Gas holdup:

$$VF = \frac{A_g}{A_{tot}} = \frac{A_g}{A_l + A_g} \quad \text{Eq. 2.3}$$

Liquid holdup:

$$LH = \frac{A_l}{A_{tot}} = \frac{A_l}{A_l + A_g} \quad \text{Eq. 2.4}$$

Gas liquid ratio:

$$GLR = \frac{Q_g}{Q_l} \quad \text{Eq. 2.5}$$

Slip ratio:

$$S = \frac{c_g LH}{VF c_l} \quad \text{Eq. 2.6}$$

Gas holdup, also known as void fraction represents the actual cross-sectional area occupied by the gas. The relationship between GVF and the gas holdup depends on the slip ratio. If the gas velocity is decreased compared to the liquid velocity while the GVF is kept the same, the area occupied by the gas will increase.

## 2.2 Flow regimes

Deciding the flow regime can be difficult. In fact scientists do not fully agree upon which regimes actually exist. A multi-phase pump is normally equipped with an upstream flow conditioning unit, which generates a homogenous flow, i.e. mixing of the phases before they enter the pump main flow path. It means that slug flow, elongated bubble flow, stratified flow and wavy flow are all transformed in to dispersed bubble flow or annular flow depending on whether the flow is gas or liquid dominated.

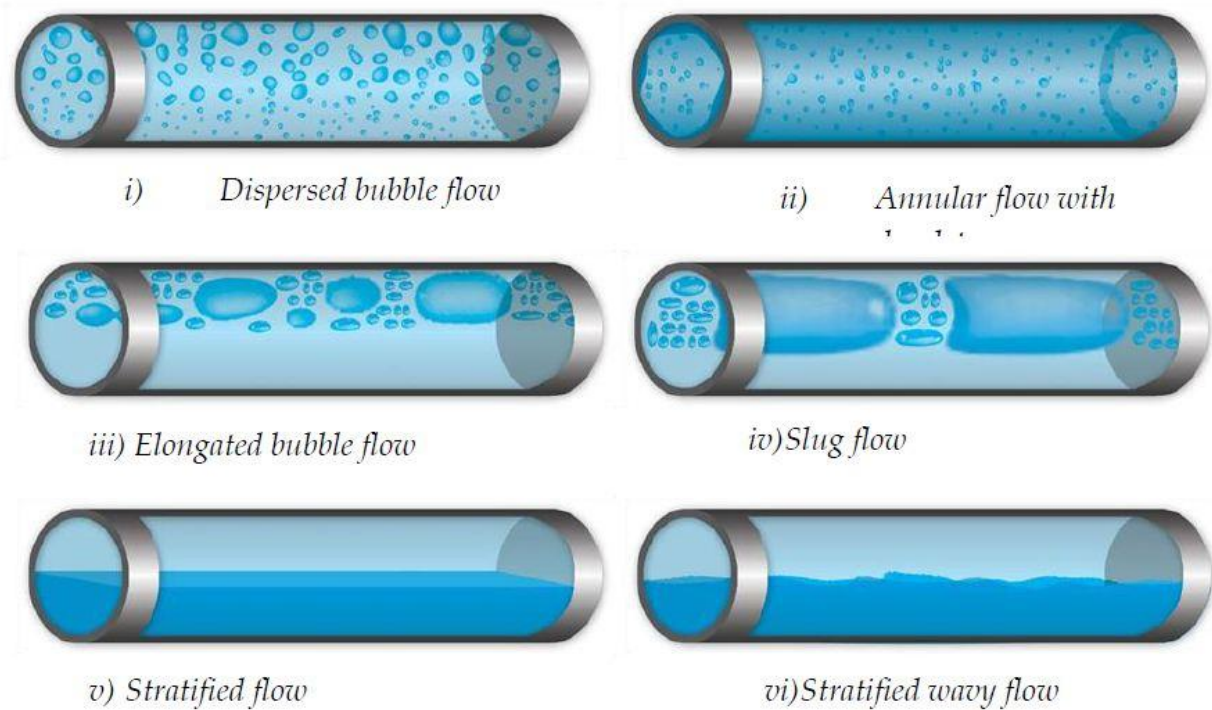


**Figure 2 Gas-liquid flow regime in horizontal pipes [ 3 ].**

## 2.3 Mixed flow model

Liquid domination means that gas bubbles are traveling in liquid (low GVF). Bubble flow is modeled as a homogenous mixture of the two-phases. The central assumption of the mixed flow model is that the two phases travel at equal velocities and mix well, and that they can therefore be treated as if there is only one phase [ 4 ].

$$\frac{dp}{dx} = -F - G \quad \text{Eq. 2.7}$$

$$F = \frac{1}{2} \lambda_m \rho_m c^2 \frac{1}{d} \quad \text{Eq. 2.8}$$

$$G = \rho_m g \cos(\theta) \quad \text{Eq. 2.9}$$

$$\rho_m = \alpha \rho_g + (1 - \alpha) \rho_l \quad \text{Eq. 2.10}$$

Eq. 2.7 represents the momentum equation for pipe flow with constant cross sectional area. The effect of mixture friction against the pipe wall (F) is given in Eq. 2.8 while gravitational effect on pressure change (G) is described by Eq. 2.9. Mixed-fluid density is determined by averaging the densities.

## 2.4 Two-fluid model

The drag force of a bubble travelling in a liquid is significant compared to its mass, therefore the bubble quickly adapts to any changes in the liquid velocity. For gas dominated flow however the drag force of the liquid droplet is small compared to its mass, and homogeneous fluid theory is therefore not valid. Instead a two-fluid model must be applied [ 4 ].

$$VF \frac{dp}{dx} = -F_d - F_g - G_g \quad \text{Eq. 2.11}$$

$$LH \frac{dp}{dx} = +F_d - F_l - G_l \quad \text{Eq. 2.12}$$

The two-fluid model separates the gas and the liquid into two different momentum equations. Because slip between the phases is expected, area fractions are introduced. Eq. 2.11 is the gas momentum equation while Eq. 2.12 represents the momentum equation for the liquid droplets. The pressure loss due to drag on the droplets is given by  $F_d$ . If a liquid film exists together with gas and liquid droplets, which is often the case for annular flow, the liquid holdup has to be separated into film holdup and droplet holdup. A third momentum equation must also be added to handle the liquid film.





### 3 Single-phase Pump Theory

A pump is meant to increase the pressure of the fluid. Energy is transferred to the fluid through one or more rotating impellers. The velocity diagrams in Figure 4 and Figure 5 display the actual, relative and circumferential velocity of the fluid, at impeller inlet and outlet. How the change in velocity generates head can be understood from Eq. 3.1. Figure 3 links the velocities to the impeller geometry, where  $c$  is the absolute velocity of the fluid,  $v$  is the relative velocity of the fluid compared to the impeller and  $u$  is the circumferential velocity of the impeller.

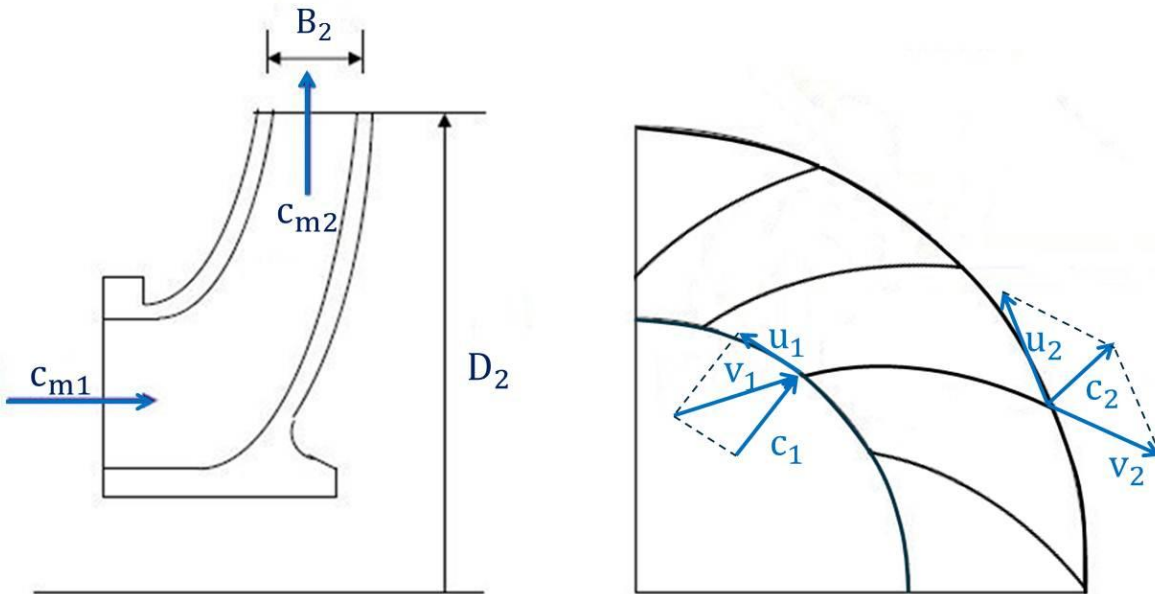


Figure 3 Velocity diagrams of a centrifugal impeller.

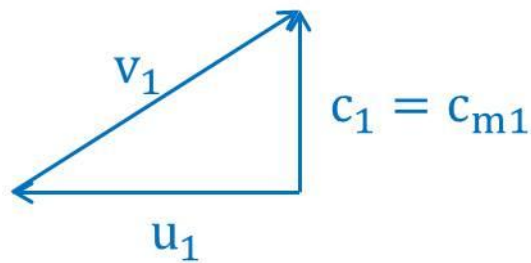


Figure 4 Velocity diagram at impeller inlet.

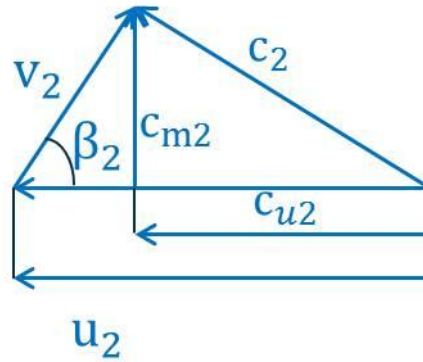


Figure 5 Velocity diagram at impeller outlet.

The theoretical head of a single-phase pump is determined by the geometry of the impeller outlet. An increase of the  $c_{u2}$  component will result in an increase of the theoretical head. Pre rotation of the fluid at the inlet, also known as swirl, reduces the impeller's ability to generate head.

$$H_{th} = u_2 c_{u2} \quad \text{Eq. 3.1}$$

$$H_{th} - H_{swirl} = u_2 c_{u2} - u_1 c_{u1} \quad \text{Eq. 3.2}$$

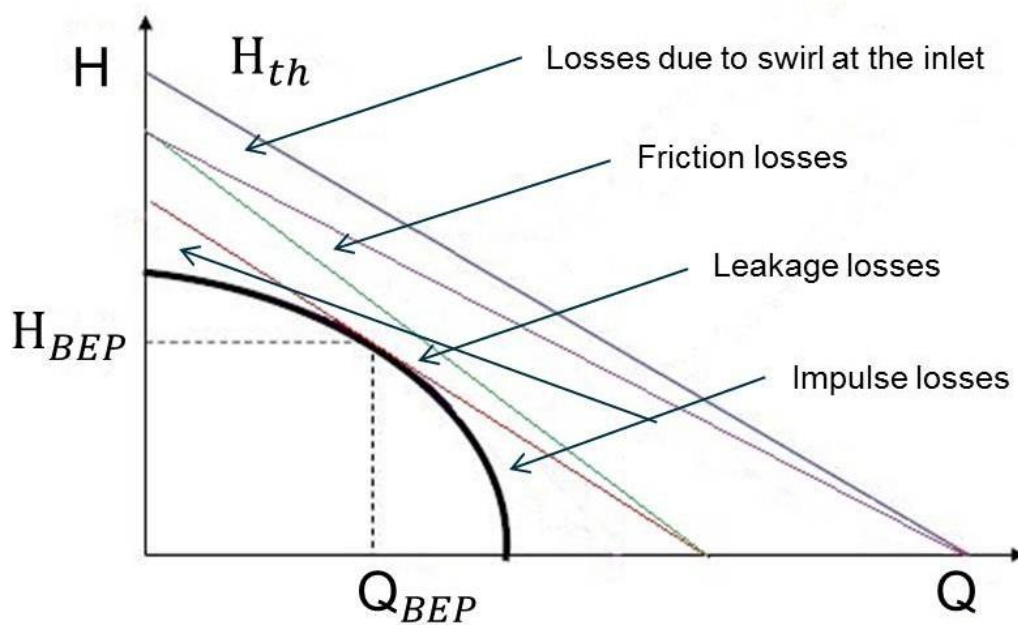


Figure 6 Pump characteristics with specified losses.

Figure 6 shows how the different losses reduce the head, and shape the actual head curve. From simple pipe flow theory it is known that friction losses increase with the flow rate. This theory also applies to pumps.

Leakage flow in a typical centrifugal pump can consist of;

- flow from the impeller discharge back to suction through the wear ring at the front shroud,
- flow from impeller suction through the wearing separating the diffuser and the shaft,
- flow through an axial thrust force balancing device.

A flow will increase if the differential pressure over its path increases. Leakage losses have the same effect, and are increasing with increasing head.

Impeller inlet and outlet are designed so that neither flow separation nor recirculation (backward facing flow) occurs at the best efficiency point [ 2 ]. These types of losses are referred to as impulse losses. When operating outside the design point, impulse losses exist due to miss match between the flow and the shape of the impeller

An accurate determination of the different losses requires details about geometry and fluid behavior. Such information is not easily obtained. Performance predictions of a single-phase pump are therefore done based on characteristics from a similar and already tested pump. A set of scaling rules are used in these calculations. Head, power consumption and flow rate are primarily scaled according to the affinity laws, in order to fit the correct diameter and rotational speed of the impeller. If the amount of stages differs between the predicted and the tested pump, head and power are also scaled according to the application/model stage count ratio. At last, if the density of the tested fluid differs from the fluid in the predictions, power consumption is scaled according to the application/model density ratio [ 2 ].

Application/model stage count ratio:

$$H = H_{ref} \left( \frac{z_{st}}{z_{st,ref}} \right) \quad \text{Eq. 3.3}$$

$$P = P_{ref} \left( \frac{z_{st}}{z_{st,ref}} \right) \quad \text{Eq. 3.4}$$

Application/model density ratio:

$$P = P_{ref} \left( \frac{\rho}{\rho_{ref}} \right) \quad \text{Eq. 3.5}$$

### 3.1 Affinity laws

The affinity laws are derived from a dimensionless analysis and are widely used for scaling performance curves of radial impeller pumps. The analysis is based on geometrical similarity and constant pump efficiency.

$$Q = Q_{ref} \left( \frac{n}{n_{ref}} \right) \left( \frac{d}{d_{ref}} \right)^3 \quad \text{Eq. 3.6}$$

$$H = H_{ref} \left( \frac{n}{n_{ref}} \right)^2 \left( \frac{d}{d_{ref}} \right)^2 \quad \text{Eq. 3.7}$$

$$P = P_{ref} \left( \frac{n}{n_{ref}} \right)^3 \left( \frac{d}{d_{ref}} \right)^5 \quad \text{Eq. 3.8}$$

### 3.2 Viscosity

Tests of the impellers are usually done on water. When pumping fluids of higher viscosity impeller performance is changed. Figure 7 shows how head and efficiency are decreased due to higher viscosity. Subscript v denotes viscous fluids, while subscript w denotes water. Head, flow rate and efficiency are corrected according to Eq. 3.9 to Eq. 3.11 [ 2 ].

$$f_h = \frac{H_v}{H_w} \quad \text{Eq. 3.9}$$

$$f_Q = \frac{Q_v}{Q_w} \quad \text{Eq. 3.10}$$

$$f_\eta = \frac{\eta_v}{\eta_w} \quad \text{Eq. 3.11}$$

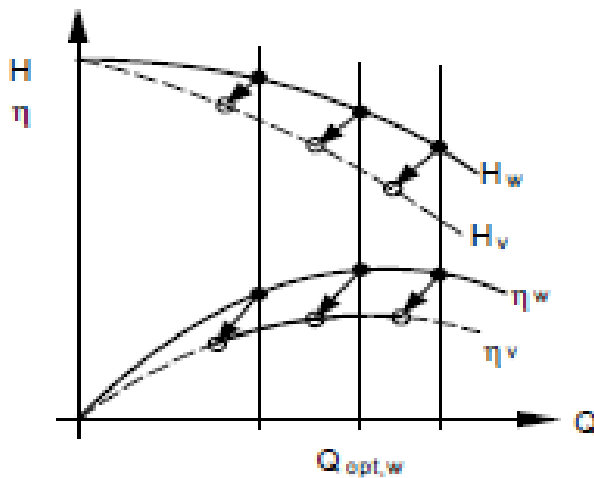


Figure 7: Correction of head and efficiency [ 2 ].

There are many available viscosity correction models, most of them are empirical. The Hydraulic Institute model is used and accepted by industry worldwide. It has been included as an ISO standard and is meant to include all centrifugal and vertical pumps, with open or closed impellers, single or double suction, pumping Newtonian fluids [ 5 ].

$$B = \frac{480 \sqrt{v}}{Q^{0.25} (g H)^{0.125}} \left\{ \frac{n_{q,Ref}}{n_q} \right\}^{0.25} \quad \text{Eq. 3.12}$$

$$n_{q,Ref} = 20 \quad \text{Eq. 3.13}$$

The model consists of equations based on a “pump performance Reynolds number”, adjusted for specific speed (parameter B).

$$f_Q = e^{-0.165(\log B)^{3.15}} \quad \text{Eq. 3.14}$$

$$f_\eta = B^{-\beta} \quad \text{Eq. 3.15}$$

$$\beta = 0.0547 B^{0.69} \quad \text{Eq. 3.16}$$

$$f_{H,BEP} = f_Q \quad \text{Eq. 3.17}$$

$$q^* = \frac{Q}{Q_{BEP}} \quad \text{Eq. 3.18}$$

$$f_H = 1 - (1 - f_{H,BEP})(q^*)^{0.75} \quad \text{Eq. 3.19}$$

The correction factor for flow and efficiency is calculated from parameter B. The head correction factor at best efficiency point equals the flow correction factor. Eq. 3.19 then adjusts the head for different flow rates.



## 4 Multi-phase Pump Theory

A significant difference between multi-phase and single-phase performance predictions is that multi-phase predictions should be done stage by stage. The outlet conditions of the previous stage acts as inlet conditions to the following stage. This is because important performance parameters such as density ratio (DR) and GVF are constantly changing throughout the compression.

### 4.1 Affinity and Similarity laws

In chapter 3.1 the affinity laws were introduced. The affinity laws scale performance of radial impellers when the outlet diameter or rotational speed is changed. Because radial impellers are more exposed to formation of gas blockages, semi-axial impellers are preferred when the gas content is significant. For typical semi-axial impellers, all geometric dimensions have to be scaled in order to keep similarity, not just the outlet diameter. The similarity laws are therefore applied instead of the affinity laws.

Similarity laws:

$$Q = Q_{ref} \left( \frac{n}{n_{ref}} \right) \left( \frac{d}{d_{ref}} \right)^3 \quad \text{Eq. 4.1}$$

$$H = H_{ref} \left( \frac{n}{n_{ref}} \right)^2 \left( \frac{d}{d_{ref}} \right)^2 \quad \text{Eq. 4.2}$$

$$P = P_{ref} \left( \frac{n}{n_{ref}} \right)^3 \left( \frac{d}{d_{ref}} \right)^5 \quad \text{Eq. 4.3}$$

The affinity and similarity laws are commonly used and accepted for centrifugal and semi-axial impellers. When pumping multi-phase flow these laws show good accuracy for liquid dominated flow. For gas dominated flow however the scaling laws does not apply [ 6 ].

A way around the limitations of the scaling laws is to avoid applying them directly on multi-phase flow. Scaling can be done on single-phase test data in order to calculate the single-phase flow coefficients before multi-phase effects are considered. The effects of operating with gas dominated flow are later captured by the two-phase multipliers and not the scaling laws.

## 4.2 Two-phase multipliers

Two-phase multipliers are used to predict two-phase performance when single-phase performance of liquid is known. The single-phase performance is found according to chapter 3. Gas entering the pump will cause degradation of the head as well as reduction in power consumption.

Rune Mode Ramberg [ 7 ] states the degradation of the head is related to the amount of gas going through the pump, the density of the mixture, the density ratio, the inlet pressure, the inlet temperature and the viscosity. He also mentions that pump speed is important. Too high speed will lead to fluid separation and reduce the performance even more. The two-phase multipliers are defined in the following way.

Head degradation factor:

$$f_{TP,H} = \frac{\psi_{TP}}{\psi_{SPL}} \quad \text{Eq. 4.4}$$

Power consumption reduction factor:

$$f_{TP,P} = \frac{P_{TP}}{P_{SPL}} \quad \text{Eq. 4.5}$$

From here on the thesis refers to the two-phase multipliers presented in Eq. 4.4 and Eq. 4.5 as head degradation factor and power consumption reduction factor. A set of two-phase multipliers generated from experiments are used as input in the performance predictions. Single- and two-phase flow coefficients form the basis when calculating the head degradation factors. The coefficients are generated from test results and related to each other by the same volumetric flow rate. They are found by measuring inlet and outlet conditions as well as impeller tip speed.

$$\psi = \frac{2 H}{u_2^2} \quad \text{Eq. 4.6}$$

In chapter 2 it was shown that liquid dominated flow could be modeled as a homogenous mixture. When it comes to multi-phase head calculations the two-fluid model is applied in order to treat the gas and the liquid differently.

$$H_{ISO,TP} = \beta Z_1 R T_1 \ln \left( \frac{p_2}{p_1} \right) + (1 - \beta) \frac{p_2 - p_1}{\rho_l} = f_{TP} \psi_{SPL} \frac{u_2^2}{2} \quad \text{Eq. 4.7}$$

$$H_{SPL} = \frac{p_{2l} - p_1}{\rho_l} \quad \text{Eq. 4.8}$$

As well as for calculating the head degradation factor from test results, Eq. 4.7 is used to predict two-phase head when the head degradation factor is known. Stage outlet pressure can be calculated from Eq. 4.7 once the two-phase head is determined. Note that Eq. 4.7 applies an isothermal compression model for the gas part of the equation. Alternatives to this approach will be presented later.



The power consumption reduction factors can be determined by relating power consumptions from single- and two-phase test data. The test data share the same flow rate and rotational speed.

Gulich [ 2 ] states that if a pump is operated with a given two-phase mixture at specific flow rate ratio  $q^*$  with different speeds, the velocity triangles remain similar. Therefore two-phase multipliers can be used independently of impeller tip speed and consequently independently of diameter and rotational speed of the pump.

#### 4.2.1 Analytical approach

Ramberg developed a head degradation factor, which can be calculated analytically from variables that are easily obtained under actual operating conditions. He evaluated the influence of GVF, density ratio, mixture density, inlet pressure, inlet temperature, pump speed and came up with the model given in Eq. 4.9.

$$H_{TP} = H_{SPL} f_{TP,H} = H_{SPL} \left( \frac{\rho_m}{\rho_l} \right) (1 + \alpha) \quad \text{Eq. 4.9}$$

$$f_{TP,H} = \left( 1 + \alpha \left( \frac{1}{DR} - 1 \right) \right) (1 + \alpha) \quad \text{Eq. 4.10}$$

By rearranging Eq. 4.9 we can see in Eq. 4.10 that Ramberg's head degradation factor only depends on the GVF and the density ratio. He has tested and validated the model against actual pump performance at the oil and gas field Gullfaks.

#### 4.2.2 MIT-model

The MIT-model is presented in the master thesis of J. E. Korenchan [ 11 ]. This model is a result of nuclear research, and an attempt to understand how pumps are affected by air or steam. Instead of looking at degradation of the head, MIT focused on how the head loss was increasing with increasing GVF. Korenchan states that by normalizing two-phase head loss compared to single-phase head loss instead of normalizing two-phase head compared with single-phase head we can diminish the dependence of pump geometry. Eq. 4.11 shows how the head-loss ratio  $H^*$  where defined.

$$H^* = \frac{\psi_{TP,th} - \psi_{TP}}{\psi_{SPL,th} - \psi_{SPL}} \quad \text{Eq. 4.11}$$

$$\psi_{TP} = 1 - \frac{f_{tp,flow} \phi_{tp2}}{\tan \beta_2} \quad \text{Eq. 4.12}$$

A lot of challenges are involved when applying the MIT-model, one of them is determination of the slip factor  $\mu$ . Note that  $\mu$  does not represent the slip between the phases, but the slip angle at the trailing edge of the impeller. The slip factor is needed to calculate the outlet flow angle  $\beta_2$  which affects the calculation of the head coefficient. An empirical method by Noorbakhsh [ 13 ] was suggested to determine the slip factor. Another challenge is to determine the slip ratio  $S$  (slip between the phases) which is needed in order to calculate the two-phase flow function  $f_{tp,flow}$ .

The idea of looking at head loss increase instead of head decrease is interesting, and might result in more accurate predictions. The uncertainty however, related to estimating the outlet flow angle is great. The empirical method of Noorbakhsh could be applied, but first it should be validated against CFD-simulations of the actual impeller.

### 4.3 Gas compression

As seen in subchapter 4.2, isothermal compression was applied in order to calculate the head degradation factor. This chapter will explain the consequences of assuming isothermal compression, and explain why the polytrophic compression is more accurate, especially in the high GVF region. It will also highlight additional input data required for an implementation a polytrophic compression model.

#### 4.3.1 Isothermal compression

A process that occurs at constant temperature is called an isothermal process. The liquid phase in a two-phase flow holds a significant larger heat capacity per unit volume compared to the gas phase. A high GVF value is needed to get a noticeable heat increase. A normal assumption is therefore that the gas goes through an isothermal compression process.

Head:

$$H = \int_1^2 v dp \quad \text{Eq. 4.13}$$

Assuming ideal gas:

$$p v = R T \quad \text{Eq. 4.14}$$

Constant temperature:

$$T = \text{const} \quad \text{Eq. 4.15}$$

Rearranging Eq. 4.14 and including constant temperature:

$$dp = \frac{R T}{dv} \quad \text{Eq. 4.16}$$

Applying the isothermal relation (Eq. 4.16) in Eq. 4.15 to get the isothermal head:

$$H_{ISO} = R T \int_1^2 \frac{dv}{v} = R T \ln \left( \frac{p_2}{p_1} \right) \quad \text{Eq. 4.17}$$

The isothermal compression is a normal simplification applied by the industry. Heat generated from compression of the gas is neglected and the temperature is assumed constant from suction to discharge.

### 4.3.2 Polytropic compression

A possible improvement of multi-phase pump performance predictions would be to replace isothermal calculations with a polytropic approach. It will influence the calculation of head degradation factor, stage outlet pressure and overall efficiency of the pump. As no heat is neglected, the polytropic compression model is believed to improve the calculations. Before showing how it can be implemented in multi-phase predictions, we shall take a short review of the polytropic gas compression process.

Polytropic relation:

$$p v^n = \text{const} \quad \text{Eq. 4.18}$$

Rearranging:

$$v_2 = v_1 \left( \frac{p_2}{p_1} \right)^{-\frac{1}{n}} \quad \text{Eq. 4.19}$$

Inserting the polytropic relation in Eq. 4.13 to get the polytropic head:

$$H_{POL} = Z R T \int_1^2 v_1 \left( \frac{p}{p_1} \right)^{-\frac{1}{n}} dp = \frac{n}{n-1} Z R T \left( \left( \frac{p_2}{p_1} \right)^{\frac{n-1}{n}} - 1 \right) \quad \text{Eq. 4.20}$$

Schultz

The polytropic head given in Eq. 4.20 is not correct because the change in polytropic exponent  $n$  along the compression path is neglected. Schultz [ 14 ] introduced the volume corrected polytropic exponent  $n_v$  and the compressibility functions X and Y.

$$n_v = \frac{1 - X}{Y \left[ \frac{1}{\kappa} \left( \frac{1}{\eta_p} + X \right) - \left( \frac{1}{\eta_p} - 1 \right) \right]} \quad \text{Eq. 4.21}$$

$$X = \frac{T}{v} \left( \frac{\partial v}{\partial Y} \right)_p - 1 \quad \text{Eq. 4.22}$$

$$Y = -\frac{p}{v} \left( \frac{\partial v}{\partial p} \right)_p \quad \text{Eq. 4.23}$$

The change in  $n_v$  along the compression path is considered to be small. Schultz defined it as constant. He introduced the compression path correction factor  $f_s$  to correct for the small variations in  $n_v$ .

$$f_s = \frac{h_{2s} - h_1}{\frac{\kappa_v}{\kappa_v - 1} Z R T \left( \left( \frac{p_2}{p_1} \right)^{\frac{\kappa_v - 1}{\kappa_v}} - 1 \right)} \quad \text{Eq. 4.24}$$

Where:

$$\kappa_v = \frac{\kappa}{Y} \quad \text{Eq. 4.25}$$

Schultz definition of the polytropic head is finally given by:

$$H_{POL} = f_s \frac{n_v}{n_v - 1} Z_1 R T_1 \left( \left( \frac{p_2}{p_1} \right)^{\frac{n_v - 1}{n_v}} - 1 \right) \quad \text{Eq. 4.26}$$

Applying Schultz's polytropic head into Eq. 4.7 would be an improvement compared to the isothermal predictions, but it requires more thermodynamic data on the gas phase. A possibility could be to involve a process simulation tool such as HYSYS in the predictions.

The following work will continue by showing how the polytropic head from Eq. 4.20 can be used to predict performance of a multi-phase pump. By applying Eq. 4.20 instead of Eq. 4.26 no process simulation program is necessary.

First we establish head degradation factor data from single and two-phase tests. The actual two-phase head is found from Eq. 4.27. Then polytropic efficiency data is calculated. It can be retrieved from test results by solving the first two sections of Eq. 4.28 iteratively. Note that the relation  $(n - 1)/n = \ln(T_2 - T_1)/\ln(p_2 - p_1)$  used for compressors, is valid only for pure gas and cannot be used to calculate polytropic efficiency from two-phase test data [ 14 ].

$$H = \frac{H_{POL}}{\eta_{pol}} = h_2 - h_1 \quad \text{Eq. 4.27}$$

$$H = \frac{\beta}{m \eta_{pol}} Z_1 R T_1 \left( \left( \frac{p_2}{p_1} \right)^m - 1 \right) + (1 - \beta) \frac{p_2 - p_1}{\rho_l \eta_{pol}} = f_{tp} \psi_{SPL} \frac{u_2^2}{2} \quad \text{Eq. 4.28}$$

$$m = \frac{n-1}{n} = \frac{\kappa-1}{\kappa \eta_{pol}} = \frac{RZ}{C_{p,m} \eta_{pol}} \quad \text{Eq. 4.29}$$

Where:

$$C_{p,mix} = \frac{\rho_l Q_l C_{p,l} + \rho_g Q_g C_{p,g}}{\rho_l Q_l + \rho_g Q_g} = \frac{C_{p,l} + \frac{GLR}{DR} C_{p,g}}{1 - \frac{GLR}{DR}} \quad \text{Eq. 4.30}$$

And

$$GLR = \frac{GVF}{1 - GVF} \quad \text{Eq. 4.31}$$

$$T_2 = T_1 + \frac{H}{C_{p,m}} \quad \text{Eq. 4.32}$$

The established test data can now be used to predict outlet pressure from last two sections of Eq. 4.28, and outlet temperature from Eq. 4.32.

#### 4.4 Viscosity

Discovery and development of new oilfields causes the industry to demand pumps that can handle fluids of higher viscosities. From chapter 3.2 we know that viscosity correction of single-phase pump performance is commonly used and accepted. For multi-phase flow, viscosity impact on fluid behavior becomes more complex. It is difficult to establish which phase is in contact with the surrounding geometry, how the viscosities affect the flow pattern and how the two phases interact with each other.

When pumping multi-phase flow the drag of the bubbles rise with the viscosity of the liquid phase. An increase in the viscosity is expected to work against phase separation. Gulich [ 2 ] found that by increasing viscosity from 10 and 18  $mm^2/s$  performance actually improved at flow rates above best efficiency flow rate. Generally, increased viscosity reduces performance of single-phase pumps.

Viscous effects can be predicted through a multi-phase fluid viscosity. This viscosity is a combination of the fluid viscosity and the liquid viscosity. Rune Mode Ramberg [ 7 ] stated that this kind of approach causes a mal-interpretation of the viscous effects. Instead he introduced the apparent liquid viscosity correlations, which are based on Reynolds number correction's to turbulent flow in pipes. The semi-empirical model corrects for efficiency, head and flow rate.

$$\frac{1 - \eta_{SPL,a}}{1 - \eta_{SPL,M}} = \frac{0.3 + 0.7 \frac{\lambda_{SPL,a}}{\lambda_{\infty}}}{0.3 + 0.7 \frac{\lambda_{SPL,M}}{\lambda_{\infty}}} \quad \text{Eq. 4.33}$$

$$\frac{\psi_{SPL,a}}{\psi_{SPL,M}} = 0.5 + 0.5 \frac{\eta_{SPL,a}}{\eta_{SPL,M}} \quad \text{Eq. 4.34}$$

$$\frac{\varphi_{SPL,a}}{\varphi_{SPL,M}} = \sqrt{0.5 + 0.5 \frac{\eta_{SPL,a}}{\eta_{SPL,M}}} \quad \text{Eq. 4.35}$$

The idea is basically to correct for viscous effects before applying the two-phase multiplier. As a result, we only have to deal with viscosity of one phase. Another favourable aspect is that we are more likely to utilize the correct two-phase multiplier when performance already is corrected for viscosity.

Ramberg has verified the correlations against both single and multi-phase test results. He found them to give reasonable results for viscosities less than 90 cSt. For higher viscosities he found degradation of head and flow rate to be at some extent overestimated.

#### 4.5 Phase transition

When a multi-phase mixture is compressed, temperature and pressure increases. A change in gas mass fraction from stage inlet to outlet can occur as a result of some gas or liquid changing phase. Phase transitions are often neglected and the gas mass fraction is assumed constant from suction to discharge.

$$H = \beta \frac{Z_1 RT_1}{m \eta_{pol}} \left( \left( \frac{p_2}{p_1} \right)^m - 1 \right) + (1 - \beta) \frac{p_2 - p_1}{\rho_l \eta_{pol}} + (\beta_2 - \beta_1) \frac{h_g - h_l}{g} \psi \quad \text{Eq. 4.36}$$

If phase transition is to be included in predictions it can either be added directly in to the head equation as in the last section of Eq. 4.36, or the gas mass fractions can be corrected to fit the end state after stage outlet temperature and pressure is predicted. In both ways a process simulation tool such as HYSYS is needed to provide the thermodynamic data.

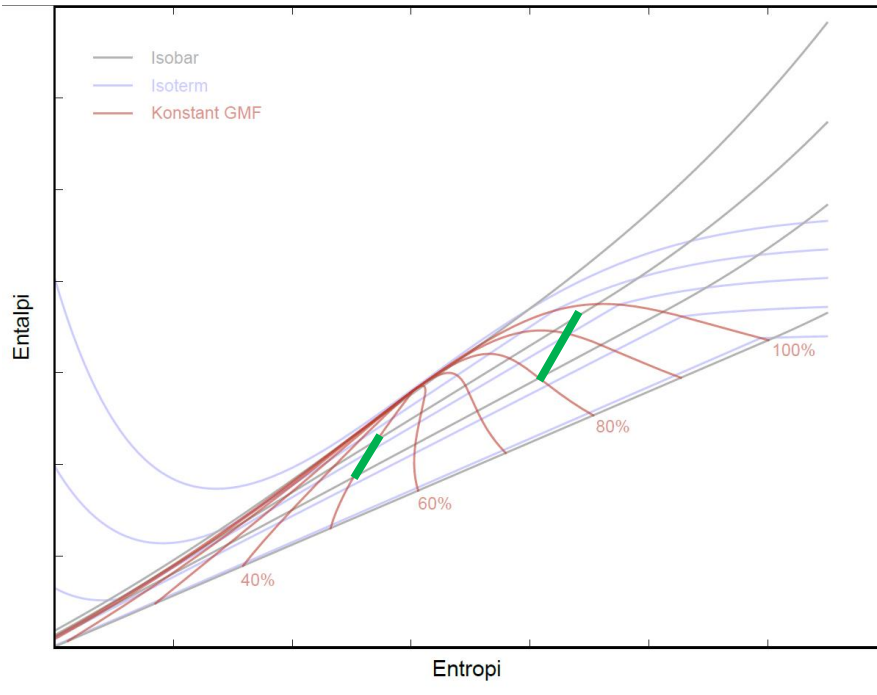


**Figure 8 Phase envelope of a typical hydrocarbon.**

From Figure 8 we can see that phase transition due to compression behaves different in different regions of the phase envelope. At 50% GMF the green compression path is close to parallel to the constant GMF line, while at 80% GMF it is almost perpendicular. Wet gas compressors operate in the higher GMF region, while multi-phase pumps operate in the lower GMF region. Phase transitions may therefore be less important for pumps than for compressors. A polytropic calculation method is a solution to the phase transition issue and will be discussed later in this thesis.





## 5 Temperature measurements

As seen in Chapter 4.3, the polytrophic compression model could be an improvement of the performance calculation routine. The polytrophic compression model requires test data containing temperature measurements. This chapter will highlight the importance of accurate temperature measurements and introduce different type of temperature sensors.

### 5.1 Accuracy

Discharge temperature measurements are usually not included in single-phase pump performance tests, as the compression is assumed isothermal. On the compressor side the ISO standard for performance tests states that a inaccuracy should be less than 1 K when it comes to temperature measurements [ 19 ]. For multi-phase flow an accuracy of 1 K is not accurate enough, as the temperature difference between impeller inlet and outlet is often just a couple degrees C. Two sensitivity analyses presented in the project thesis “MultiBooster Performance” [ 17 ], written by the author of this Master thesis will now be revisited.

The polytrophic efficiency is calculated, according to the method presented in Chapter 4.3.2. Figure 9 and Figure 10 shows the deviations of the polytrophic efficiency given in percentage points. The analysis is done on an example meant to represent a single stage in a Multi-phase pump. First sensitivity analysis is done with a temperature inaccuracy of 0.2K which is typical for the commonly used PT100 RTD temperature sensor. More details about RTDs and other sensors will follow later in this chapter.

Temperature measurement sensitivity analysis	
Medium	Air/Water
$\Delta P$	10 bar
$T_1$	25 °C
GVF	0-95 %
$\eta_p$	55-75 %
Temperature measurement uncertainty	0.2 °C and 0.002 °C

**Table 1 Temperature measurement sensitivity analysis**

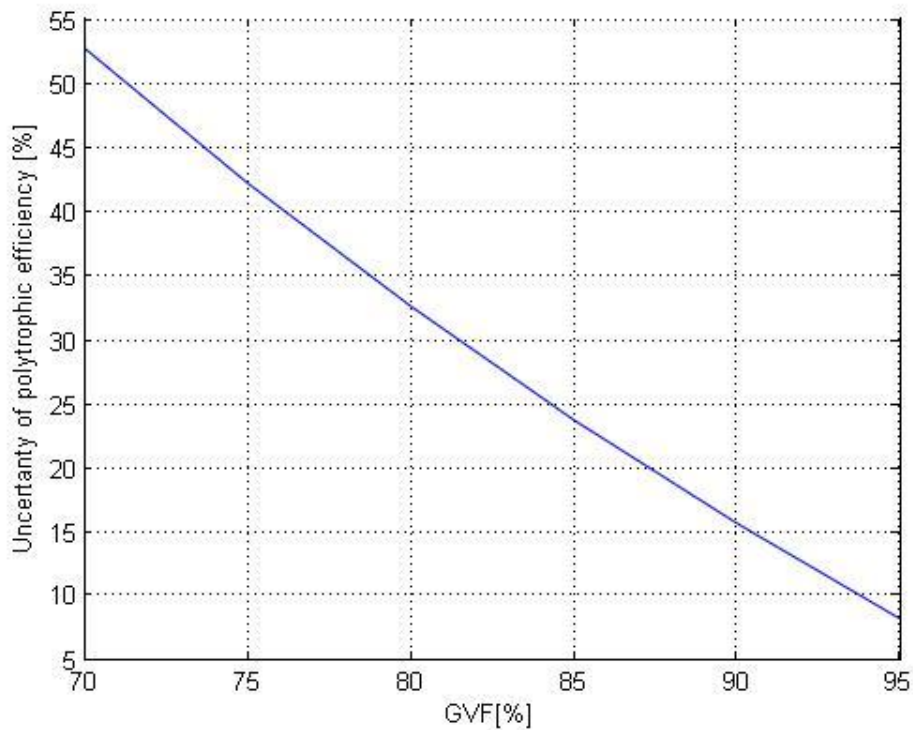


**Figure 9 Temperature sensitivity analysis, with an inaccuracy of 0.2 K.**

Figure 9 shows that 0.2 K is not accurate enough for single stage calculations. Even at 95% GVF the deviation exceed 8 percentage points. An uncertainty of this magnitude will cause inaccurate predictions of stage outlet temperature and pressure.

The hydropower industry uses temperature measurements in order to calculate efficiency of water turbines. These measurements have to be very precise, as the temperature increase is limited. By applying thermistors they can measure temperature with inaccuracy down to 0.002 K. A new sensitivity analysis is performed in order to see if a temperature inaccuracy of 0.002 K is sufficient when it comes to calculating the polytropic efficiency.

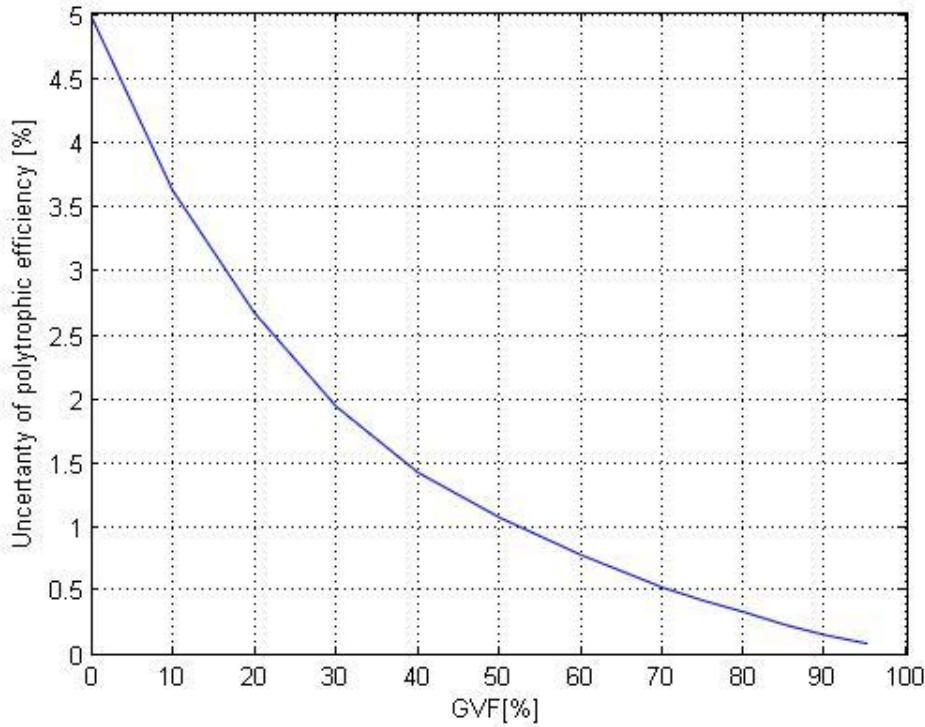


**Figure 10** Temperature sensitivity analysis, with an inaccuracy of 0.002 K.

Figure 10 shows that calculations of the polytrophic efficiency are significantly improved when the inaccuracy of the temperature measurements is reduced to 0.002 K. At GVFs above 60% it is less than 0.75 percentage points, which must be found acceptable.

## 5.2 Sensor technologies

Accurate temperature measurements are crucial when it comes to evaluating performance of multi-phase pumps. Temperature cannot be measured directly, instead we measure quantities that are temperature dependant. This chapter will describe and evaluate different types of temperature sensors that are relevant for measuring multi-phase flow.

### 5.2.1 Thermocouples

Thermocouples are the most versatile thermometer. They utilize the fact that when a homogenous conductor is heated locally it generates a voltage potential. The hot part becomes positively charged compared to the cold part, and the voltage measured between them is proportional to the temperature difference and the Seebeck coefficient of the conductor.

$$E = C_1(T_1 - T_2) - C_2(T_1^2 - T_2^2) \quad \text{Eq. 5.1}$$

When two conductors made of different materials are connected together and exposed to different temperatures, a voltage potential between the two junctions can be measured. The measured voltage depends on the temperature difference and the Seebeck coefficients of the two conductors. Eq. 5.1 shows the relation between the measured voltage  $E$ , the Seebeck coefficients  $C$  and the temperature difference.

The relation between the Seebeck coefficients and the temperature is none linear. In order to generate accurate measurements the temperature of the reference junction could be held constant. Another more commonly used method is to utilize hardware or software based cold junction compensation. Cold junction compensation reduces the generated voltage to a voltage that corresponds with the reference temperature.

Thermocouples can measure over a large temperature span, and if the hot junction is sufficiently small they can respond quickly to changes in temperature. The main limitation is their accuracy.

### 5.2.2 Resistance temperature detectors (RTD)

Resistance temperature detectors (RTDs) are more accurate thermometers. They measure the resistance of a conductor. The resistance of a conductor depends on temperature and on the material. The relation between temperature and resistance can be expressed by Eq. 5.2. The number of joints required in the equation, depends on the wanted accuracy and temperature span.

$$R = R_0(1 + \alpha_1 T + \alpha_2 T^2 + \dots + \alpha_n T^n) \quad \text{Eq. 5.2}$$

Resistance is measured by subjecting the conductor to a current. As the current heats the conductor, the temperature rises above the surrounding temperature, and the measurements becomes inaccurate. To reduce this effect, a larger conducting element could be chosen. Although this reduces the temperature gradient, it generates another limitation. The extra mass increases the response time of the detector, which is an important parameter when it comes to measuring multi-phase flow. The final selection of conductor will have to be a trade-off between response time and accuracy. Either way it is important to keep the measuring current low.

Typically RTDs are made from Platinum or Nickel. Platinum has a wide temperature span and good linearity. Nickel is the cheapest option, but its temperature span is limited.

### 5.2.3 Thermistors

Thermistors are made from semiconducting material, and the most sensitive thermometers considered in this thesis. They are temperature resistance devices based on the same principle as the RTD's. Unlike RTD's most thermistors have a negative temperature coefficient (NTC), it means that the resistance decreases as the temperature rises. Eq. 5.3 shows the relation between temperature and the measured resistance of a semiconductor and is called the Stein-Hart equation.

$$\frac{1}{T} = A + B \ln(R) + C (\ln(R))^3 \quad \text{Eq. 5.3}$$

Thermistors are usually made from oxides, but silicates and sulfides are also used.

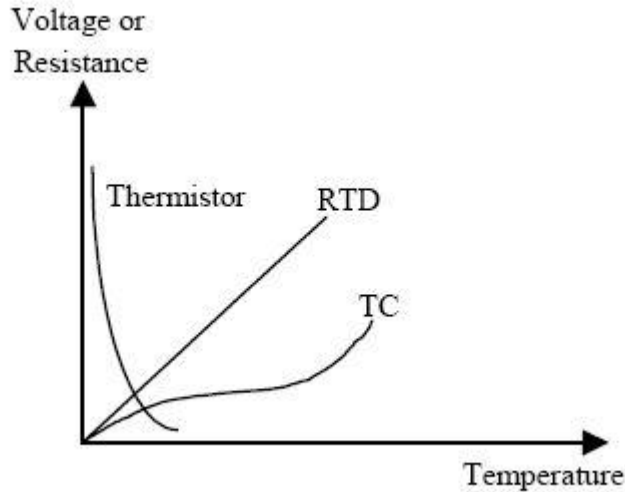


**Figure 11 Comparison of RTDs, NTC thermistors and Thermo couples.**

#### 5.2.4 Pyrometers

A pyrometer has the benefit of being able to measure temperatures without being in actual contact of the medium it is measuring. Pyrometers measure the radiation emitted from a body. The power and wave length distribution is analyzed in order to calculate the temperature of the body. Instruments like infrared thermometers, optical pyrometers and temperature radiation meters are all based on this principle.

$$E_{b\lambda} = \frac{C_1 \lambda_w^{-5}}{e^{C_2/\lambda T} - 1} \quad \text{Eq. 5.4}$$

Pyrometers are limited by the fact that they are unable to measure temperature of gasses. Another limitation is the uncertainties involved with deciding the emissivity of the body that is being measured. The emissivity depends on substance, size, shape and roughness of the body.

### 5.3 Two-phase temperature measurements

When a gas is compressed the temperature rises. Heat transfer between the phases will cause a temperature rise in both phases. This means that the total temperature increase is less for two-phase flow than for pure gas. This sub chapter will discuss some of the challenges related to measuring temperature in multi-phase flow.

First of all GVF affects the temperature increase. For single-phase pumps pressure increase is the main concern. On the compressor side the temperature increase is highly significant. For multi-phase pumps operating on gas/liquid mixtures, temperature measurements need to be very accurate, as the temperature increase is limited by the liquid content.

There is some uncertainty related to kinetics involved with heat exchange between the gas and liquid phases. If the gas is heated rapidly, a temperature difference might develop between the phases. If the phases are not in thermal equilibrium, the local phase temperatures need to be measured separately. It is also important to know which of the two phases that is actually being measured.

For liquid dominated flow, HZDR-innovation provides a thermo-needle-probe system which is designed to do local phase temperature measurements for multi-phase flow [ 27 ]. The probe combines temperature measurements and conductivity measurements. The temperature sensor consists of a small thermocouple which responds fast enough to measure temperatures of passing gas bobbles. The conductivity tells us which phase the needle is subjected to. If the conductivity is zero for a longer time than the response time of the thermocouple, the probe is measuring the gas temperature. Figure 12 shows the measured temperature and conductivity of a passing bobble.

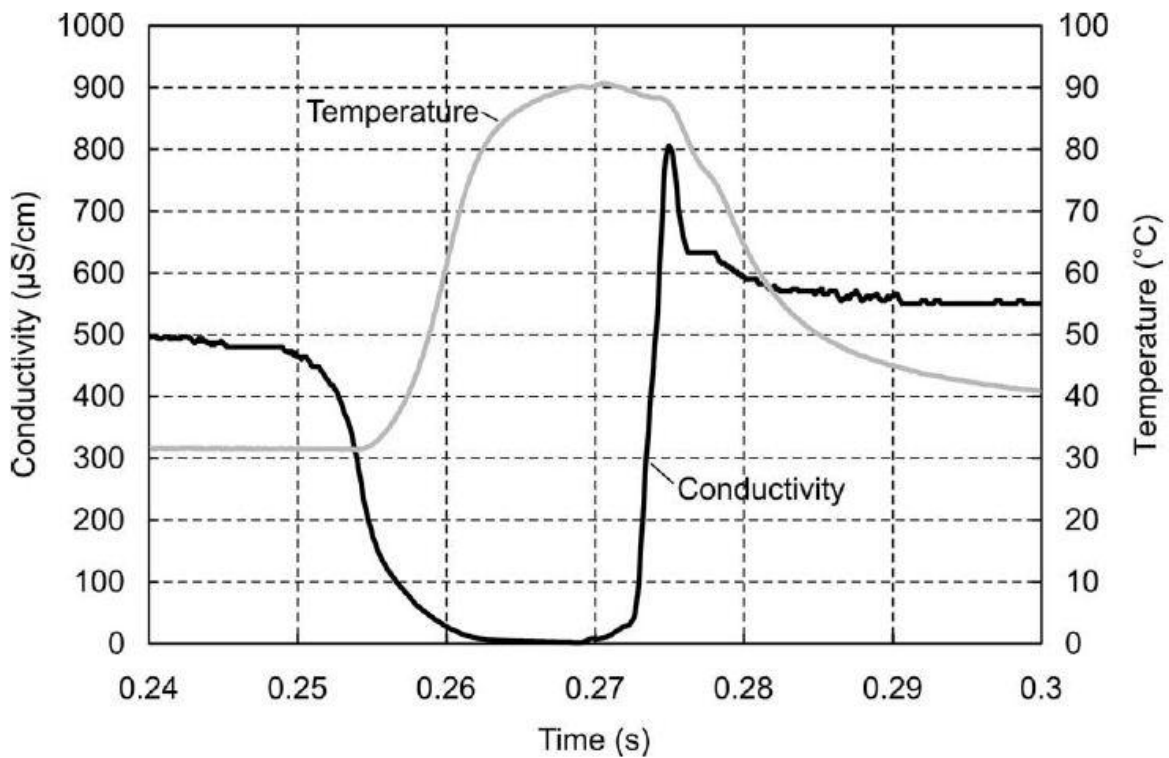


Figure 12 Temperature and conductivity measurement of a passing bobble [ 27 ].

For gas dominated flow the combined temperature conductivity sensor only work as a standard temperature sensor. The conductivity which is measured between the probe tip and ground potential will be zero both when the probe tip is subjected to gas and when it is covered by a liquid droplet. Ground potential is often the pipe wall, and unless there exists continues liquid between it and the probe tip, no conductivity will be measured.

Due to the nature of gas dominated flow the heat exchange between the phases is slower than for liquid dominated flow. The heat capacity of the liquid droplets is high and the surface area is small, therefore it is more likely that a temperature difference will occur in gas dominated flow.

Another problem related to temperature measurements in gas dominated flow is the formation of liquid films on all surfaces including the sensors. If the probes are covered with liquid, they will simply measure the liquid temperature, and it will be impossible to decide the actual enthalpy of the mixture.

At last but not least it is worth mentioning that the sensitivity analysis presented early in this chapter was based upon the assumption that thermal equilibrium existed at the measuring point. When measuring local phase temperature in none equilibrium mixtures, the gas temperature measurements does not have to be as accurate as the liquid temperature measurements. It is because a given change in gas temperature will have less effect on the enthalpy than the same change in liquid temperature.





## 6 Laboratory rig

The goal of this chapter is to plan a test rig that can validate different temperature sensors ability to give accurate measurements of multi-phase flow. Main focus will be appointed to conditions where thermal equilibrium is not met.

A polytrophic compression model can improve performance predictions of multi-phase pumps. Unlike the isothermal model they require temperature measurements. These measurements will have to be taken stage-by-stage, in locations where the phases might not be in thermal equilibrium. Temperature measurements will have to be measured locally in each phase. Although the industry seems to assume thermal equilibrium, no documentation has so far been found on this topic.

For multi-phase pumps, the temperature increase is limited, especially when it comes to stage-by-stage and low GVF calculations. As explained earlier, the limited temperature is caused by the high heat capacity per unit volume of the liquid compared to the heat capacity per unit volume of the gas. Temperature measurements will therefore have to be highly accurate. The test rig shall generate conditions where the two-phase mixture is not in thermal equilibrium. And the temperature sensors will be evaluated by their ability to do accurate local temperature measurements.

Validating temperature sensors ability to measure multi-phase flow is difficult because no available sensor can tell us the exact temperature of the phases. The idea behind the test rig is to measure the local gas phase temperature in a location where the actual temperature can be calculated from other measured values. Measurements used for the calculations are:

- Single-phase liquid temperature and pressure before mixing.
- Single-phase gas temperature and pressure before mixing.
- Local liquid Temperature after mixing.
- Pressure after mixing.

The local liquid temperature is easier to measure compared to the local gas temperature, as it can be measured in the liquid film near the pipe wall.

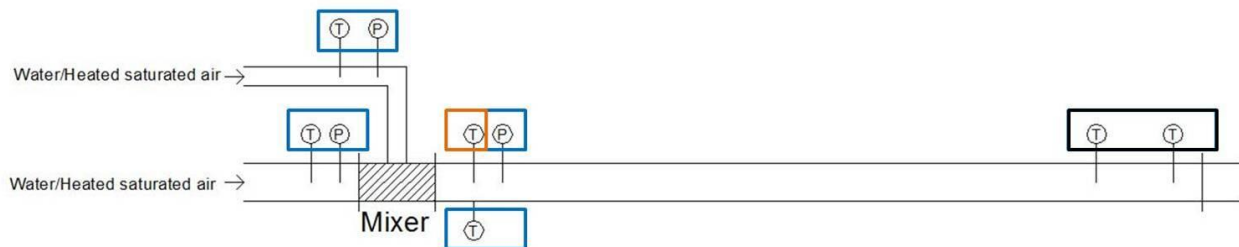


Figure 13 Simple drawing of the test rig.

The orange square in Figure 13 is the local gas phase measurement. The measured gas temperature will be validated against the calculated gas temperature. Blue squares indicate inputs to the calculations. The black square downstream indicates two temperature measurements that will measure the equilibrium temperature.

Test procedure, conditions, equipment and different challenges involved with planning the test rig will be presented in the following subchapters. Data sheets related to the suggested components can be found in Appendix B.

Most of the simulations in this chapter are done in HYSYS. HYSYS is a process modeling system that allows us to choose different equations of state, fluid compositions and process components. Hunseid [ 21 ] found GERG to be the best equation of state for predicting outlet conditions of a wet gas compressor. GERG is not implemented in the student version of HYSYS, Peng Robinson is therefore used in the following simulations. In the work of Hunseid, Peng Robinson was found to be the second best equation of state for predicting outlet conditions.

## 6.1 Conditions and setup

The test rig will be constructed so that sensors can be tested on the whole multi-phase pump GVF range (0-90%GVF). Figure 13 show how two single-phase streams are brought together to form a two-phase homogeneous mixture in a flow conditioner device (mixer). The single-phase streams will be water at ambient temperature and heated saturated air. Which stream is entering in which pipe depends on the mixer. Two different mixers will be applied, depending which phase is dominating the flow. In the mixer generating liquid dominated flow, a perforated tube will be fitted to feed bobbles into the liquid stream. In the mixer generating gas dominated flow, nozzles will be applied to distribute droplets in the gas.

The total flow rate in the test section (downstream of the mixer) will be kept constant at 200 m<sup>3</sup>/h, by adjusting the liquid and gas flow rate.

GVF [%]	90	80	70	60	50	40	30	20	10	0
QL [m <sup>3</sup> /h]	20	40	60	80	100	120	140	160	180	200
QG [m <sup>3</sup> /h]	180	160	140	120	100	80	60	40	20	0

**Table 2 Fluid conditions 2**

The tests are limited by the fact that they are not done on hydrocarbons. And that the pressure, density ratio, heat capacity ratio, droplet sizes, bobble sizes and heat exchange between the phases might differ from the actual operating condition. However it is important to be aware that prototypes usually are tested on air/water mixtures with density ratios and pressures different from

actual operating conditions, and that the performance of the pump often is predicted from air/water test results. Being able to do local phase temperature measurements of air/water mixtures is therefore important in a research and developing point of view as well as a step into doing local phase measurements in the field.

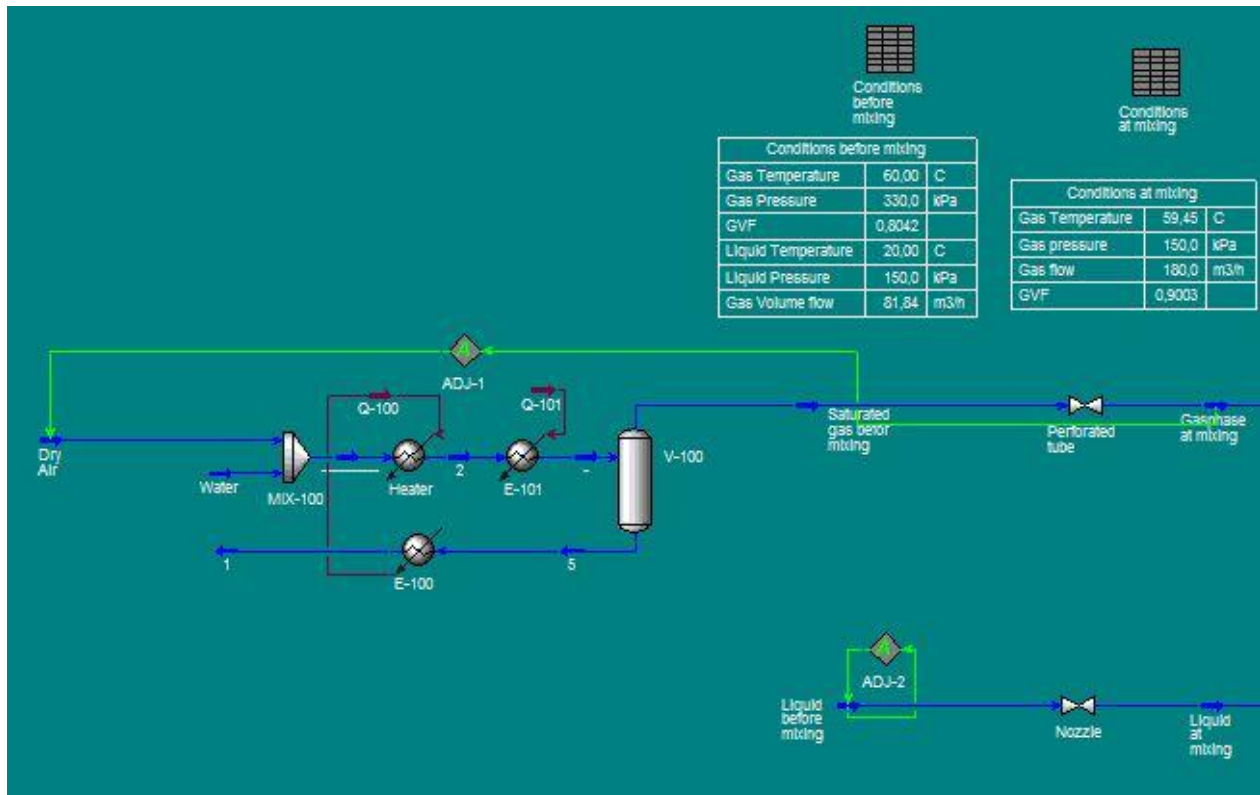


**Figure 14 Heater and saturator simulations.**

In order to generate a temperature difference between the phases, the gas enters the mixer fully saturated and heated to 60 degree C. Liquid enters with an ambient temperature. The reason for saturating the air will be explained later.

Figure 14 shows how the heater and saturator is simulated in HYSYS. The heater must be able to deliver at least 10.58 kW of heat, to maintain a gas temperature of 60 degree C at a GVF of 90%. The saturator must be able to feed at least 10.8 kg/h of water to saturate gas.

## 6.2 Engineering

This subchapter will go through the challenges and solutions related to the engineering of the test rig, by taking a closer look at the following subjects.

- Temperature measurements
- Test section

- Gas phase humidity
- Gas volume fraction
- Mixers

### 6.2.1 Temperature measurements

When it comes to choosing temperature sensors, it is all about deciding what you need the measurements for. As seen in chapter 5 thermistors provide the most accurate measurements, but do not respond quickly to changes in temperature. They are also limited to a relatively narrow temperature span. RTDs can also be quite accurate but have the same limitations when it comes to response time. They are preferred by the industry in stationary flow, and can be useful in thermal equilibrium conditions when accuracy is important.

RTDs and thermistors can also be used to decide whether or not the phases are in thermal equilibrium. Framo Engineering used this approach when they tested their wet gas compressor. Four temperature measurements were done downstream of the compressor discharge. The distances between the probes were 2 meters. The idea was that Thermal equilibrium was reached when two or more probes showed the same value. They experienced that thermal equilibrium was reached already at the discharge, as all four sensors showed the same value within the given uncertainty of the probes. Note that the tests were done at 95% GVF and above.

In conditions where thermal equilibrium is absent, temperature sensors will be exposed to rapid changes in temperature, as bobbles or droplets hit the probe tip. There are two obvious ways of measuring local phase temperature:

- Applying a sensor which responds quick enough, to measure the temperature of a passing bobble or a droplet.
- Make sure the sensor is only subjected to one of the phases.

The thermo needle probe system delivered by HZDR utilizes the first measurement principle. They can do local temperature measurements, and have been tested on liquid dominated flow with a velocity up to 20m/s. They consist of fast responding small thermocouple junctions. The probes can also do conductivity measurements. From here on the combined temperature and conductivity probes will be referred to as CTC-probes. Contact has been established, and an official offer on a 5 customized sensors including cables and software has been received from HZDR. The offer can be found in Appendix A.

The alternative measurement principle suggests that a more accurate, but slower sensor is subjected to only one of the two phases. Two different approaches subjecting a PT100 sensor to only the gas phase will be presented in the next subchapter. Also the liquid phase temperature will be measured using this principle, by positioning a sensor in the liquid film at the bottom of the pipe.

Table 3 shows some data on the sensors chosen for this assignment. More can be found in the data sheets in Appendix B. Details concerning the mounting of the sensors will follow in the next subchapter.

Name:	Type:	Accuracy:	Response time
CTC	Thermocouple	0.7 °C	20 ms
PT100	RTD	0.164 °C	200 ms
SBE38	Thermistor	0.001 °C	500 ms

**Table 3 Temperature sensor data**

The total enthalpy of the two-phase mixture is highly sensitive to the liquid temperature and not so sensitive to the gas temperature. This means that for HYSYS to calculate the gas temperature from the liquid temperature, it needs the liquid temperature measurements to be very accurate.

GVF [%]	$T_L$ [°C]	$T_G$ [°C]	$\Delta T_L$ [°C]	$\Delta T_G$ [°C]
89.58	20.13	39.94	0.001	0.06

**Table 4 Sensitivity of liquid temperature measurements on gas temperature calculations.**

A sensitivity analysis displayed in Table 4, shows how an uncertainty in the liquid temperature measurements affects the uncertainty of the calculated gas temperature. Under the given conditions, an uncertainty of 0.001 °C in the measured liquid temperature generates an uncertainty in the calculated gas temperature of 0.06 [°C]. From table 3 we read that the SBE38 thermistor will be accurate enough to measure the liquid temperature, when the goal is to validate gas temperature measurements taken with the CTC and the RTD100.

### 6.2.2 Test section

The test section is defined as the pipe work downstream of the mixer. A pressure sensor and two temperature sensors measuring the gas and liquid phase temperatures are positioned right after the mixer. Two temperature sensors are also positioned further downstream. Their job is to capture the equilibrium temperature.

In order to determine the flow regime and view how the sensors are affected by the stream, the flow will be monitored visually through Plexiglas pipes. The chosen Plexiglas pipes are casted, have a wall thickness of 10 mm, can withstand a service temperatures of up to 80°C and pressures well above test conditions. More detailed information can be found in the Plexiglas data sheet in Appendix B.

The flow regime in the test section should be as close to the actual discharge conditions of a multi-phase pump as possible. A pipe diameter of 100 mm combined with a volumetric flow rate of 200 m<sup>3</sup>/h, generates a fluid velocity of approximately 7m/s, which is a velocity that could also be found in an actual application. Table 5 shows data related to the flow conditions.

Q [m <sup>3</sup> /h]	r [m]	A [m <sup>2</sup> ]	v [m/s]
200	0.05	0.00785	7.08

**Table 5 Fluid conditions**

Three different gas phase temperature measuring concepts will now be presented. First up is the CTC-probe which measures both temperature and conductivity. Note that the pressure sensor is not included in the concept drawings.

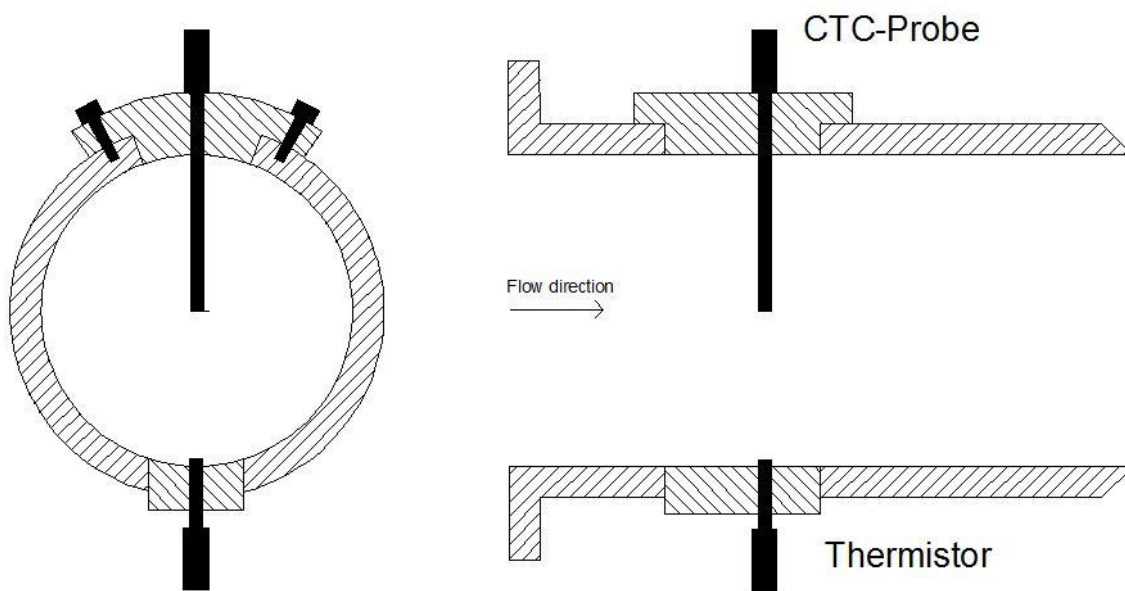


**Figure 15 Concept number one - CTC probe setup.**

The fact that conductivity measurements do not work in gas dominated flow, makes the CTC-concept most promising in liquid dominated flow. The CTCs fast response time of 20 ms might allow measurements also in gas dominated flow. But without the conductivity functionality, an important validation tool is lost. A SBE38 thermistor is positioned in the bottom of the pipe, to measure the liquid temperature.

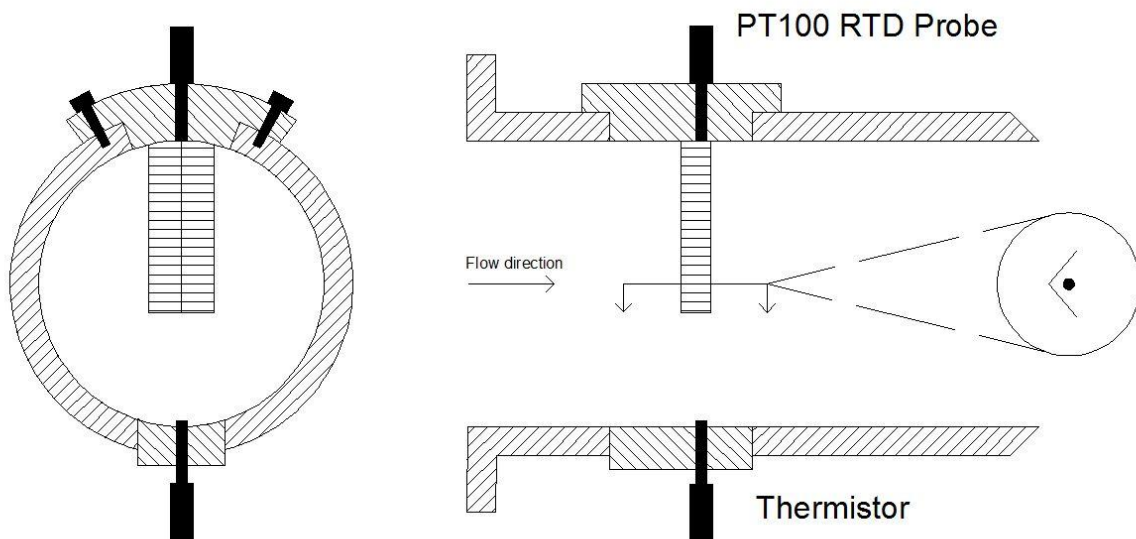


**Figure 16 Concept number two - PT100 RTD shield setup.**

Concept number two is in the first place intended for gas dominated flow. It utilizes a RTD probe protected by a shield. The idea is that the liquid will be guided around the probe. And as the probe is not in contact with the shield it will not be affected by the cooling of the liquid. The drawback of this concept is that gas behind the shield might not be replaced fast enough. If so, the gas will be cooled by the liquid hitting the shield, which will affect the measurements. As for the CTC-concept this concept also uses a thermistor to measure the liquid temperature in the bottom of the pipe. The circle to the right in Figure 16 shows how the probe is hidden behind the shield.

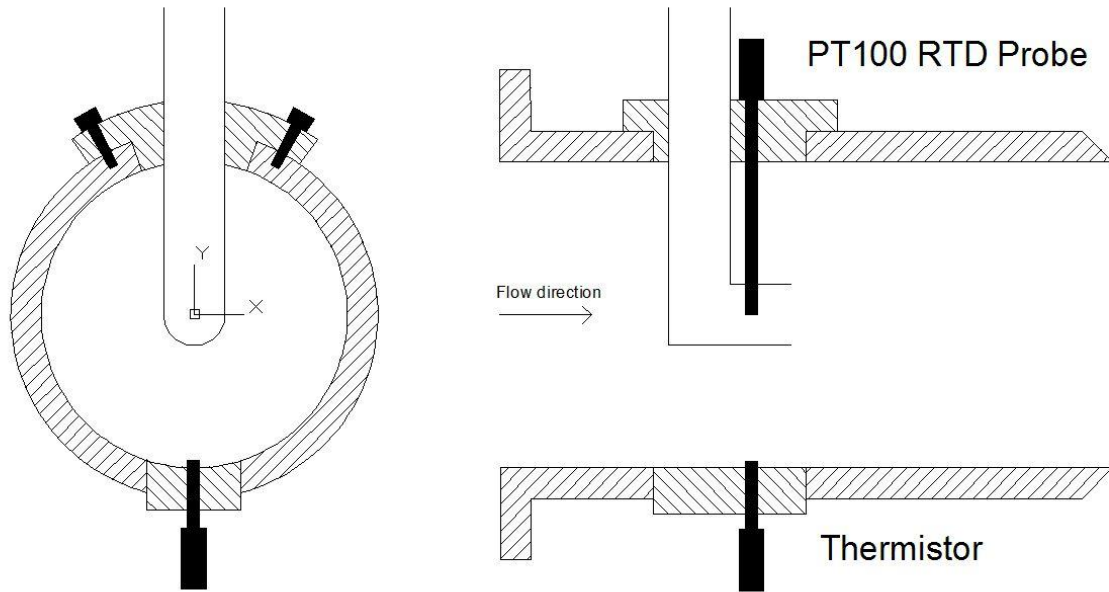


**Figure 17 Concept number three - PT100 Gas suction setup.**

Concept number three is a further development of concept two. It is also intended for gas dominated flow. The idea is to shield the probe from the liquid and at same time replace the gas surrounding the probe. This way temperature will not be affected by the cold shield. Some gas will be sucked out through the pipe shielding the sensor. It is important that the suction is slow, so that it doesn't bring with it any liquid. The drawback with this solution is that it will affect the equilibrium condition measured by the downstream temperature sensors, as some of the gas is extracted from the stream. Also this concept utilizes a thermistor positioned in the bottom of the pipe to measure the liquid temperature. See Figure 17 for illustration.

Two types of connection points will be used to mount sensors to the Plexiglas pipe, one for the gas phase temperature measurements and one for all the other sensors. The first type is designed so that the different gas temperature concepts can be mounted and remounted in different axial locations of the test section. Why it is so important to be able to move the sensors will be explained later. The second type will be fabricated from Plexiglas rods and welded onto drilled holes in the Plexiglas pipe. For illustration, see how the sensors are connected in Figure 17.

Thermal equilibrium will be absent at the moment of mixing, and the goal is to do local temperature measurements of both phases before equilibrium is reached. No documentation on the heat transfer between the phases has been found. Focus on multi-phase heat transfer seems to have been on calculating the heat transfer between the mixture and the surroundings, and not the heat transfer between the phases. It is therefore difficult to estimate how far the liquid needs to travel down the pipe in order to reach thermal equilibrium. The length of the test section will have to be decided by a calculated guess. The suggestion is at least 3m. During tests the equilibrium temper-



ature can be found by slowly moving the two SBE 38 sensors, positioned with some axial distance, further downstream. The thermal equilibrium is reached at the first sensor when both of them measure the same value.

The downstream SBE38 sensors will be used to confirm or disprove the measurements in cases where the local phase temperature sensors do not find a temperature difference between the phases. If all temperature sensors in the test section measures the same temperature, it means that thermal equilibrium is met already upstream of the local temperature measurements. In that case, if possible, the local temperature measurements should be moved closer to the mixer.

Uncertainty related to the humidity of the gas, generates a lower boundary on how close to the mixer the gas measurement can be done. This limitation will be further explained in the next chapter. Because the position of the sensors is crucial, and that the best position will change with the conditions, the pipe section will be fitted with as many connection points as possible.

Summary of the needs for measuring instruments in the test section:

- One of the concepts above (CTC or RTD) measuring the local gas phase temperature in the centre of the flow right after mixing.
- One SBE38 sensor measuring the liquid temperature at the bottom of the pipe right after mixing.
- Two SBE38 sensors measuring the Temperature of the mixture when thermal equilibrium is reached in a downstream section of the pipe.
- One pressure sensor positioned as close to the local gas phase measurement as possible.

### 6.2.3 Gas phase humidity

When non saturated air is mixed with water it starts a saturation process. This process requires heat and causes the temperature of the mixture to drop. It will continue until the air is fully saturated. An example has been run in HYSYS to demonstrate how the saturation affects the temperature, when single-phase liquid and gas with the same temperature is mixed.

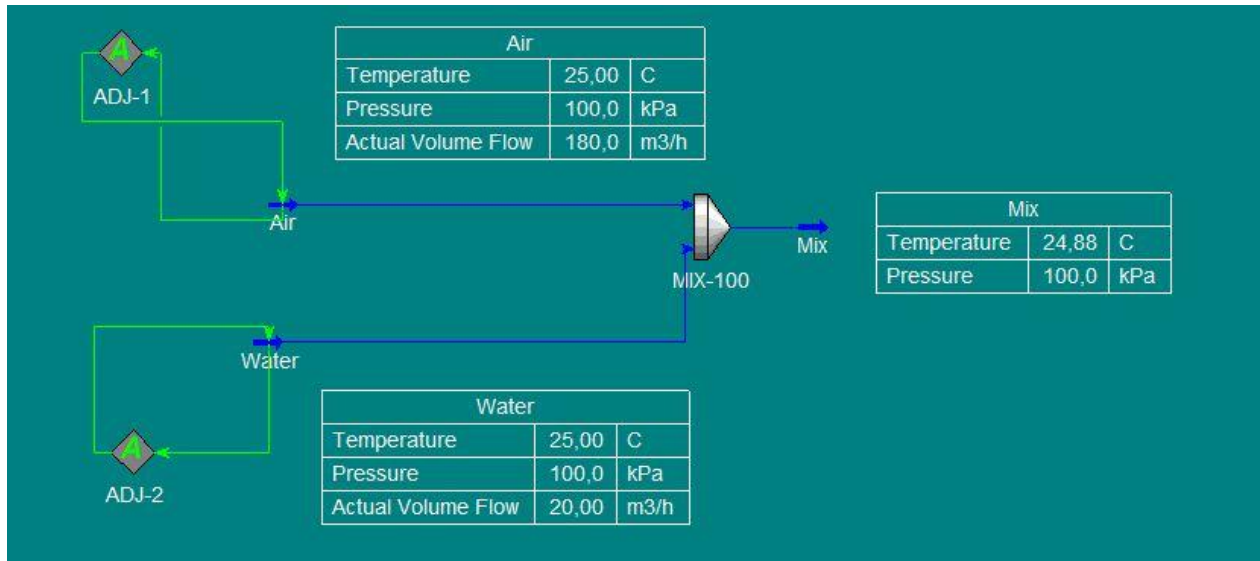


**Figure 18 Saturation example**

Figure 18 shows the mixing process. Dry air and water are mixed together to form a two-phase flow at 90% GVF. Even though both air and water enters the mixer at 25°C, the saturation causes the temperature to drop 0.12°C. Note that the cooling effect of saturation is decreasing with decreasing GVF. At 60% GVF the temperature drop was only 0.02°C

When dry air and water is mixed in test rig we cannot calculate the gas phase temperature from the liquid phase temperature if we do not know the humidity of the gas. The solution is to saturate the gas before mixing.

If the temperature of a fully saturated gas is reduced it condenses some liquid, but remains fully saturated. For gas dominated flow leaving the mixer, we know that the gas phase is gradually cooled by the liquid phase. It is therefore reasonable to assume that the gas phase is fully saturated through out the test section.

For liquid dominated flow the gas is throttled into the liquid trough a perforated tube, and is no longer fully saturated. But if the pressure drop is kept small enough, the gas will reach fully saturation at some point before it reaches thermal equilibrium. “The fully saturation temperature” can be calculated in a HYSYS simulation which will be presented and explained in chapter 6.3.

A humidity, temperature and pressure sensor will be placed in the gas stream right before mixing, in order to make sure that the gas is fully saturated.

#### 6.2.4 Gas volume fraction

Standard single-phase flow meters will be positioned in the single-phase gas and liquid streams as the last instruments before the mixer. Data from the flow meters will be used to calculate the GVF. It is important to notice that liquid contained in the saturated gas starts to condense when the temperature drops due to heat exchange with the liquid phase. The GVF has therefore changed between the flow meters and the point of the local phase temperature measurements. An example has been performed in HYSYS to show how the condensation of water affects the GVF.

	$T_g$ [°C]	$T_l$ [°C]	GVF [%]	P [kPa]
Before mixing	60	25	90	100
At local phase measurement	40	25.5	87.96	100

**Table 6 Effect of condensation on GVF**

Table 6 shows that the GVF needs to be recalculated at the local phase temperature measurement point. Note that for liquid dominated flow the GVF will change even more, as the gas is expanding through the perforated tube.

#### 6.2.5 Generating liquid dominated flow

To be able to evaluate the temperature sensors ability to measure local phase temperatures in actual pump applications, sensors must be exposed to a relevant flow regime in the test rig. Two different mixers will be applied, one for generating annular droplet flow (gas dominated flow) and one for generating bobble flow (liquid dominated flow). First up is the liquid dominated flow mixer.

For generating liquid dominated flow the first idea was to use a flow homogenizer to transform stratified flow into bobble flow. But since the gas will be in contact with the liquid for a substantial amount of time, it is a concern that the phases will be in thermal equilibrium before local temperature measurements can be performed. The solution is to apply a perforated tube instead. It will be used to distribute air bobbles into the water stream.

The perforated tube will be customized to fit this project, and fabricated after the following specifications:

Tube diameter	20mm
Hole diameter	5mm
Number of holes	25

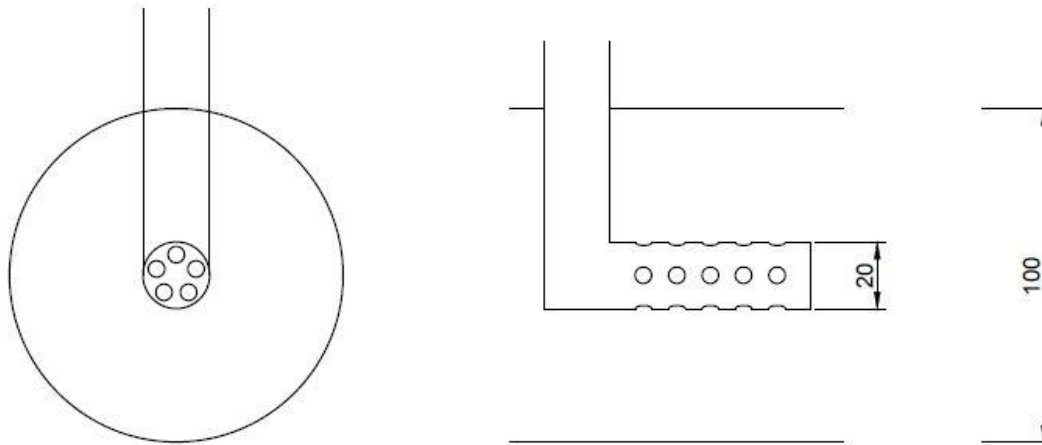


**Figure 19 Perforated tube in mixer.**

When digging in to the challenges related to knowing the exact humidity of the gas phase, it was found that the differential pressure across the perforated tube was too high. Because of the expansion, the gas would simply not be saturated again before the mixture had reached thermal equilibrium. This would leave us without a possible zone along the test pipe where measurements could be validated. The number of holes in the perforated tube was therefore increased to reduce the differential pressure.

The number of holes was chosen to 25, which at a differential pressure of 217 kPa generates a gas flow rate of 140 m<sup>3</sup>/h (70% GVF). Fully saturation occurs when the gas is cooled to 42.2 °C, while the thermal equilibrium occurs at 20.09 °C. This means that if the gas temperature is measured between 42.2 °C and 20.09 °C we know that the gas is fully saturated, that the phases are not in thermal equilibrium and that the measurements can be validated. For a lower GVF-value the fully saturation temperature increases and the equilibrium temperature decreases. This means that the zone of possible validation increases.

Type:	Tube diameter = 20mm, Hole diameter=5mm and Number of holes =25.							
GVF [%]	70	60	50	40	30	20	10	0
$Q_{g1}$ [m <sup>3</sup> /h]	44.3	42,7	41.0	38,5	34,7	28,6	17,7	0
$Q_{g2}$ [m <sup>3</sup> /h]	140	120	100	80	60	40	20	0
dp [kPa]	217	179	144	108	73	40	12	0

**Table 7 Perforated tube Flow rate/Pressure calculations**

Table 7 shows the differential pressure ( $dp$ ) needed to get the correct gas flow rate. It also shows the gas flow rate in ( $Q_{g1}$ ) and out ( $Q_{g2}$ ) of the mixer. Because there is some uncertainty related to when the flow will transform from liquid to gas domination, a differential pressure of more than 217 kPa should be available. The same holds for differential pressure across the nozzles in the next chapter.

### 6.2.6 Generating gas dominated flow

One or more nozzles will distribute water droplets into the mixer in order to generate a gas dominated flow. The nozzle is chosen so that it provides the correct GVF range at the available liquid pressure range. The droplet sizes can be reduced by increasing the number of nozzles. Two different options have been assessed.

The first option is to use a single nozzle in the centre of the stream. It can easily be operated by adjusting the inlet pressure. One of the disadvantages is that the nozzle must be chosen so that it can handle the whole range of GVFs from 50-90%. This means that it either will need a very high differential pressure to manage 50% GVF, or that it due to the low differential pressure will have problems distributing the droplets at 90% GVF. Positioned in the centre of the pipe it will also have substantial impact on the flow conditions.

Type:	BETE NF 2250 303 Stainless steel				
GVF [%]	90	80	70	60	50
QL [m <sup>3</sup> /h]	20	40	60	80	100
Number of Nozzles	1	1	1	1	1
Dp [bar]	0.4	1.7	3.8	6.8	10.6
Droplet sizes [ $\mu$ m]	22987	1949	1537	1289	1129

**Table 8 Nozzle GVF calculations option 1**

The second option applies two to ten smaller nozzles to generate different flow rates. This way, the GVF range can be achieved while the differential pressure is kept moderate simply by varying the amount of nozzles. A disadvantage is that it is more complicated to operate ten nozzles than one.

Type:	BETE NF 400 303 Stainless steel				
GVF [%]	90	80	70	60	50
QL [m <sup>3</sup> /h]	20	40	60	80	100
Number of Nozzles	2	4	6	8	10
Dp [bar]	3.3	3.3	3.3	3.3	3.3
Droplet sizes [μm]	797	797	797	797	797

**Table 9 Nozzle GVF calculations option 2**

The single nozzle option will affect the flow more than a set of nozzles located near the pipe wall. The combination of good positioning possibilities and constant differential pressure makes the multiple nozzles option the best solution.

Figure 20 shows how the nozzles will be mounted to the pipe. The expansion of the pipe walls at the nozzle mounting has three advantages:

- Creates more space for mounting of the nozzles.
- Less impact of the nozzles on the stream.
- Droplets are sprayed in the flow direction.

The left drawing shows a cross-sectional view of the mixing device, while the right drawing shows an axial view. The idea of the mounting is taken from a visual inspection of the wet gas compressor rig at NTNU.

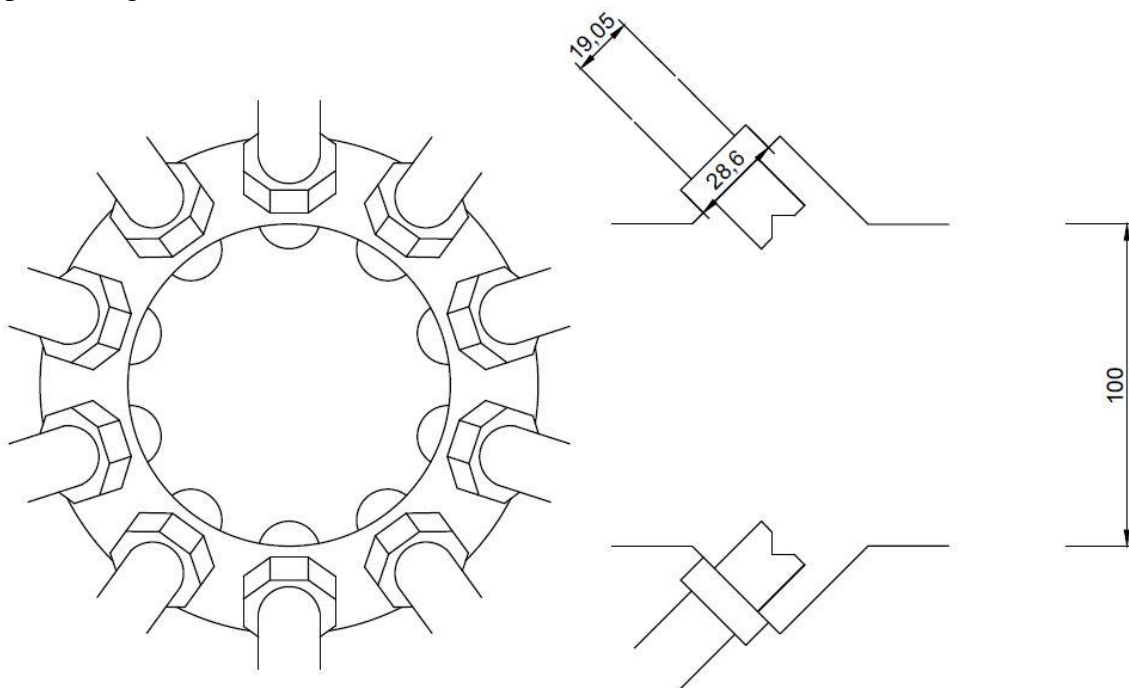


**Figure 20 Nozzle mounting.**

A large droplet contains more heat per unit surface than a smaller droplet, and it therefore requires more time to reach the equilibrium temperature. The size and size distribution of the droplets are expected to have an influence on the functionality of the sensors. Unfortunately no documentation on typical droplet sizes for multi-phase pumps or wet gas compressors have been found. The calculated droplet sizes are displayed in Table 8 and Table 9.

### 6.3 Test procedure

This subchapter presents a complete test procedure that should be followed during tests. A simulation environment in HYSYS representing the test rig will be used as a tool in the validation. A screenshot of the simulation environment is displayed in Figure 21. For a better view, look to the enlarged version of Figure 21 in Appendix D.

Values that will be measured during the tests are shown in the list below. They will be referred to with their list reference in the rest of this subchapter. For example will the volumetric flow rate of liquid before mixture be referred to as 2c. The measurement points can also be found in the HYSYS simulation environment.

1. Saturated gas before mixing
  - a. Temperature
  - b. Pressure
  - c. Volumetric flow rate
  - d. Humidity
2. Liquid before mixing
  - a. Temperature
  - b. Pressure
  - c. Volumetric flow rate
3. Two-phase flow after mixing, but before thermal equilibrium
  - a. Gas Temperature
  - b. Liquid Temperature
  - c. Pressure
4. Two-phase flow equilibrium temperature 1
5. Two-phase flow equilibrium temperature 2

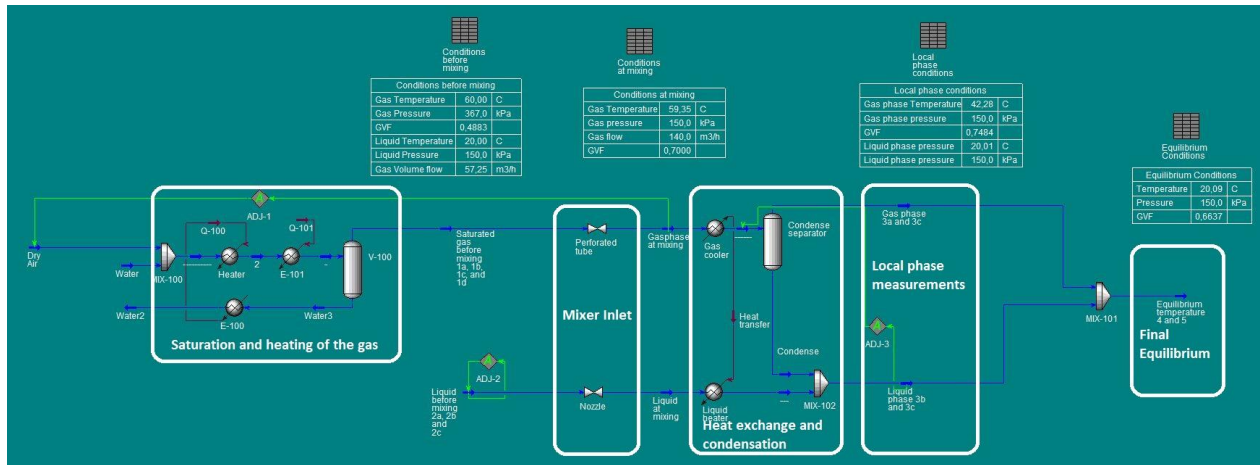


Figure 21 HYSYS test procedure simulations

### Test procedure:

- First task is to generate inlet conditions that correspond to one of the GVFs in Table 2. Liquid and gas flow rates is set according to Table 7 and Table 9 by adjusting the inlet pressures. The Gas should be fully saturated and preheated to 60°C, while the liquid enters with the ambient temperature. When all measurements of point 1 and 2 are done, they will be entered into the HYSYS simulation displayed in Figure 21.
- A visual inspection of the flow regime will uncover which phase is dominating the flow. The mixer should be chosen thereafter. If the liquid domination mixer is applied, the air is throttled into the water and is no longer fully saturated. But as it is gradually cooled by the liquid, it will reach fully saturation at some point. The task is to calculate at which temperature the “gas phase after mixing” reaches fully saturation. It can be done in HYSYS by adjusting 3a until the point where liquid starts to separate from the gas stream in the third white square (counting from left) in Figure 21. 3a, 3b and 3c are then placed so that 3a measures a value between the saturation temperature and the thermal equilibrium temperature (found in the fourth square in Figure 21). If the gas dominated flow mixer is applied, 3a, 3b, and 3c only have to be positioned somewhere before thermal equilibrium is reached.
- When all measurements of point 3 are done, 3b and 3c will be entered into the HYSYS simulation, together with the already known values from point 1 and 2. The gas phase temperature at the measuring point can now be simulated in HYSYS and compared to the measured value.
- Measurement point 4 and 5 are not necessary but can be used to validate the calculated equilibrium temperature. Tests will be repeated to include all the different GVFs showed in Table 2.



### **Explanation of the simulation environment displayed in Figure 21:**

The first with square simulates the heating and saturation process. Dry gas enters from the left. The single phase heated and saturated gas before mixing can be found to the right of the first square. The liquid before mixing can be found beneath it.

The second square simulates the mixing device. If the liquid domination mixer is applied the gas stream is throttled, while the liquid is throttled when the gas domination mixer is applied. Gas and liquid phase conditions directly after mixing, can be found between the second and the third square. Note that no heat or mass transfer between the phases has accrued at this point.

The third square simulates heat and mass transfer between the phases that have occurred upstream of the local measurements (3a, 3b and 3c). The local measurements are found between the third and fourth square. The final thermal equilibrium condition is found in the last square.

### **6.4 Sources of Error**

Differences in bubble and droplet sizes will cause a temperature variation from bobble to bobble and droplet to droplet as the heat exchange occurs at different rates, depending on the total mass and the surface area. A liquid film will also have a different rate of heat transfer and may not have the same temperature as the droplets travelling in the gas. The measured local phase temperature is therefore not necessarily representative for the entire phase at the given position.

Heat loss through the wall along the pipe between the measured single phase temperatures and the local phase temperatures is not included in the calculations. This uncertainty may cause a difference between the calculated temperature and the measured temperature. Actual heat loss is difficult to predict as the temperature profile is unknown. Isolation will therefore be used to keep the heat transfer as low as possible.

Friction loss along the pipe between the measured single phase temperatures and the local phase temperatures is not included in the calculations. A simulation has been run in HYSYS, and the temperature rise in the test rig caused by friction loss where found to be insignificant, at least compared to the accuracy of the applied sensors.

The focus of this thesis has been on temperature measurements. The accuracy of the pressure measurements has not been assessed. The uncertainty related pressure measurements in multi-phase flow might have a relevant influence on the calculated gas phase temperature.



## 7 Validation of direct integration in HYSYS

Direct integration is a polytrophic calculation method equivalent with Schultz method. It calculates performance through numeric's and can be quite accurate. Aspen tech has implemented this method in their process simulation tool HYSYS. The goals of this chapter are to explain the method, document the implementation in HYSYS and validate the implementation in HYSYS against a self made implementation done in Matlab.

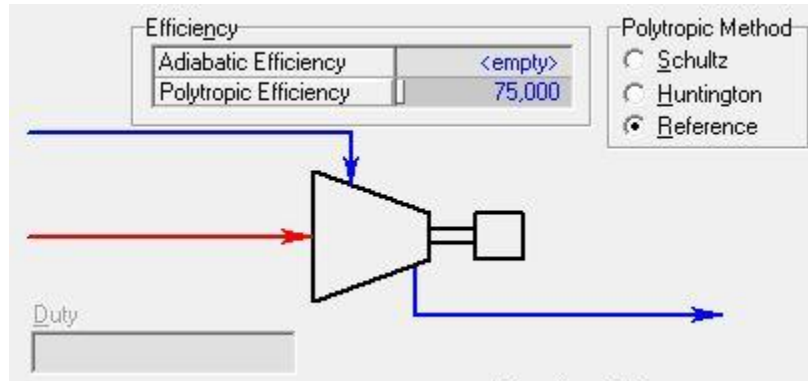


Figure 22 HYSYS compressor calculation options

Figure 22 shows the compressor calculation options available in HYSYS. The well established Schultz and Huntington methods are also available. Note that the Direct Integration method goes under the name Reference method in HYSYS. In this chapter it will be referred to as the Direct Integration method.

### 7.1 Direct Integration

Direct Integration was presented by R. A. Huntington in the Journal of Engineering for Gas Turbines and Power [ 25 ] in 1985. At the time, Shultz method was the most commonly used and accepted polytrophic calculation method. Previously Mallen and Saville had proposed an alternative calculation method for high pressure gasses, and found that the results were deviating from Shultz method. The differences in the results were obvious, but they had not proven the model to be better than Shultz's. Huntington needed a reference method that didn't rely on simplifications to validate the two previous models. He thereby came up with the Direct Integration Model. Note that Huntington and the reference model are not the same. Huntington just used the reference method in the purpose of validating other methods.

$$H_p = \int_1^2 v dp \quad \text{Eq. 7.1}$$

$$H_p = \eta_p H \quad \text{Eq. 7.2}$$

The direct integration model breaks the polytropic compression path between two pressure levels into several sub paths. Huntington states that if the compression path is divided sufficiently, Eq. 7.1 could be linearized without significant error.

$$H_p = \sum H_i \quad \text{Eq. 7.3}$$

$$H_i = v_{avg} \Delta p_i \quad \text{Eq. 7.4}$$

$$H_i = \eta_p \Delta h_i \quad \text{Eq. 7.5}$$

Direct Integration can be applied to calculate outlet temperature of a pump or a turbine at a given outlet pressure when the polytropic efficiency is known. It can also be used to calculate polytropic efficiency from test results when the outlet temperature and pressure is known. Either way numerical calculation methods must be applied to equal Eq. 7.4 and Eq. 7.5. Today computers can easily solve the numeric task related to the Direct Integration Model. The Direct Integration Model is suggested to replace methods such as Shultz.

## 7.2 Implementation of direct integration in HYSYS

This chapter will look at how direct integration is implemented in HYSYS. The documentation available in HYSYS simply refers to Huntington's article [ 25 ]. It does not mention how many steps the differential pressure is divided into, and not which iteration method or tolerance Aspen Tech has applied. E-mail's sent directly to Aspen Techs support office were never replied. And a replied email sent through my supervisor did not answer the given questions. It has therefore been difficult to establish any facts concerning the implementation.

Comparing Direct Integration Method in HYSYS to Schultz method in HYSYS revealed an interesting discovery. As expected there is a deviation between the result of Schultz and Direct Integration when calculating outlet temperature for a given polytropic efficiency. But when calculating polytropic efficiency from given inlet and outlet conditions, the two methods return the exact same value. Two examples showing the discovery, is given in the tables below.

$T_1$	20 °C
$p_1$	3000 kPa
$p_2$	4000 kPa
$\eta_p$	75 %

**Table 10 Conditions**

Method:	$T_2$
Schultz	24,4048343866527 °C
Direct Integration HYSYS	24,4048155879620 °C

**Table 11 Outlet temperature calculations**

Table 11 shows that when calculating outlet temperature with the conditions given in Table 10, Schultz and Direct Integration returns different results. In the next example polytrophic efficiency is calculated from given inlet and outlet conditions. The outlet conditions calculated with Schultz method in the last example are inputs for the new example.

$T_1$	20 °C
$T_2$	24,404834 °C
$p_1$	3000 kPa
$p_2$	4000 kPa

**Table 12 Conditions**

Method:	$\eta_p$
Schultz	74,9998997648932 %
Direct Integration HYSYS	74,9998997648932 %

**Table 13 Polytrophic efficiency calculations**

Table 13 shows that when calculating polytrophic efficiency with the conditions given in Table 12, Schultz and Direct Integration returns the same results. This suggests that HYSYS uses the same calculation method for both Schultz and Direct Integration when calculating polytrophic efficiency.

Applying the direct integration for polytrophic efficiency calculations is much more complicated and time consuming (will be further explained in the next subchapter). It is therefore reasonable to believe that Aspen Tech hasn't implemented Direct Integration for polytrophic efficiency calculations, but simply applies Schultz instead.

### 7.3 Implementation of direct integration in Matlab

Because information about the implementation of the Direct Integration in HYSYS is a limited, Direct Integration has been implemented in Matlab. The Matlab implementation will serve as a tool in the validation of the HYSYS implementation. It is done through a Matlab script which runs one of two functions, depending on whether the outlet temperature or the polytropic efficiency is known.

Rather than implementing the equation of state for all the substances, the script connects to HYSYS through ActiveX. This way it can utilize equations of state and components available in HYSYS. A brief summary of the actions performed by the script are given in the list below. The complete script and functions can be found in Appendix E.

Actions:

- Sets inlet condition (pressure, temperature and GVF), outlet pressure and either polytropic efficiency or outlet temperature.
- Sets calculation options such as number of pressure steps and accuracy demands.
- Connects to HYSYS.
- Opening HYSYS simulation case.
- Runs `DirectIntegrationEtha()` if the outlet temperature is known or `DirectIntegrationT()` if the polytropic efficiency is known.

#### 7.3.1 `DirectIntegrationT()`

`DirectIntegrationT()` is a function used to calculate outlet temperature when inlet conditions, outlet pressure and polytropic efficiency are known. The implementation is based on the reference method presented by Huntington.

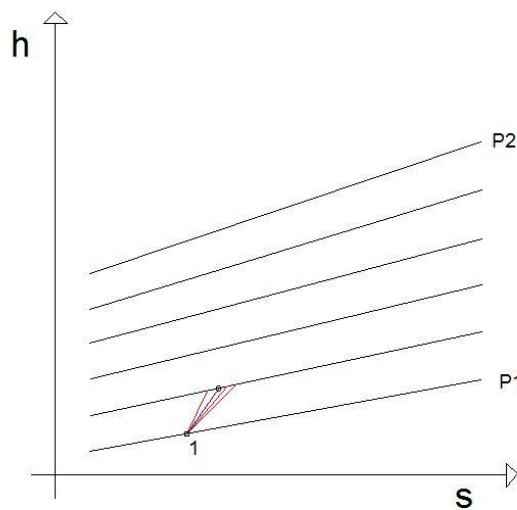
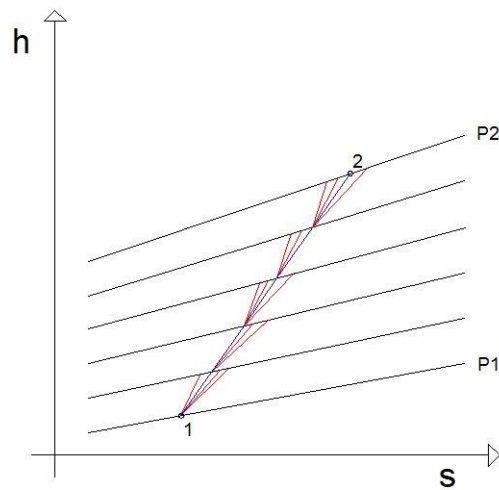


Figure 23 `DirectIntegrationT()` first step iteration

First it divides the differential pressure into a given number of steps and opens a stream from HYSYS which corresponds to the given GVF. Then it calculates the conditions for each different sub pressure level by applying the bisection iteration method to Eq. 7.4 and Eq. 7.5. Figure 23 shows how the conditions after the first step are calculated through iteration.



**Figure 24 DirectIntegrationT() after last step iteration**

When the bisection iteration method has found a solution to the conditions after the first step, which meets the demands of accuracy, the results serve as inlet conditions for the next step. The final compression path is formed, and the outlet temperature is calculated, when the conditions after the last step has been decided (see the blue line in Figure 24). The red lines represent the calculated outlet conditions that did not meet the demands of accuracy.

In theory the accuracy of the calculations will increase with the amount of calculation steps. But since the data retrieved from HYSYS is limited to a certain amount of digits, the amount of steps is limited as well. For very small steps, data from HYSYS starts to treat  $\Delta p$  and  $\Delta h$  as zero. Eq. 7.4 will then equal Eq. 7.5, even though the outlet temperature and polytrophic efficiency are wrong. HYSYS is simply not accurate enough to cope with too many steps.

### 7.3.2 DirectIntegrationEtha()

DirectIntegrationEtha() is a function used to calculate the polytrophic efficiency when the inlet and outlet temperatures and pressures are known. The implementation has an extra dimension compared to DirectIntegration(T), as the polytrophic efficiency is not known. The function first guess a polytrophic efficiency and then run the same procedure as in DirectIntegrationT(). When the calculated outlet condition is found it is compared to the measured one. And a new poly-

trophic efficiency is decided according to the Bisection method. The `DirectIntegrationT()` procedure is then run again with the new polytrophic efficiency. The iteration process is repeated until the difference between the calculated and known outlet conditions are within the demand of accuracy. The polytrophic efficiency used in the last iteration is returned as the result of the function.

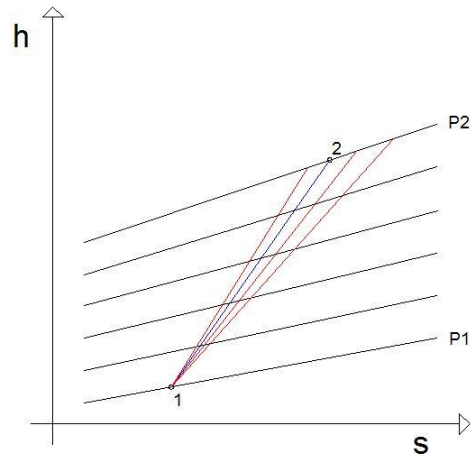


**Figure 25 DirectIntegrationEtha()**

The blue line in Figure 25 represents the last iterations, while the red lines represent the iterations that did not meet the demands of accuracy. Each single line has been created through the `DirectIntegrationT()` procedure.

As mentioned, the `DirectIntegrationT()` will become inaccurate if the number of steps is too high. The same thing holds for the `DirectIntegrationEtha()`, only `DirectIntegrationEtha()` can also become unstable. If the deviation between the calculated and measured value is caused by HYSYS and not the polytrophic efficiency, accuracy will not be improved by changing the polytrophic efficiency. The function will either continue to run for ever, or hit an outlet condition within the accuracy demand just by pure luck.

## 7.4 Validation

This subchapter tries to validate the Direct Integration method implemented in HYSYS, by comparing it to the Direct Integration method implemented in Matlab. From subchapter 7.2 it is already known that HYSYS does not apply Direct Integration when calculating polytrophic efficiency. This subchapter will therefore focus on the validation of outlet temperature calculations. The conditions displayed in Table 14 will be applied for all examples.



$T_1$	20 °C
$p_1$	3000 kPa
$p_2$	4000 kPa
$\eta_p$	75 %

**Table 14 Conditions**

Calculated outlet temperatures for a typical hydro carbon mixture at 60% GVF can be found in Table 15. The temperatures are calculated from Schultz model in HYSYS, Direct Integration model in HYSYS and the Direct Integration Model implemented in Matlab. The tolerance in the Matlab implementation is set so low that a decrease in tolerance would not affect the results within the amount of digits displayed in Table 15.

Method:	$T_2$
HYSYS Compressor Schultz	24,404834 °C
HYSYS Compressor Direct Integration	24,404815 °C
Matlab Direct Integration (1 step)	24.383473 °C
Matlab Direct Integration (2 steps)	24.361063 °C
Matlab Direct Integration (5 steps)	24.354671 °C
Matlab Direct Integration (10 steps)	24.353754 °C
Matlab Direct Integration (20 steps)	24.353524 °C

**Table 15 Outlet temperature calculations of a hydrocarbon mixture at 60% GVF**

The purpose of this example was to decide how many steps HYSYS applies in the implementation of Direct Integration. The Matlab implementation was run with different amount of pressure steps without closing in on the HYSYS implementation. The deviation can therefore not be caused just by different number of steps.

If the difference between the Direct Integration Model in HYSYS and Matlab is not caused by a difference in the number of steps, it can only be caused by a difference in tolerance limits. The example above was repeated for numerous of different conditions, and the results were the same. The direct Integration method in HYSYS was always closer to Schultz than to the Direct Integration method implemented in Matlab. It is difficult to say much about what kind of tolerance HYSYS uses. But high tolerance would not generate a systematic inaccuracy in the direction of Shultz. It would be a random inaccuracy occurring on both sides of the Direct Integration Matlab results.

The Direct Integration in HYSYS was so close to Schultz and so far from the Matlab implementation that it raised doubts about the implementation in Matlab. The Matlab implementation has therefore been thoroughly checked both against the paper of Huntington and the implementation of a fellow student, and is at the time of writing believed to be correct.

Before writing off the HYSYS implementation completely, the two implementations will be compared from another perspective. When simulating multi-phase flow with the Schultz method, HYSYS utilizes the mixed flow model. This means averaging the specific volumes of the two phases, and treating the whole mixture as a single-phase compressible gas. This approach might be acceptable for wet-gas calculations, but for multi-phase pumps the liquid content is too high to treat the mixture as compressible.

The good thing about the Direct Integration Model is that it is not limited to either gas or liquid. For instance, if the medium is pure liquid the head calculation reduces to Eq. 7.6 which is the same equation used for single-phase pumps.

$$\Delta h = \frac{v\Delta p}{\eta_p} \quad \text{Eq. 7.6}$$

An example has been performed in order to see how the different models perform on pure liquid. HYSYS's pump calculation is included, and will serve as reference for the other methods. As explained above Schultz is expected to treat the whole mixture as gas and therefore fail on this example, while the Direct Integration Models are expected to return the same value as the HYSYS pump.

Method:	$T_2$
HYSYS Compressor Schultz	20,1422°C
HYSYS Compressor Direct Integration	20,1417°C
Matlab Direct Integration (1 step)	20.0842°C
HYSYS Pump	20,0843°C

**Table 16 Outlet temperature calculations of water**

The results given Table 16, shows that the implementation of the Direct Integration model implemented in Matlab return an outlet temperature fairly close to the calculated pump outlet temperature. The Direct Integration Model Implemented in HYSYS on the other hand, returns a value close to the Schultz implementation. As explained earlier Schultz treats the mixture as a gas and cannot be used to calculate outlet temperature of a pure liquid. How the Direct Integration method is implemented in HYSYS is not known, but this example proves that it is not implemented according to Huntington's paper.

## 8 Influence of heavy components on the performance calculations

The performance of a multi-phase pump is affected by the properties of the fluid. If the fluid is a Hydrocarbon mixture, the composition is decided through an analysis of the mixture. The cost of the analysis is increasing with the amount of hydrocarbons considered. To reduce costs, industry actors sometimes tend to neglect the heavier components. This chapter will investigate the importance of including heavy components in the calculations and explain the consequences of neglecting them. Examples will be performed and the results will show the effects on performance parameters and compression path.

Direct Integration is chosen as the calculation method. Earlier chapters of this thesis have shown that the Direct Integration method implemented in HYSYS, do not perform the calculation such as Huntington intended. Another drawback with the simulations in HYSYS is that it does not display the compression path, only inlet and outlet conditions. The direct integration model implemented in Matlab will therefore be used instead. The Matlab implementation can return all data related to the compression path, and the method is believed to be more correct.

### 8.1 Compositions

To be able to study the effects of neglecting some parts of the composition two different mixtures will be compared. The first mixture (A) represents the actual fluid composition and contains Nitrogen, CO<sub>2</sub> and hydrocarbons from C1 to C30. The second mixture (B) represents the results from a low-cost analysis performed on the first mixture. It contains the same amount of Nitrogen, CO<sub>2</sub> and hydrocarbons from C1 to C9, while C10-C30 are considered as C10+.

Table 17 presents actual fluid compositions and low cost analyzes for 90, 60, 30 and 0% GVF mixtures. The compositions are generated from a typically wet-gas case, handed over to me by my supervisor. The compositions in Table 17 representing the different GVFs were generated by extracting some of the lighter components. The GVF is calculated at a temperature of 5 °C and at a pressure of 3000 kPa.

GVF: Composition:	90%		60%		30%		0%	
	A	B	A	B	A	B	A	B
Nitrogen	0,0004	0,0004	0,0002	0,0002	0,0002	0,0002	0,0002	0,0002
CO2	0,0259	0,0259	0,0162	0,0162	0,0103	0,0103	0,0065	0,0065
Methane	0,5029	0,5029	0,2686	0,2686	0,1944	0,1944	0,1475	0,1475
Ethane	0,1738	0,1738	0,1445	0,1445	0,0941	0,0941	0,0576	0,0576
Propane	0,0818	0,0818	0,1240	0,1240	0,1024	0,1024	0,0640	0,0640
i-Butane	0,0139	0,0139	0,0262	0,0262	0,0277	0,0277	0,0207	0,0207
n-Butane	0,0250	0,0250	0,0490	0,0490	0,0558	0,0558	0,0453	0,0453
i-Pentane	0,0149	0,0149	0,0307	0,0307	0,0396	0,0396	0,0401	0,0401
n-Pentane	0,0141	0,0141	0,0294	0,0294	0,0388	0,0388	0,0416	0,0416
n-Hexane	0,0187	0,0187	0,0395	0,0395	0,0546	0,0546	0,0675	0,0675
n-Heptane	0,0290	0,0290	0,0614	0,0614	0,0860	0,0860	0,1123	0,1123
n-Octane	0,0283	0,0283	0,0598	0,0598	0,0840	0,0840	0,1119	0,1119
n-Nonane	0,0134	0,0134	0,0283	0,0283	0,0398	0,0398	0,0533	0,0533
n-Decane/C10+	0,0120	0,0579	0,0254	0,1223	0,0357	0,1722	0,0480	0,2315
n-C11	0,0073		0,0154		0,0216		0,0290	
n-C12	0,0065		0,0137		0,0193		0,0260	
n-C13	0,0057		0,0121		0,0171		0,0229	
n-C14	0,0054		0,0113		0,0159		0,0214	
n-C15	0,0042		0,0089		0,0125		0,0168	
n-C16	0,0031		0,0065		0,0091		0,0122	
n-C17	0,0027		0,0057		0,0080		0,0107	
n-C18	0,0023		0,0049		0,0068		0,0092	
n-C19	0,0019		0,0040		0,0057		0,0076	
n-C20	0,0015		0,0032		0,0045		0,0061	
n-C21	0,0011		0,0024		0,0034		0,0046	
n-C22	0,0008		0,0016		0,0023		0,0031	
n-C23	0,0008		0,0016		0,0023		0,0031	
n-C24	0,0004		0,0008		0,0011		0,0015	
n-C25	0,0004		0,0008		0,0011		0,0015	
n-C26	0,0004		0,0008		0,0011		0,0015	
n-C27	0,0004		0,0008		0,0011		0,0015	
n-C28	0,0004		0,0008		0,0011		0,0015	
n-C29	0,0004		0,0008		0,0011		0,0015	
n-C30	0,0004		0,0008		0,0011		0,0015	

Table 17 Hydrocarbon composition Actual mixtures VS Low cost analyzes

## 8.2 Compression path and performance parameters

Fictive test results have been generated to serve as input values for the following examples. The conditions can be seen in Table 18. The fictive outlet conditions are generated by applying the direct integration method to the actual fluid composition, with the inlet conditions given in Table 18 and a polytropic efficiency of 75%.

<b>GVF:</b> <b>Composition:</b>	90%		60%		30%		0%	
	A	B	A	B	A	B	A	B
Calc. inlet GVF [%]	90	90,64	60	61.68	30	31.48	0	0
$p_1$ [kPa]	3000	3000	3000	3000	3000	3000	3000	3000
$p_2$ [kPa]	4000	4000	4000	4000	4000	4000	4000	4000
$T_1$ [°C]	5	5	5	5	5	5	5	5
$T_2$ [°C]	13,583	13,583	9,036	9,036	7,410	7,410	5,357	5,357

**Table 18 Imagined test results**

The first thing worth noticing is that the calculated GVF of composition B differs from the actual GVF. The simplification in composition B has caused the whole phase envelope to change. It is not only the GVF that's affected by change in composition. Enthalpy, entropy, specific volume and mol weight, in fact all properties relevant for the calculations changes for a given inlet temperature and pressure.

Results from prototype tests are often used to predict performance on actual operating pumps. Test data such as polytropic efficiency, head and power consumption are related to inlet GVF, inlet volumetric flow rate and pump speed. One effect of neglecting some of the heavier components is a miss calculation of GVF and volumetric flow rate, which in turn leads to an incorrect relation between different test data.

The Direct Integration Model has been used to calculate the polytropic efficiency from the fictive test results in Table 18. The results are presented in Table 19.

<b>Composition:</b>	90%		60%		30%		0%	
	A	B	A	B	A	B	A	B
$T_2$ [°C]	13,583	13,583	9,036	9,036	7,410	7,410	5,357	5,357
$\Delta h$ [kJ/kmol K]	526	463	272	202	199	132	190	157
Calculated $\eta_p$ [%]	75	84	75	96	75	103	75	81

**Table 19 Performance Calculations**

Table 19 shows that the calculated polytropic efficiency for composition B deviates from the actual polytropic efficiency. The head deviation is also comprehensive. From chapter 4 we know that the head degradation factor is calculated from the single and two-phase head. From Eq. 8.1 it is evident that two-phase performance predictions will be affected by a simplification of the composition.

$$f_{TP,H} = \frac{\psi_{TP}}{\psi_{SPL}} = \frac{H_{TP} u_{SP,2}^2}{H_{SP} u_{TP,2}^2} \quad \text{Eq. 8.1}$$

The compression paths from the examples in Table 19 will now be presented in a numerous of h-s diagrams. Because of the differences in fluid properties of composition A and B, they are not plotted in the same graph.

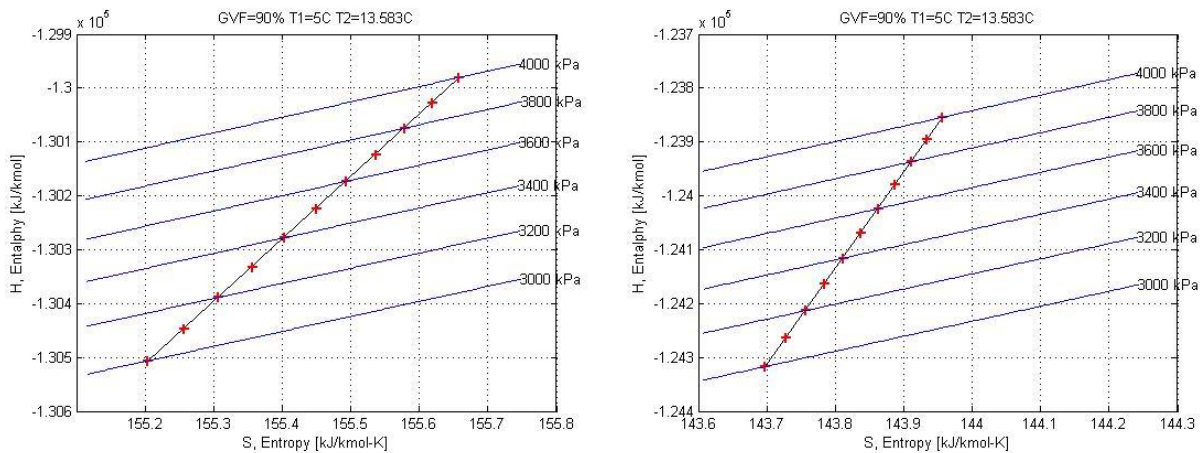


**Figure 26 Direct integration, Composition A VS B, Number of steps = 10, GVF 90%.**

First up is the 90% GVF example. The graph to the left in Figure 26 shows the compression path at 90% GVF of the actual composition. The compression path of the simplified composition is plotted in the graph to the right. Figure 26 show that the simplification of the composition causes an inaccuracy in the inlet enthalpy and entropy. The increased polytropic efficiency found in Table 19 can be seen in the right figure as an increase of steepness of the compression path.

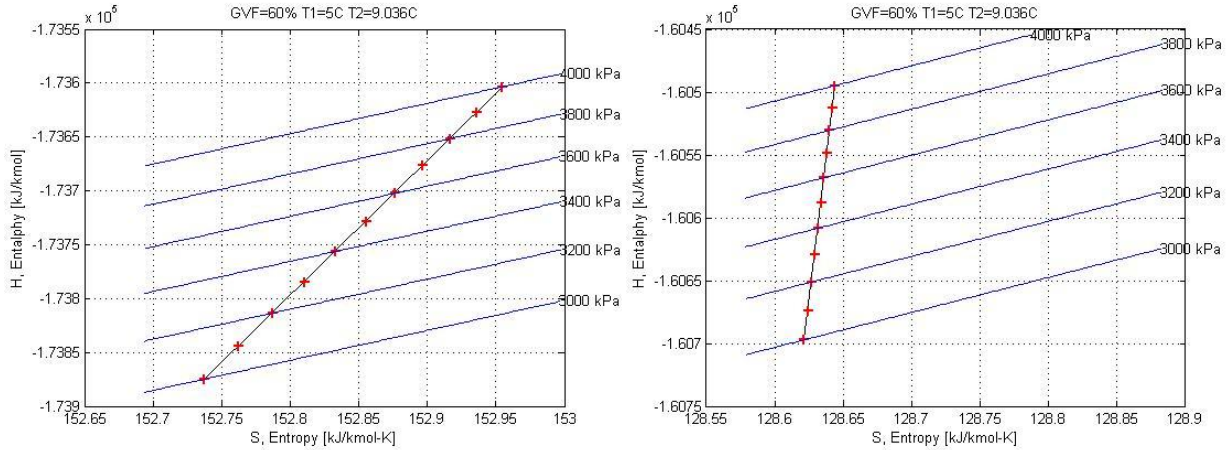


**Figure 27 Direct integration, Composition A VS B, Number of steps = 10, GVF 60%.**

When increasing the liquid content, Figure 27 shows that the importance of the heavy components seems to increase. This behavior is expected as the heavier components are more dominant at lower GVFs. At 60% GVF the simplification of the mixture causes a mal positioning of the compression path, in terms of inlet enthalpy and entropy, which is more than twice of what was found at 90% GVF. Table 19 showed that the polytropic efficiency calculated from composition B was 96 %, which is far off the actual polytropic efficiency of 75 %. This can also be seen on the steepness of the compression path, in the right graph.

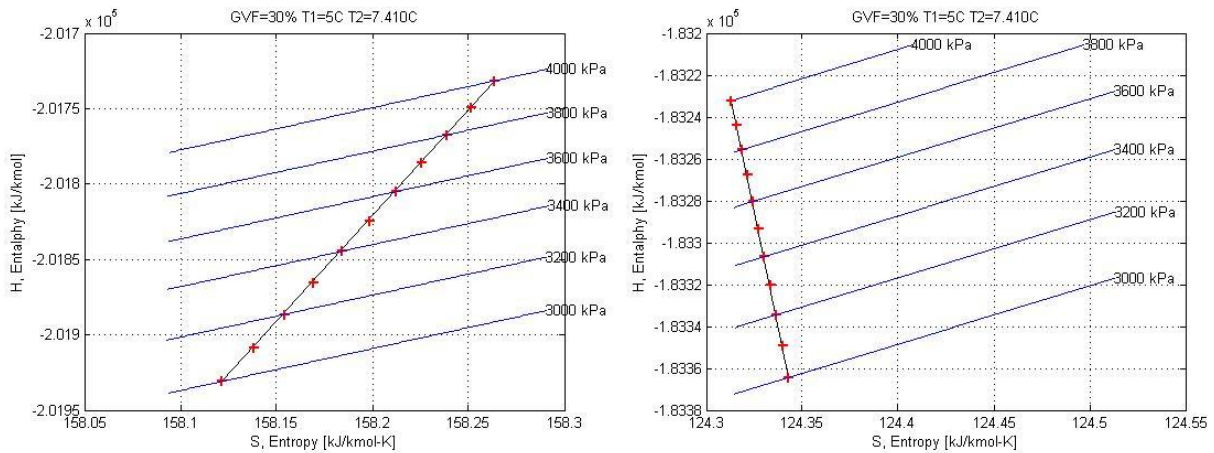


**Figure 28 Direct integration, Composition A VS B, Number of steps = 10, GVF 30%.**

A further increase of the liquid content shows that developed trend continues. At 30% GVF the polytropic efficiency calculated from the simplified composition reaches 103% which is an unphysical number. Figure 28 shows how the entropy is actually decreasing. Results like this should create some mind trouble for the involved test engineers.

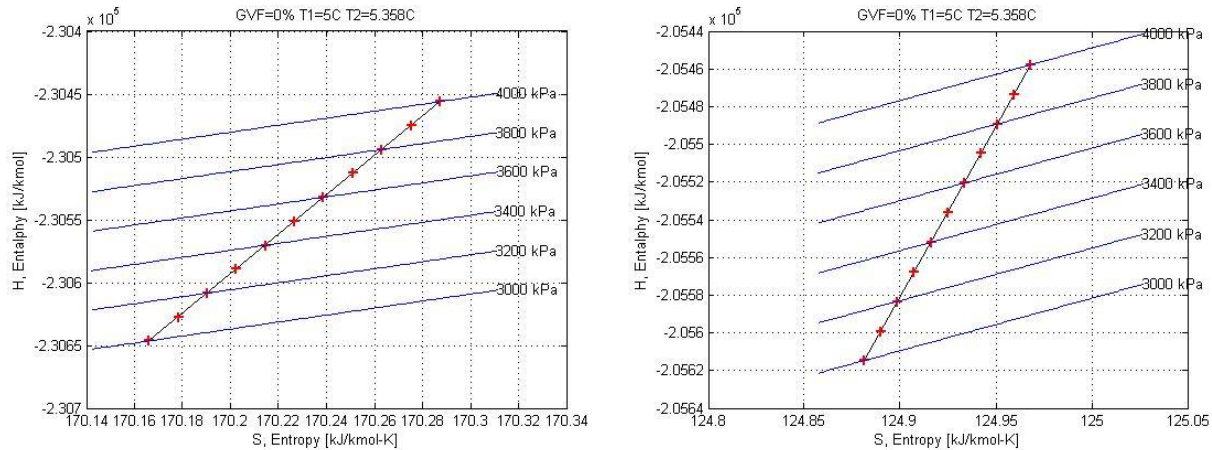


**Figure 29 Direct integration, Composition A VS B, Number of steps = 10, GVF 0%.**

At the bubble point, the mal positioning of the compression path, calculated from the simplified composition, still increases according to the trend. The polytropic efficiency calculated from composition B however, is now 81%, which is much closer to the actual value than for 30% GVF.

Knowing the exact composition of fluid is important when dealing with single-phase pumps and dry gas compressors. This chapter has showed that for multi-phase applications it is even more important. The displacement of the phase envelope impacts all properties relevant for the performance calculations. The exact inlet and outlet properties of a stage or a pump can only be found if the exact composition is known. It was no big surprise that head calculations using composition B worsen as the actual composition becomes heavier. It was however interesting to find that the polytropic efficiency calculations was especially sensitive in the two-phase area.



## 9 Conclusions and Suggestions to Further Work

Because the heat capacity per unit volume of a liquid is much higher than the heat capacity per unit volume of a gas, the temperature increase is limited in the whole GVF range of Multi-phase pumps (0-90%GVF). In the lower GVF range the temperature increase is in fact so small that the common practice in the industry is to simplify calculations by assuming an isothermal compression process. In the higher GVF region (60-90%GVF) the isothermal calculations becomes inaccurate. Polytropic calculations can provide accurate calculations, but is highly sensitive to the accuracy of the temperature measurements, especially for the liquid phase. For the gas phase a sensitivity analysis performed in this thesis has showed that temperature measurements can be less accurate, due to a lower heat capacity.

The implementation of the Direct Integration method in HYSYS is not found to be implemented according to the Reference Method presented by Huntington. For polytropic efficiency calculations it does not seem to be implemented at all. If Direct Integration is to be used in future performance calculations, better results will be achieved by applying the Matlab implementation presented in this thesis.

It was found that accurate performance calculations depend on accurate determination of the composition. The calculations of polytropic efficiency showed to be especially sensitive when operating far into the two-phase area. Both when analyzing test results and predicting performance of a subsea pump, engineers needs to acknowledge the importance of the fluid composition.

### **Suggestions for further work**

A sensitivity analysis of all the measured parameters connected to the calculation of the local gas temperature in the test rig should be conducted. Due to the time limit of this thesis, sensitivity analyzes has so far only been done on the temperature measurements.

After the sensitivity analyzes has been performed, the tests should be carried out. Results will show whether or not the accuracy of the different concepts presented in Chapter 6.2.2 are high enough.

If the tests show that measurements of the local gas phase is possible and that the accuracy is found high enough, the next step is to look at how the concepts can be moved into an actual pump application. Challenges like positioning and durability will have to be tackled.

Collaboration with AspenTech should be established in order to clarify how their reference method is implemented in HYSYS. If their implementation is found incorrect, AspenTech should be encouraged to improve their version of the reference method. Calculation options such as number of pressure steps and tolerance levels should be included in the user interface.

## References

[ 1 ]	Wallis B. G., “One-dimensional Two-phase Flow”, McGraw-Hill Book Company, 1996.
[ 2 ]	Gülich J.F., “Centrifugal Pumps 2 <sup>nd</sup> edition”, Springer-Verlag, 2010.
[ 3 ]	Bratland O., “Pipe flow 2 – Multiphase flow assurance”, 2010. <a href="http://drbratland.com/">http://drbratland.com/</a> (15.09.2012).
[ 4 ]	Faghri A., Zhang, Y., Transport Phenomena in Multiphase Systems, Elsevier, Burlington, MA, 2006.
[ 5 ]	British Standards Institution, “Centrifugal pumps handling viscous liquids –Performance corrections”, PD ISO/TR 17766, 2005.
[ 6 ]	Ramberg R. M., “Multiphase pump performance modelling”, Doctoral Thesis, NTNU, 2007.
[ 7 ]	Ramberg R. M., Bakken L. E., “Influence of viscous fluids on multiphase pump performance”, FEDSM98-4869, 1998.
[ 8 ]	Abelson, C., Hybrid Pump Performance Prediction Model. Aker Solutions 10001162103-PDC-000
[ 9 ]	Walski, T., Zimmerman, K., Dudinyak, M., Dileepkumar, P., Some Surprises in Estimating the Efficiency of Variable-Speed Pumps with the Pump Affinity Laws. World Water and Environmental Resources Congress, 2003.
[ 10 ]	Moran M. J., Shapiro H. N., Fundamentals of Engineering Thermodynamics, 5 <sup>th</sup> edition, John Wiley and Sons, Inc, 2006.
[ 11 ]	Korenchan J. E., Application of Analytical Centrifugal-Pump Performance Models in Two-Phase Flow. Master Thesis, S.B.M.E., Illinois Institute of Technology, 1982.
[ 12 ]	Wilson D. G., Analytical Models and Experimental Studies of Centrifugal Pump Performance in Two-phase Flow. Electric Power Research Institute Report EPRI NP-677, 1979.
[ 13 ]	Nourbakhsh S. A., Theoretical and Real Slip Factor in Centrifugal Pumps, Von Karman Inst., Technical Note 93, 1973.
[ 14 ]	Schultz J. M., The Polytropic Analysis of Centrifugal Compressors. Journal of Engineering for power, 84:69, 1962.

[ 15 ]	Murakami M., Minemura K., Effects of Entrained Air on the Performance of a Centrifugal Pump, JSME, Vol. 17, No 110, August, 1974.
[ 16 ]	Test report, High Viscosity Fluid Pump Test PAZFLORE PROJECT. Aker Solutions, 10000104797.
[ 17 ]	Knudsen H., MultiBooster Performance, Project Thesis, Norwegian University of Science, 2012.
[ 18 ]	Gié P., Buvat P., Bratau C., Durando P., Poseidon Multiphase Pump: Field Tests Results. Offshore Techn Conf OTC 7037, 4 (1992), 489-501
[ 19 ]	API 610, Centrifugal Pumps for Petroleum, Petrochemical and Natural Gas Industries. Eleventh Edition, September 2010
[ 20 ]	Turbo compressors – Performance test code. ISO 5389:2005, Geneva, Switzerland, 2005.
[ 21 ]	Hunseid Ø., Bakken L. E., Evaluation of Performance Models for Wet Gas Compressors. Doctoral Thesis, Norwegian University of Science, 2008
[ 22 ]	Saravanamutto H.I.H., Rogers G.F.C., Cohen H. Gas Turbine Theory. Pearson Education, 6 <sup>th</sup> edition, 2009.
[ 23 ]	Falcimagine J., Decarre S., Multiphase Production. IFP Publications, Paris 2008. ISBN 978-27108-0913-5
[ 24 ]	Ripka P., Tipek A., Modern Sensors Handbook, ISTE, 2007.
[ 25 ]	Huntington R. A., Evaluation of Polytropic Calculation Methods for Turbo machinery Performance, Journal of Engineering for Gas Turbines and Power, October 1985, Vol. 107.
[ 26 ]	Mallen M., Saville G., Polytropic Processes in the Performance Prediction of Centrifugal Compressors, Institute of Mechanical Engineers, Paper No. C183, pp 89-96.
[ 27 ]	Schleicher E., Da Silva M. J., Hampel U., Enhanced Local Void and Temperature Measurements for Highly Transient Multiphase Flows, IEE Transactions on Instrumentation and Measurement, Vol. 57, No. 2, February 2008.
[ 28 ]	Consolation with Arne Veland FRAMO Engineering AS
[ 29 ]	Taitel Y., Duckler A. E., A Model for Predicting Flow Regime Transitions in Horizontal and Near Horizontal Gas-Liquid Flow. AIChE Journal, 22/1.

[ 30 ]	Standard Specification for Industrial Platinum Resistance Thermometers, E1137/E1137M, American Society for Testing and Materials, 2008.
[ 31 ]	White F. M., Fluid Mechanics, Sixth Edition, University of Rhode Island, McGrawHill Higher Education.



## Appendix

- A - Offer on Thermo-Needle Probe System
- B - Data Sheets
- C - Liquid Dominated Mixer Calculations
- D - Simulation Environment Test Rig
- E - Matlab Implementation of Direct Integration
- F - Direct Integration Results





# A - Offer on Thermo-Needle-Probe System



HZDR Innovation GmbH | Bautzner Landstraße 400 | D-01328 Dresden

Professor Lars Erik Bakken  
Institutt for energi- og prosessteknikk  
Norges teknisk-naturvitenskapelige universitet  
7491 TRONDHEIM  
NORWAY

Division  
Multiphase measurement  
technology

Bautzner Landstraße 400  
D-01328 Dresden  
Tel +49 351 440091-120  
Fax+49 351 440091-199  
contact@hzdr-innovation.de  
www.hzdr-innovation.de

## Offer 1119 Thermo-Needle-Probe System

Unser Zeichen:  
1119 / 20.02.2013

Dear Professor Bakken,

Referring to consultation with Mr. Halfdan Knudsen and Mr. Eckhard Schleicher we offer the following goods and services: Manufacturing and delivery of

### 5 pieces Thermo Needle Probes

- Thermo couple (probe tip size): 250  $\mu\text{m}$  ( $\tau = 25 \text{ ms}$ )
- shaft outer diameter: 10 mm)
- shaft length: min. 300 mm
- insulation: PEEK
- maximum pressure: 5 MPa
- maximum temperature: 250 °C

### Lump Sum Price for 5 Pcs.

16.500,00 €

### 5 pieces Thermo Needle Probe Amps (TNP-2) including

- TNP-2 device 5 pcs.
- power supply 5 pcs.
- triaxial cable (0.5 m) 5 pcs.
- thermo cable (0.5 m) 5 pcs.
- Ethernet Switch 1 pc
- data acquisition software

### Lump Sum Price for 5 Pcs.

35.500,00 €

### Granting the Right of Use of the Data evaluation software "VoidWizard"

900.00 €

### Subtotal

52,900.00 €

### Transport and insurance fees DAP

500.00 €

### TOTAL

53,400.00 €

HZDR Innovation GmbH  
Bautzner Landstraße 400  
D-01328 Dresden  
contact@hzdr-innovation.de  
www.hzdr-innovation.de

Geschäftsführer:  
Prof. Dr. Andreas Koltsch  
Dipl.-Kfr. Beate-Victoria Ermisch  
Gesellschafter: HZDR e.V., GWT-TUD GmbH  
Registriergericht: Amtsgericht Dresden  
Registernummer: HRB 30595

Bankverbindung: Commerzbank AG  
Konto 800484800 | BLZ 85040000  
SWIFT/BIC COBADEFF850  
IBAN DE73850400000800484800  
Steuer-Nr. 202/110/06464  
USt.-ID DE 279973320

Seite 2

All amounts are net amounts and subject to additional statutory VAT.

The HZDR will issue the invoice after service delivery. Payment is due 14 days after receipt of auditable invoice. All bank fee levied to HZDR shall be borne by orderer.

**Delivery date**

4 - 5 months after order

**Additional**

Goods are delivered according to INCOTERMS 2010: delivery DAP to Trondheim/Norway.

**Other**

Needle-Probe-System is a patented technology of Helmholtz-Zentrum Dresden-Rossendorf. HZDR Innovation GmbH has been granted a license for manufacturing and distribution.

In addition the General Sales and Delivery Conditions of HZDR shall apply.

**Quotation deadline**

This offer is valid until May 31, 2013.

We would be happy to receive the corresponding order from your company to the following contact: [susann.rosky@hzdr-innovation.de](mailto:susann.rosky@hzdr-innovation.de).

**THE OFFER IS SUBJECT TO CHANGE.**

Dresden, 20.02.2013



Beate-Victoria Ermisch  
Financial Managing Director

## **B - Data Sheets**

- Sea-bird Electronics SBE 38
- BETE NF Standard Fan Nozzle
- GEVACRIL Plexiglas Pipe

# Digital Oceanographic Thermometer

SBE 38



Sophisticated A/D acquisition electronics, ultra-stable thermistor, and state-of-the-art calibration provide the standards-level performance of an expensive AC bridge and platinum thermometer at a small fraction of the cost. The SBE 38 is unaffected by shock and vibration, has high accuracy and stability, and is easy to use. It has a rugged, corrosion-proof, 10,500 meter (34,400 foot) titanium pressure housing. Real-time temperature data is transmitted in ASCII characters (°C or raw counts) via an RS-232 or optional RS-485 serial interface for display or logging by PC or data logger.

The SBE 38's measurement range is -5 to +35 °C; absolute accuracy is better than 0.001 °C (1 mK) and resolution is approximately 0.00025 °C (0.25 mK). Each sensor includes certification that demonstrates drift of less than 0.001 °C (1 mK) during a six-month period.

Applications include calibration baths, oceanographic/aquatic research, and environmental monitoring. The SBE 38 is frequently integrated as a remote temperature sensor with an SBE 21 Thermosalinograph or SBE 45 MicroTSG, to provide accurate sea surface temperature. It can also be integrated as a secondary temperature sensor with an SBE 16*plus*, 16*plus*-IM, 16*plus* V2, 16*plus*-IM V2, or 19*plus* V2 SEACAT CTD.

## OPERATION

The SBE 38 operates in one of three modes:

- RS-232 (full duplex) with one SBE 38 connected to the interface
- RS-485 (half duplex) with one SBE 38 connected to the interface
- RS-485 (half duplex) with several RS-485 sensors sharing one pair of wires

On power-up, the SBE 38 reads its EEPROM, which includes calibration coefficients and other setup information. As programmed, the SBE 38 samples and transmits temperature continuously, or waits for a command. For RS-485 applications with several sensors sharing one pair of wires, the SBE 38 cannot sample continuously.

## MEASUREMENT METHOD

Temperature is determined by applying an AC excitation to reference resistances and an ultra-stable aged thermistor with a drift rate of less than 0.002 °C per year. Each of the resulting outputs is digitized by a 24-bit A/D converter. The reference resistor is a hermetically sealed VISHAY. AC excitation and ratiometric comparison using a common processing channel removes measurement errors due to parasitic thermocouples, offset voltages, leakage currents, and gain errors. The maximum power dissipated in the thermistor is 0.5 microwatts, and contributes less than 200 µK of overheat error.

A raw count (ratio) is related to resistance measurements:

$$\text{raw counts} = 1048576 * NT / NR$$

where NR is the output from the reference resistor and NT is the thermistor output.

The number of acquisition cycles (raw counts) averaged per sample is user-programmable. Increasing the number of cycles per sample increases the time to acquire the sample and the interval between samples, while reducing the RMS temperature noise from the sensor. The interval between samples is:

$$\text{interval [seconds]} = (0.133 * N_{\text{Avg}}) + 0.339$$

where N<sub>Avg</sub> is the number of acquisition cycles per sample.

The SBE 38's converted output is computed from the raw count and the calibration coefficients that are stored in EEPROM.



Sea-Bird Electronics, Inc.

13431 NE 20th Street, Bellevue, Washington 98005 USA

Website: <http://www.seabird.com>

E-mail: [seabird@seabird.com](mailto:seabird@seabird.com)

Fax: (425) 643-9954

Telephone: (425) 643-9866



# Digital Oceanographic Thermometer

## SBE 38



### CALIBRATION

The SBE 38 is calibrated in Sea-Bird's state-of-the-art calibration laboratory, which maintains primary temperature standards (water triple point [TPW] and gallium melting point [GaMP] cells), ITS-90 certified and standards-grade platinum resistance thermometers, and a low-gradient temperature bath.

Temperature is computed using the Steinhart-Hart polynomial for thermistors (Steinhart and Hart, 1968; Bennett, 1972), which is based on thermistor physics. The equation characterizes the non-linear temperature versus resistance response of the sensor. Note that thermistors require individualized coefficients to the Steinhart-Hart equation, because the thermistor material is an individualized mix of dopants:

$$t_{sol} = \{ [1.0 / (a_0 + a_1 * [\ln(n)] + a_2 * [\ln^2(n)] + a_3 * [\ln^3(n)])] - 273.15 \} * \text{Slope} + \text{Offset} \text{ [}^\circ\text{C]}$$

where n is the SBE 38 output.

### SPECIFICATIONS

#### Interface and Power Requirements:

RS-232 (standard)

Power: 8-15 VDC at 15 milliamps average

RS-485 half duplex (optional)

Power: 8-15 VDC at 10 milliamps average

#### Housing:

Titanium, rated at 10,500 meters (34,400 feet)

#### Weight:

In Air

0.9 kg (2.0 lbs)

In Water

0.5 kg (1.2 lbs)

#### Range:

-5 to +35 °C

#### Initial Accuracy<sup>1</sup>:

± 0.001 °C (1 mK)

#### Resolution:

0.00025 °C (0.25 mK)

#### Stability:

0.001 °C (1 mK) in six months, certified

#### Response Time<sup>2</sup>:

500 milliseconds

#### Self-heating Error:

less than 200 µK

<sup>1</sup> NIST-traceable calibration applying over the entire range.

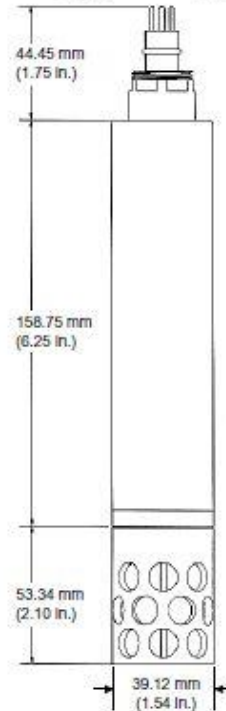
<sup>2</sup> Time to reach 63% of final value following a step change in temperature.

#### Pin Signal

- 1 Common
- 2 RS-232 Receive or RS-485 A
- 3 RS-232 Transmit or RS-485 B
- 4 Power

Optional connector:  
Wet-Pluggable  
MCBH-4MP (WB), TI  
(3/8" length base,  
1/2-20 Thread)

Standard connector:  
XSG-4-BCL-HP-SS



### ACTUAL CALIBRATION DATA for Sensor Number 80

CALIBRATION DATE: 02 September 1997

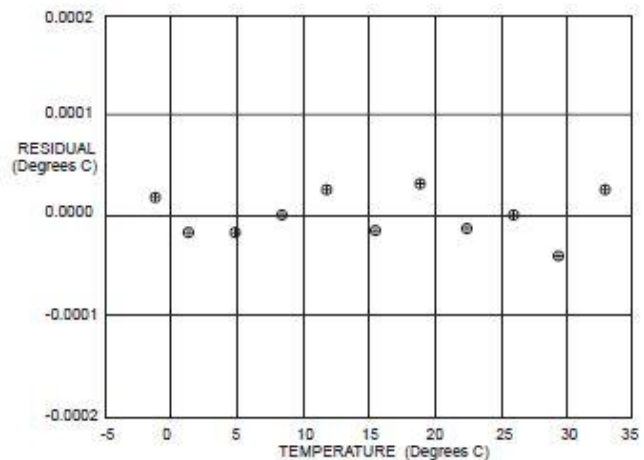
a0 = -2.809379e-05

a2 = -2.619655e-06

a1 = 2.783483e-04

a3 = 1.598734e-07

Bath Temperature [°C]	Instrument Output [n]	Instrument Temperature [°C]	Residual (Instrument - Bath) [°C]
-1.52985	824162.7	-1.52983	0.00002
1.03108	733633.1	1.03106	-0.00002
4.60520	625547.1	4.60518	-0.00002
8.11169	536776.4	8.11169	-0.00000
11.61533	462132.6	11.61536	0.00003
15.17575	398167.3	15.17574	-0.00001
18.63931	345476.6	18.63934	0.00003
22.14032	300170.8	22.14031	-0.00001
25.66793	261276.6	25.66793	0.00000
29.13948	228549.1	29.13944	-0.00004
32.61481	200420.3	32.61484	0.00003



04/09



Sea-Bird Electronics, Inc.

13431 NE 20th Street, Bellevue, Washington 98005 USA

Website: <http://www.seabird.com>

E-mail: [seabird@seabird.com](mailto:seabird@seabird.com)

Fax: (425) 643-9954

Telephone: (425) 643-9866

# NF

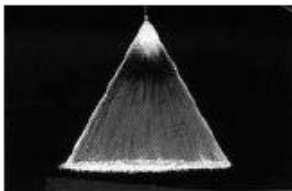
## Standard Fan Nozzle

### DESIGN FEATURES

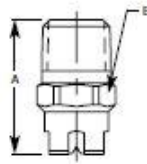
- One-piece construction
- No internal parts
- Sizes for all applications
- Male connection

### SPRAY CHARACTERISTICS

- High impact
  - Uniform distribution with tapered edges for overlapping sprays
  - Extra-wide angles available
- Spray pattern:** Fan and Straight Jet  
**Spray angles:** 0° to 120°  
**Flow rates:** 0.161 to 3430 l/min



Fan 50°



3/8" - 2" Metal

Dimensions are approximate. Check with BETE for critical dimension applications.

NF Flow Rates											NF Dimensions						
Call BETE to verify spray angle performance at operating pressures above 5 bar.											BSP or NPT						
Fan and Straight Jet, 0°, 15°, 30°, 50°, 65°, 80°, 90°, 110°, and 120° Spray Angles, 1/8" to 2" Pipe Sizes																	
Male Pipe Size	Nozzle Number	K Factor	LITERS PER MINUTE @ BAR										Equivalent Orifice Dia. (mm)	Pipe Size	Dim. for Metal Only (mm)		Wt. (g) Metal Plus.
			0.5 bar	0.7 bar	1 bar	2 bar	3 bar	5 bar	10 bar	30 bar	A	B					
1/8 or 1/4	NF01	0.228	0.16	0.19	0.23	0.32	0.39	0.51	0.72	1.25	0.66	1/8	22.2	11.1	28.4	7.09	
	NF015	0.342	0.24	0.29	0.34	0.48	0.59	0.76	1.08	1.87	0.79						
	NF02	0.455	0.32	0.38	0.46	0.64	0.79	1.02	1.44	2.49	0.91						
	NF025	0.569	0.40	0.48	0.57	0.81	0.99	1.27	1.80	3.12	1.02						
	NF03	0.683	0.48	0.57	0.68	0.97	1.18	1.53	2.16	3.74	1.09						
	NF04	0.911	0.54	0.76	0.91	1.29	1.58	2.04	2.88	4.99	1.32						
	NF05	1.14	0.81	0.95	1.14	1.61	1.97	2.55	3.60	6.24	1.45						
	NF06	1.37	0.97	1.14	1.37	1.93	2.37	3.06	4.33	7.49	1.57						
NF08	1.82	1.28	1.52	1.82	2.57	3.15	4.06	5.74	9.95	1.83	1/4	27.0	14.3	42.5	10.6		
NF10	2.28	1.61	1.91	2.28	3.22	3.95	5.10	7.21	12.5	2.03							
NF15	3.42	2.42	2.96	3.42	4.83	5.92	7.64	10.8	18.7	2.38							
NF20	4.56	3.22	3.91	4.56	6.45	7.89	10.2	14.4	25.0	2.78							
NF30	6.84	4.83	5.72	6.84	9.67	11.8	15.3	21.5	37.4	3.57							
NF40	9.12	6.45	7.63	9.12	12.9	15.8	20.4	28.8	49.9	3.97							
NF50	11.4	8.06	9.53	11.4	16.1	19.7	25.5	36.0	62.4	4.37							
NF60	13.7	9.67	11.4	13.7	19.3	23.7	30.6	43.2	74.9	4.76							
NF70	16.0	11.3	13.3	16.0	22.6	27.5	35.7	50.4	87.4	5.16	3/8	31.8	17.5	56.7	14.2		
NF80	18.2	12.9	15.3	18.2	25.8	31.6	40.8	57.7	99.9	5.56							
NF90	20.5	14.5	17.2	20.5	29.0	35.5	45.9	64.9	112	5.95							
NF100	22.8	16.1	19.1	22.8	32.2	39.5	51.0	72.1	125	6.35							
NF120	27.3	19.3	22.9	27.3	38.7	47.4	61.1	85.5	150	6.75							
NF150	34.2	24.2	28.6	34.2	48.3	59.2	76.4	108	187	7.54							
NF200	45.6	32.2	38.1	45.6	64.5	78.9	102	144	250	8.73							
NF300	68.4	48.3	57.2	68.4	96.7	118	153	216	374	10.7						1/2	38.1
NF400	91.2	64.5	76.3	91.2	129	158	204	288	499	12.7							
NF400	91.2	64.5	76.3	91.2	129	158	204	288	499	12.7							
NF750	171	121	143	171	242	296	382	540	936	17.5							
NF800	182	129	153	182	258	316	408	577	999	18.3							
NF1150	262	185	219	262	371	454	586	829	1440	21.8							
NF1500	342	242	286	342	483	592	764	1080	1870	24.6							
NF2250	513	382	429	513	725	890	1150	1620	2810	30.2	3/4	44.5	28.6	170	42.5		
NF300	68.4	48.3	57.2	68.4	96.7	118	153	216	374	10.7							
NF400	91.2	64.5	76.3	91.2	129	158	204	288	499	12.7							
NF400	91.2	64.5	76.3	91.2	129	158	204	288	499	12.7							
NF750	171	121	143	171	242	296	382	540	936	17.5							
NF800	182	129	153	182	258	316	408	577	999	18.3							
NF1150	262	185	219	262	371	454	586	829	1440	21.8							
NF1500	342	242	286	342	483	592	764	1080	1870	24.6						1	55.6
NF2250	513	382	429	513	725	890	1150	1620	2810	30.2							
NF300	68.4	48.3	57.2	68.4	96.7	118	153	216	374	10.7							
NF400	91.2	64.5	76.3	91.2	129	158	204	288	499	12.7							
NF400	91.2	64.5	76.3	91.2	129	158	204	288	499	12.7							
NF750	171	121	143	171	242	296	382	540	936	17.5							
NF800	182	129	153	182	258	316	408	577	999	18.3							
NF1150	262	185	219	262	371	454	586	829	1440	21.8	1 1/4	63.5	44.5	340	85.1		
NF1500	342	242	286	342	483	592	764	1080	1870	24.6							
NF2250	513	382	429	513	725	890	1150	1620	2810	30.2							
NF300	68.4	48.3	57.2	68.4	96.7	118	153	216	374	10.7							
NF400	91.2	64.5	76.3	91.2	129	158	204	288	499	12.7							
NF400	91.2	64.5	76.3	91.2	129	158	204	288	499	12.7							
NF750	171	121	143	171	242	296	382	540	936	17.5							
NF800	182	129	153	182	258	316	408	577	999	18.3						1 1/2	76.2
NF1150	262	185	219	262	371	454	586	829	1440	21.8							
NF1500	342	242	286	342	483	592	764	1080	1870	24.6							
NF2250	513	382	429	513	725	890	1150	1620	2810	30.2							
NF300	68.4	48.3	57.2	68.4	96.7	118	153	216	374	10.7							
NF400	91.2	64.5	76.3	91.2	129	158	204	288	499	12.7							
NF400	91.2	64.5	76.3	91.2	129	158	204	288	499	12.7							
NF750	171	121	143	171	242	296	382	540	936	17.5	2	88.9	63.5	1588	284		
NF800	182	129	153	182	258	316	408	577	999	18.3							
NF1150	262	185	219	262	371	454	586	829	1440	21.8							
NF1500	342	242	286	342	483	592	764	1080	1870	24.6							
NF2250	513	382	429	513	725	890	1150	1620	2810	30.2							
NF300	68.4	48.3	57.2	68.4	96.7	118	153	216	374	10.7							
NF400	91.2	64.5	76.3	91.2	129	158	204	288	499	12.7							
NF400	91.2	64.5	76.3	91.2	129	158	204	288	499	12.7							

Flow Rate (l/min) = K √(P-bar) Standard Materials: Brass, 303 Stainless Steel, 316 Stainless Steel, PVC and PTFE (PTFE not available in nozzle numbers NF025 and under).

Spray angle performance varies with pressure. Contact BETE for specific data on critical applications.

[www.BETE.com](http://www.BETE.com)

CALL 413-772-0846  
 Call for the name of your nearest BETE representative.



**GEVACRIL®**

**Technical Properties**

**2011**

**GEVACRIL SRL**

Strada Vic. Paolina 1  
20066 Melzo  
Italy

T +39.02.95737351  
F +39.02.95737357  
E [info@gevacril.com](mailto:info@gevacril.com)

**GEVACRIL ACRYLICS**

Rischerstr. 10  
69123 Heidelberg  
Germany

T +49.6221.752652  
F +49.6221.752653  
E [info@gevacril.com](mailto:info@gevacril.com)



## Technical Properties

Typical property values (at 20° C and 50% relative humidity)

Mechanical Properties	NORM <sup>1</sup>	Unit	Cast	Extruded	Polycarbonate
Specific weight	DIN 53479	gr/cm <sup>3</sup>	1,19	1,19	1,20
Impact strength (Charpy)	DIN 53453	kJ/m <sup>2</sup>	15	15	65
Notched impact strength a <sub>IN</sub> (Izod)	DIN 53453	kJ/m <sup>2</sup>	1,6	1,6	4,5
Tensile strength $\sigma_M$	D638	Mpa			
-40° C			110	100	-
20° C			80	70	50
70° C			40	35	-
Elongation at break	DIN 53455	%	5,5	4,5	-
Flexural strength (st. test specimen 80 x 10 x 4 mm <sup>3</sup> )	D790	Mpa	115	105	100
Compressive yield stress	-	MPa	110	103	-
Max. safety stress $\sigma_{max}$ (up to 40° C)	-	Mpa	5 ... 10	5 ... 10	5 ... 10
Modulus of elasticity E <sub>t</sub> (short-term value)	D790	MPa	3300	3300	2300
Indentation hardness H <sub>961/30</sub>	DIN 53456	MPa	175	175	110
Abrasion resistance in Taber abrader test (100 rev.; 5,4 N; CS-10F)	-	% Haze	20 ... 30	20 ... 30	30 ... 40
Coefficient of friction $\mu$	-	-			
a) plastic/plastic			0,8	0,8	-
b) plastic/steel			0,5	0,5	-
c) steel/plastic			0,45	0,45	-
Poisson's ratio $\mu$ (dilatation speed of 5%/min; up to 2% dilatation; at 20°C)	-	-	0,37	0,37	-
Resistance to puck impact from thickness (FMPA Stuttgart – Germany)	similar to DIN 18032	-	12 mm	8 mm	-
Sound velocity	-	m/s	2700 ... 2800	2700 ... 2800	-
Weighted sound reduction index R <sub>w</sub> at thickness	-	dB			
4 mm			26	26	-
6 mm			30	30	-
10 mm			32	32	-

<sup>1</sup> The norms indicated in this table are taken from: a) DIN: German Society for Standardisation; b) D (or ASTM): American Society for Testing Materials.





Optical Properties	NORM <sup>2</sup>	Unit	Cast	Extruded	Polycarbonate
Transmittance $\tau_{0.65}$	DIN 5036	%	~ 92	~ 92	~ 88
UV transmission	-	-	no	yes	yes
Reflection loss the visible range (each surface)	-	%	4	4	4
Adsorption in the visible range	-	%	<0,05	<0,05	-
Refractive index $n_D^{20}$	-	-	1,491	1,491	-

ELECTRICAL PROPERTIES	NORM <sup>3</sup>	Unit	Cast	Extruded	Polycarbonate
Volume resistivity $\rho_D$	DIN VDE 0303	ohm . cm	$>10^{15}$	$>10^{15}$	$>10^{13}$
Dielectric strength $E_d$ (1 mm specimen thickness)	DIN VDE 0303	kV/mm	~ 30	~ 30	-
Dielectric constant	DIN 53483	-			-
at 50 Hz			3.6	3.7	
at 0,1 MHz			2.7	2.8	
Dielectric loss factor	DIN 53483	-			-
at 50 Hz			0.06	0.06	
at 0,1 MHz			0.02	0.03	

<sup>2</sup> The norms indicated in this table are taken from: a) DIN: German Society for Standardisation; b) D (or ASTM): American Society for Testing Materials.

<sup>3</sup> The norms indicated in this table are taken from: a) DIN: German Society for Standardisation; b) D (or ASTM): American Society for Testing Materials.



THERMAL PROPERTIES	NORM <sup>4</sup>	Unit	Cast	Extruded	Polycarbonate
Coefficient of linear thermal expansion	DIN 53752	mm/m °C	0,07	0,07	0,065
Possible expansion to heat and moisture	-	mm/m	5	5	6
Thermal conductivity at 20°C	DIN 52612	W/(mK)	0,19	0,19	-
U-value for thickness:	DIN 4701	W/m <sup>2</sup> K			
1 mm			5,8	5,8	-
3 mm			5,6	5,6	-
5 mm			5,3	5,3	-
10 mm			4,4	4,4	-
Specific Heat c	-	J/g K	1,47	1,47	-
Forming temperature	-	°C	160... 175	150... 160	160... 180
Max. surface temperature (IR radiator)	-	°C	200	180	-
Max. service temperature (without mech. stress)	-	°C	80	70	120
Ignition temperature	DIN 51794	°C	425	430	-
Fire rating (material thickness > 2 mm)	DIN 4102	-	B2, normally flammable	B2, normally flammable	B2, normally flammable
Heat deflection temperature under load (HDT)	-	°C			-
deflection 1,8 MPa			105	90	
deflection 0,45 MPa			113	95	

Behavior Towards Water	NORM <sup>5</sup>	Unit	Cast	Extruded	Polycarbonate
Water absorption (24 h., 20° C) from dry state; specimen 60 x 60 x 2 mm <sup>3</sup>	DIN 53495	mg	41	38	45
Max. weight gain during immersion	DIN 53495	%	2,1	2,1	2,1

Our technical advices for the use of our materials are typical values supplied in accordance with our tests and with the regular commercially acceptable standards. They are given without any obligation. The buyer is responsible for the application and processing of our products and is also liable for observing any third party rights.

<sup>4</sup> The norms indicated in this table are taken from: a) DIN: German Society for Standardisation; b) D (or ASTM): American Society for Testing Materials.

<sup>5</sup> The norms indicated in this table are taken from: a) DIN: German Society for Standardisation; b) D (or ASTM): American Society for Testing Materials.

## C - Liquid dominated Mixer Calculations

The total flow rate entering the holes of the perforated tube can be calculated from the orifice equation [ 31 ].

$$Q_{1g} = n C_d A \left( \frac{2}{\rho_1 \Delta p} \right)^{\frac{1}{2}} 3600 \quad \text{Eq. 0.1}$$

Perforated tube data	
Tube diameter, D [mm]	20
Hole diameter, d [mm]	5
Number of holes, n	25
Discharge coefficient, $C_d$	21,89

**Table 20 Perforated Tube Data**

The differential pressures generating the wanted outlet gas flow rates were calculated from an iteration process combining a nozzle in HYSYS and Eq. 0.1. A  $\Delta p$  was first guessed and inserted into the HYSYS nozzle together with  $Q_{2g}$ . From HYSYS  $Q_{g1}$  and  $\rho_1$  was fed into Eq. 0.1, which was used to calculate a new  $\Delta p$ . This iteration process was repeated until satisfying results were found, typically 8-12 iterations.

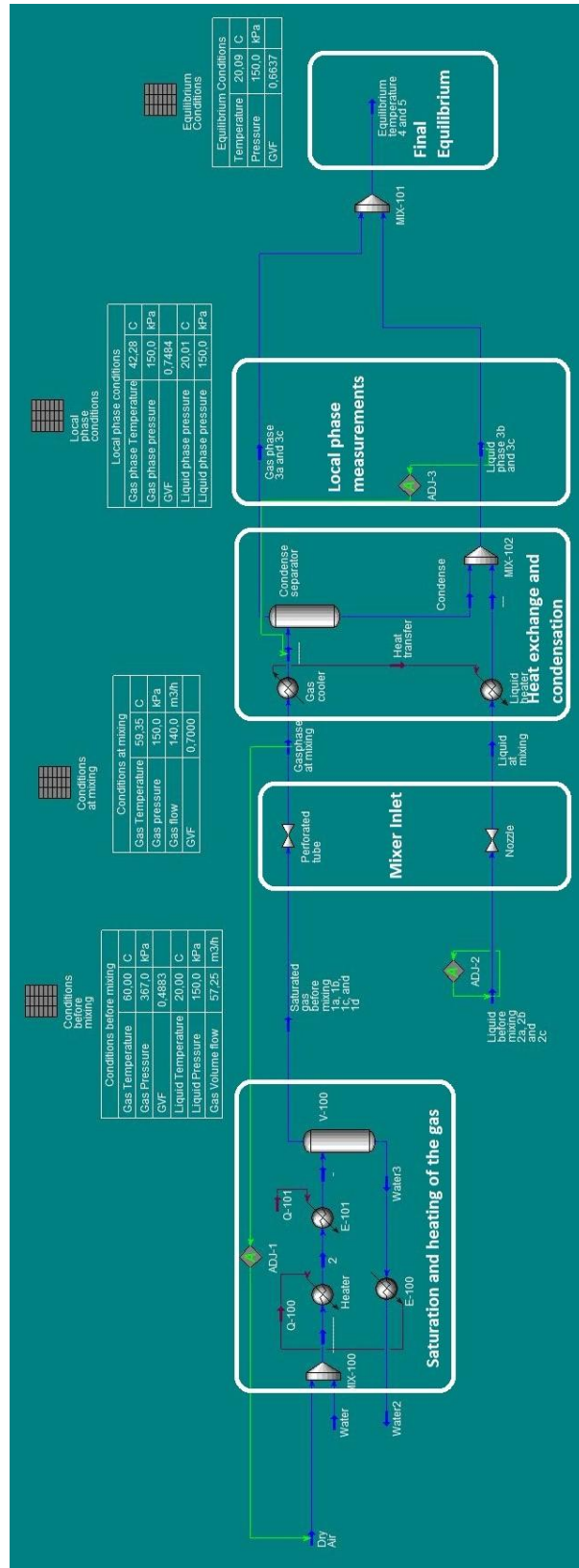
The calculations was repeated to generate inlet conditions in the GVF range of 0-70 %. The results can be found in the table below. Discharge coefficient was chosen from a table of recommended values of air passing through a thin plated orifice.

Type:	Tube diameter = 20mm, Hole diameter=5mm and Number of holes =25.							
GVF [%]	70	60	50	40	30	20	10	0
$Q_{g1}$ [m3/h]	44.3	42,7	41.0	38,5	34,7	28,6	17,7	0
$Q_{g2}$ [m3/h]	140	120	100	80	60	40	20	0
dp [kPa]	217	179	144	108	73	40	12	0

**Table 21 Perforated Tube Results**



# D - Simulation Environment Test Rig





## E - Matlab Implementation of Direct Integration

### Script #1 - Run

```
clear all
%% Inlet values
p1=3000; %% kPa
T1=5; %% Degrees C
GVF=80;

% Outlet values
p2=4000; %% kPa
T2=11.292;
%T2=11.292116178565436; %% Degrees C

%Calculation Options
NSteps=10;
%etha_pol=0.75;

%%Starting Hysys
hy = feval('actxserver', 'Hysys.Application');
c =invoke (hy.SimulationCases, 'Open',
'C:\Users\halfdanr\Dropbox\Skole\ProjektMaster
oppgave\Matlab\HYSYSM\COMPOSITIONGENERATOR.HSC');

[etha_pol,hh1, hh2,
GGVF,h_vec,s_vec,stream]=DirectIntegrationEtha(GVF, p1, p2, T1,
T2, NSteps,c);
```

### Function # 1 – DirectIntegrationEtha()

```
%% Calculates polytrophic efficiency from test results according
to the direct integration method presented by Huntington.
function [ etha_pol, h1, h2, GVF_act, h_vec, s_vec, stream] =
DirectIntegrationEtha( GVF, p1, p2, T1, T2, NSteps,c )

dp=(p2-p1)/NSteps;

if GVF == 90
stream= get (c.Flowsheet.Streams, 'Item', '90GVF');
end
if GVF == 80
stream= get (c.Flowsheet.Streams, 'Item', '80GVF');
end
if GVF == 70
stream= get (c.Flowsheet.Streams, 'Item', '70GVF');
end
```

```

if GVF == 60
stream= get (c.Flowsheet.Streams, 'Item', '60GVF');
end
if GVF == 50
stream= get (c.Flowsheet.Streams, 'Item', '50GVF');
end
if GVF == 40
stream= get (c.Flowsheet.Streams, 'Item', '40GVF');
end
if GVF == 30
stream= get (c.Flowsheet.Streams, 'Item', '30GVF');
end
if GVF == 20
stream= get (c.Flowsheet.Streams, 'Item', '20GVF');
end
if GVF == 10
stream= get (c.Flowsheet.Streams, 'Item', '10GVF');
end
if GVF == 0
stream= get (c.Flowsheet.Streams, 'Item', '0GVF');
end

% Calculating inlet enthalpy, volume and entropy
stream.PressureValue=p1;
stream.TemperatureValue=T1;
h1=stream.MolarEnthalpyValue;
s1=stream.MolarEntropyValue;
v1=1/stream.MolarDensityValue;
GVF_act=stream.DuplicateFluid.FluidPhases.Item(0).ActualVolumeFlowValue/stream.DuplicateFluid.ActualVolumeFlowValue;

% Calculating outlet enthalpy and volume.
stream.PressureValue=p2;
stream.TemperatureValue=T2;
h2=stream.MolarEnthalpyValue;
v2=1/stream.MolarDensityValue;
s2=stream.MolarEntropyValue;

%h_vec=zeros(NSteps+1);
h_vec(1)=h1;
s_vec(1)=s1;
%% Erasing Temperature value
stream.TemperatureValue=-32767;

%% Applying direct integration
etha_1=1;
etha_2=0;

```



```

while abs(etha_1-etha_2) >= 1e-4
    etha_pol=(etha_1+etha_2)/2;

    p_start=p1;
    h_start=h1;
    v_start=v1;

    for n=1:1:NSteps
        p_end=p_start+dp;

        Itt1=0;
        Itt2=etha_pol*(h2-h1)*2;
        while abs(Itt1-Itt2)>1e-4
            Itt=(Itt1+Itt2)/2;

            h_end=Itt/etha_pol+h_start;
            stream.MolarEnthalpyValue=h_end;
            stream.PressureValue=p_end;
            v_end=1/stream.MolarDensityValue;
            v_avg=(v_start+v_end)/2;

            reff=v_avg*dp;

            if reff>=Itt
                Itt1=Itt;s
            else
                Itt2=Itt;
            end
        end

        h_start=h_end;
        p_start=p_end;
        v_start=v_end;
        h_vec(n+1)=h_end;
        s_vec(n+1)=stream.molarEntropyValue;
    end

    h2_end=h_end;
    stream.MolarEnthalpyValue=h_end;
    stream.PressureValue=p_end;
    T2_end=stream.TemperatureValue;
    if T2_end >= T2
        etha_2 = etha_pol;
    else
        etha_1 = etha_pol;
    end
end

```

```
end
```

```
end
```

## Function # 2 - DirectIntegrationT()

```
function [ T2] = DirectIntegrationT(GVF, p1, p2, T1, etha_pol,
NSteps)
%% Calculates Outlet temperature from polytrophic efficiency
acording to the direct integration method presented by Hunting-
ton.

dp=(p2-p1)/NSteps;

%%Starting Hysys
hy = feval('actxserver', 'Hysys.Application');

c =invoke (hy.SimulationCases, 'Open',
'C:\Users\halfdanr\Dropbox\Skole\ProsjektMaster
oppgave\Matlab\HYSYSM\COMPOSITIONGENERATOR.HSC');

if GVF == 90
stream= get (c.Flowsheet.Streams, 'Item', '90GVF');
end
if GVF == 80
stream= get (c.Flowsheet.Streams, 'Item', '80GVF');
end
if GVF == 70
stream= get (c.Flowsheet.Streams, 'Item', '70GVF');
end
if GVF == 60
stream= get (c.Flowsheet.Streams, 'Item', '60GVF');
end
if GVF == 50
stream= get (c.Flowsheet.Streams, 'Item', '50GVF');
end
if GVF == 40
stream= get (c.Flowsheet.Streams, 'Item', '40GVF');
end
if GVF == 30
stream= get (c.Flowsheet.Streams, 'Item', '30GVF');
end
if GVF == 20
stream= get (c.Flowsheet.Streams, 'Item', '20GVF');
```

```

end
if GVF == 10
stream= get (c.Flowsheet.Streams, 'Item', '10GVF');
end
if GVF == 0
stream= get (c.Flowsheet.Streams, 'Item', '0GVF');
end

% Calculating inlet entalpy, volume and enropy
stream.PressureValue=p1;
stream.TemperatureValue=T1;
h1=stream.MolarEnthalpyValue;
s1=stream.MolarEntropyValue;
v1=1/stream.MolarDensityValue;

h_vec(1)=h1;
s_vec(1)=s1;

% % Calculating outlet enthalpy and volume.
stream.PressureValue=p2;
%% Erasing Temperature value
stream.TemperatureValue=-32767;
stream.MolarEntropyValue=s1;
h2s=stream.MolarEnthalpyValue;
%% Erasing Entrpy value
stream.MolarEntropyValue=-32767;

p_start=p1;
h_start=h1;
v_start=v1;

for n=1:1:NSteps
    p_end=p_start+dp;

    Itt1=0;
    Itt2=etha_pol*(h2s-h1)*2;
    while abs(Itt1-Itt2)>1e-4
        Itt=(Itt1+Itt2)/2;

        h_end=Itt/etha_pol+h_start;
        stream.MolarEnthalpyValue=h_end;
        stream.PressureValue=p_end;
        v_end=1/stream.MolarDensityValue;
        v_avg=(v_start+v_end)/2;
    end
end

```

```
    reff=v_avg*dp;

    if reff>=Itt
        Itt1=Itt;
    else
        Itt2=Itt;
    end
end

    h_start=h_end;
    p_start=p_end;
    v_start=v_end;
    h_vec(n+1)=h_end;
    s_vec(n+1)=stream.molarEntropyValue;
end
stream.MolarEnthalpyValue=h_end;
stream.PressureValue=p_end;
T2=stream.TemperatureValue;

end
```

## F - Complete Direct Integration Results

<b>GVF:</b>	90%		80%		70%		60%	
<b>Composition:</b>	A	B	A	A	A	B	A	B
Calc. inlet GVF [%]	90	90,64	80	81,08	70	71,43	60	61,68
$p_1$ [kPa]	3000	3000	3000	3000	3000	3000	3000	3000
$p_2$ [kPa]	4000	4000	4000	4000	4000	4000	4000	4000
$T_1$ [°C]	5	5	5	5	5	5	5	5
$T_2$ [°C]	13,583	13,583	11,292	11,292	9,962	9,962	9,036	9,036
$h_1$ [kJ/kmol K]	-130506	-124317	-149727	-140668	-162951	-151716	-173875	-160697
$h_2$ [kJ/kmol K]	-129981	-123854	-149335	-140345	-162633	-151467	-173603	-160495
$\Delta h$ [kJ/kmol K]	526	463	392	323	318	248	272	202
Calculated $\eta_p$ [%]	75	84	75	89	75	92	75	96

**Table 22 Direct Integration results 90%-60%GVF**

<b>GVF:</b>	50%		40%		30%		20%	
<b>Composition:</b>	A	B	A	B	A	B	A	B
Calc. inlet GVF [%]	50	51,78	40	41,72	30	31,48	20	21,01
$p_1$ [kPa]	3000	3000	3000	3000	3000	3000	3000	3000
$p_2$ [kPa]	4000	4000	4000	4000	4000	4000	4000	4000
$T_1$ [°C]	5	5	5	5	5	5	5	5
$T_2$ [°C]	8,352	8,352	7,827	7,827	7,410	7,410	6,709	6,709
$h_1$ [kJ/kmol K]	-183673	-168708	-192908	-176163	-201931	-183364	-211019	-190526
$h_2$ [kJ/kmol K]	-183433	-168537	-192691	-176014	-201732	-183232	-210832	-190385
$\Delta h$ [kJ/kmol K]	240	171	217	149	199	132	188	141
Calculated $\eta_p$ [%]	75	99	75	101	75	103	75	90

**Table 23 Direct Integration results 50%-20%GVF**

<b>GVF:</b>	10%		0%	
<b>Composition:</b>	A	B	A	B
Calc. inlet GVF [%]	10	10,27	0	0
$p_1$ [kPa]	3000	3000	3000	3000
$p_2$ [kPa]	4000	4000	4000	4000
$T_1$ [°C]	5	5	5	5
$T_2$ [°C]	5,933	5,933	5,357	5,357
$h_1$ [kJ/kmol K]	-220461	-197866	-230646	-205615
$h_2$ [kJ/kmol K]	-220276	-197717	-230456	-205458
$\Delta h$ [kJ/kmol K]	185	149	190	157
Calculated $\eta_p$ [%]	75	83	75	81

**Table 24 Direct Integration results 10%-0%GVF**

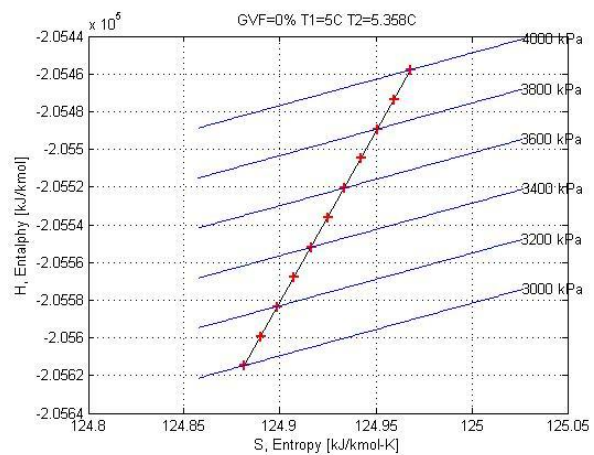
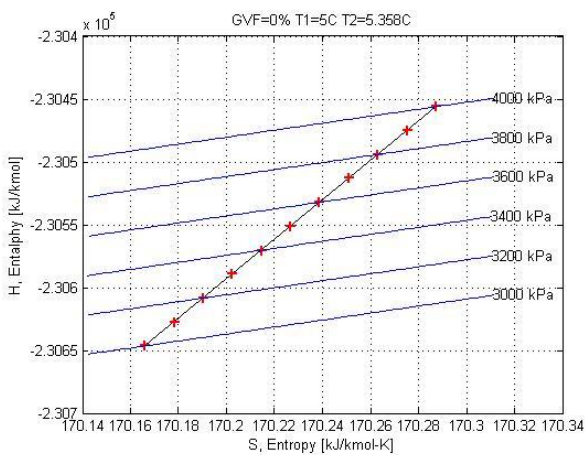


**Figure 30 Direct integration, Composition A VS B, Number of steps = 10, GVF 0%**

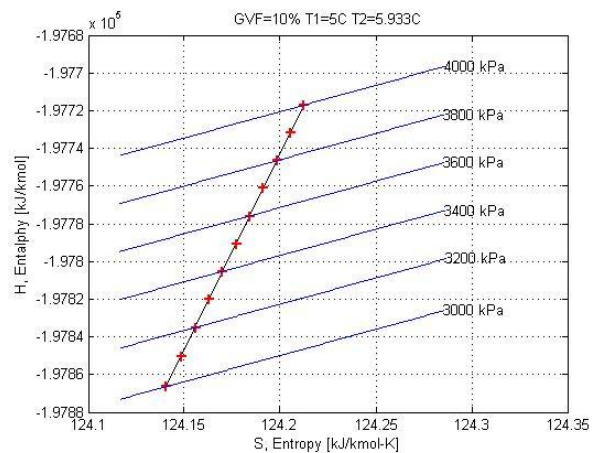
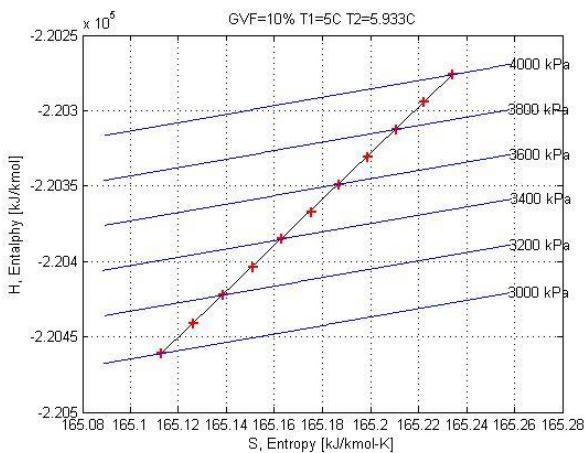


**Figure 31 Direct integration, Composition A VS B, Number of steps = 10, GVF 10%.**

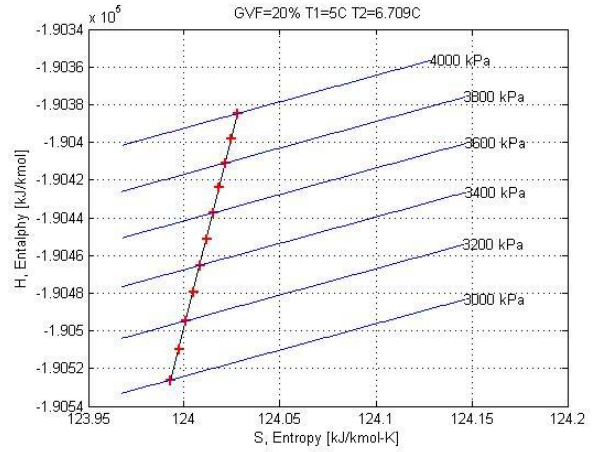
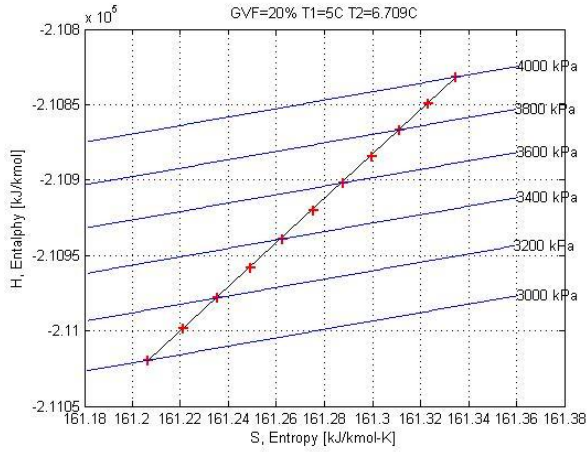


**Figure 32 Direct integration, Composition A VS B, Number of steps = 10, GVF 20%.**

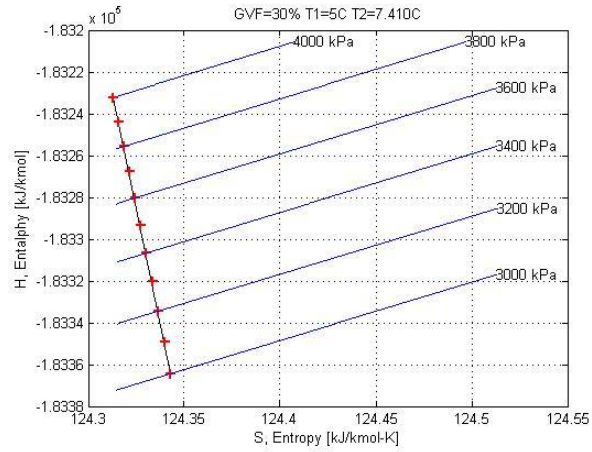
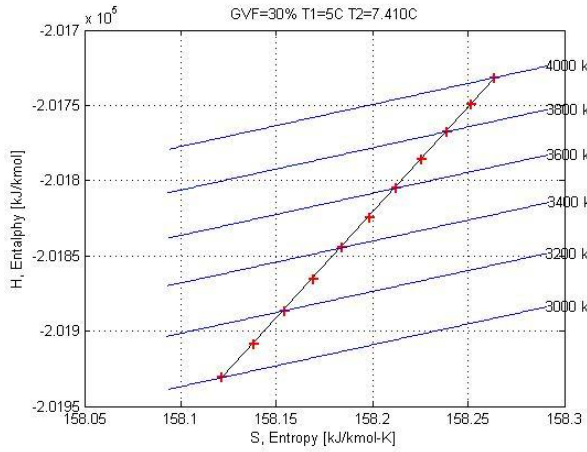


**Figure 33 Direct integration, Composition A VS B, Number of steps = 10, GVF 30%.**

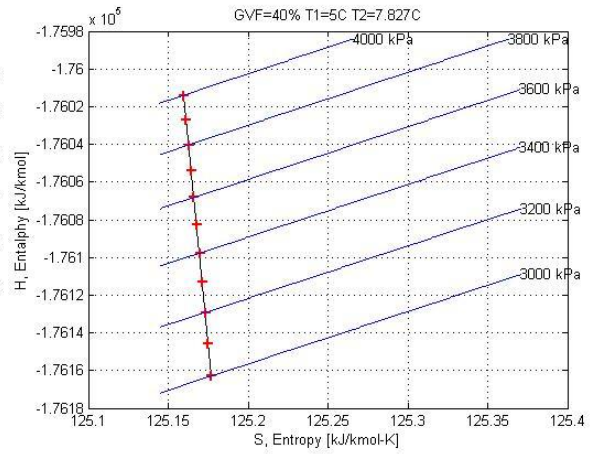
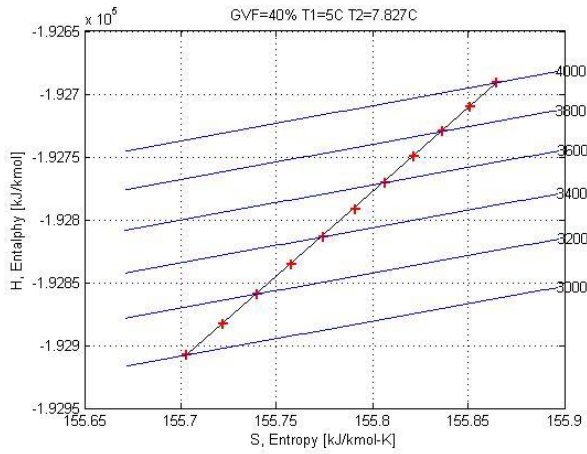


**Figure 34 Direct integration, Composition A VS B, Number of steps = 10, GVF 40%.**



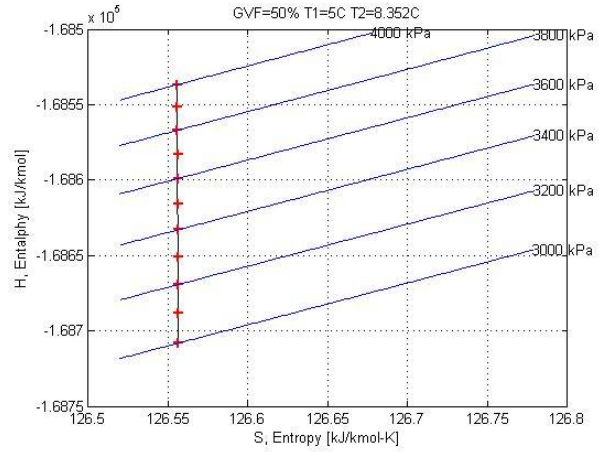
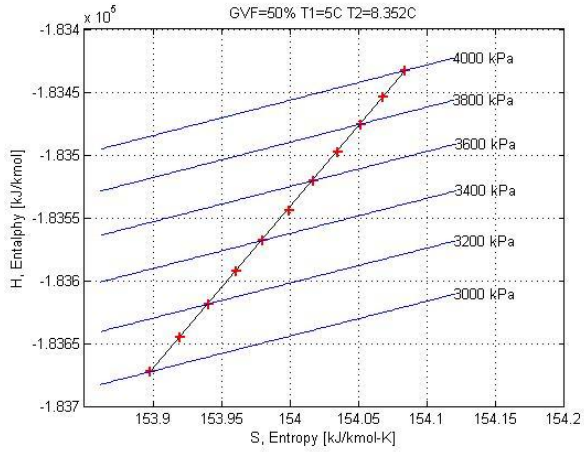


**Figure 35 Direct integration, Composition A VS B, Number of steps = 10, GVF 50%.**

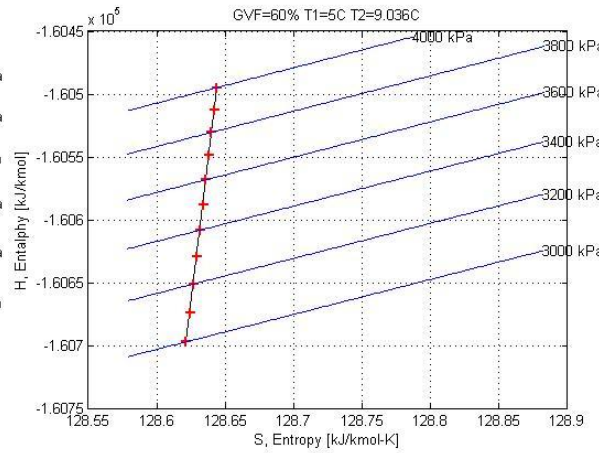
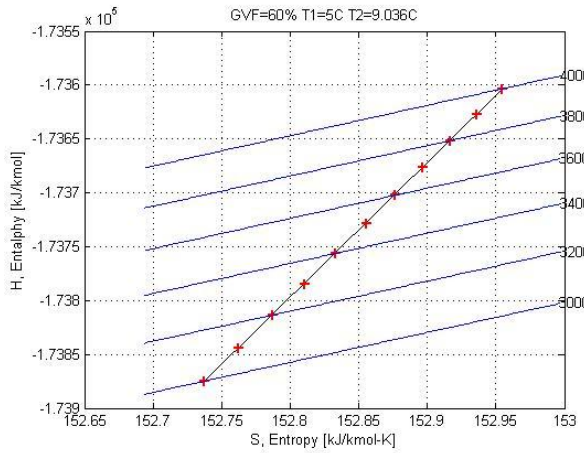


**Figure 36 Direct integration, Composition A VS B, Number of steps = 10, GVF 60%.**

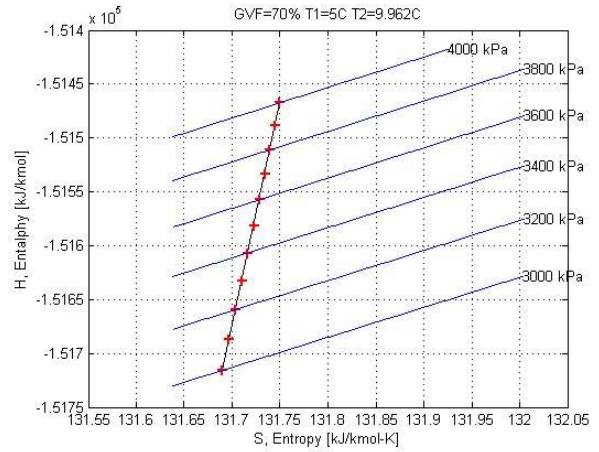
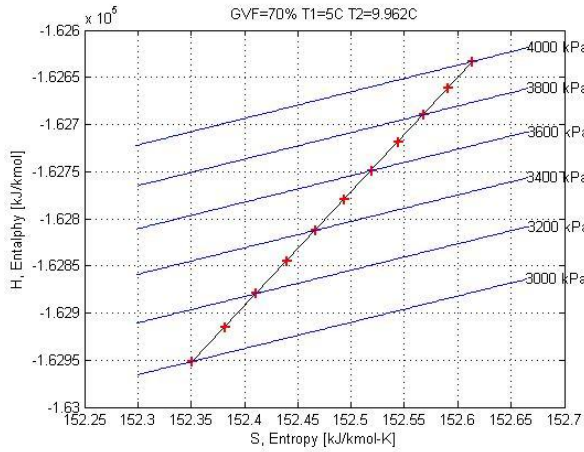


**Figure 37 Direct integration, Composition A VS B, Number of steps = 10, GVF 70%.**



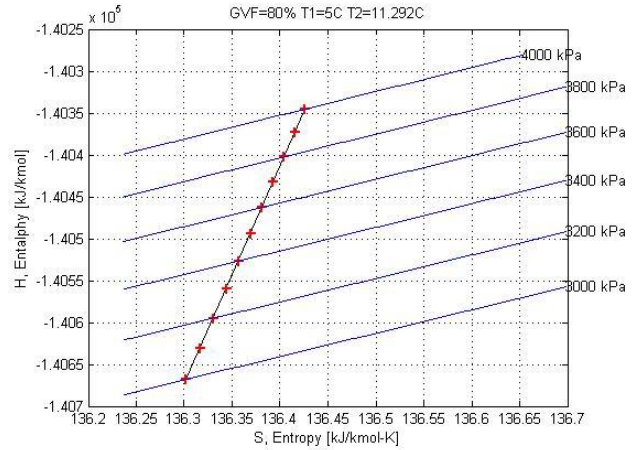
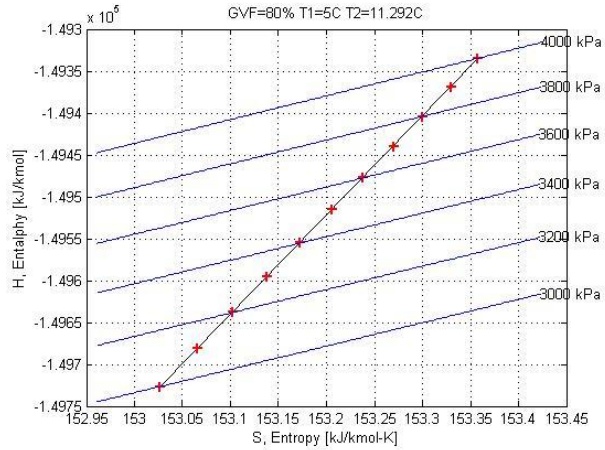


**Figure 38 Direct integration, Composition A VS B, Number of steps = 10, GVF 80%**

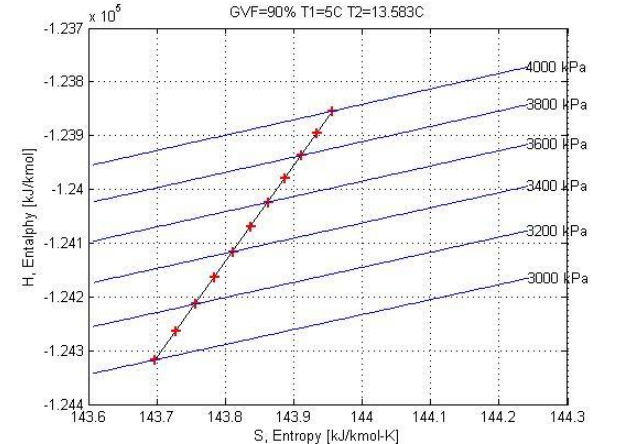
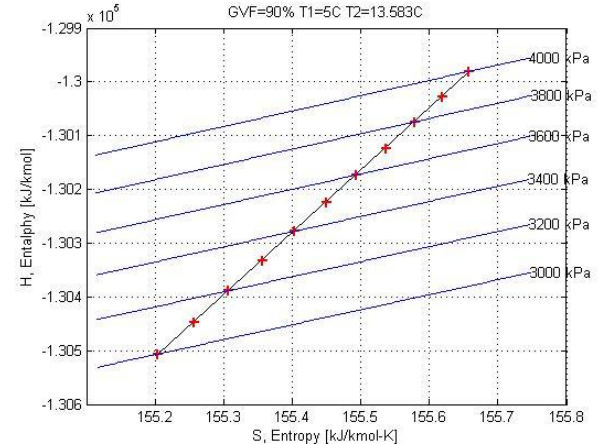


**Figure 39 Direct integration, Composition A VS B, Number of steps = 10, GVF 90%.**